CHARACTERIZATION AND MODELING OF RADIATION EFFECTS ON NASA/MSFC SEMICONDUCTOR DEVICES

by

David V. Kerns, Jr.

and

Koy B. Cook, Jr.

Department of Electrical Engineering
Auburn University
Auburn, AL 36830

NASA Contract NAS8-32634
Final Report

Prepared for

George C. Marshall Space Flight Center
Marshall Space Flight Center, AL 35812

TECHNICAL REPORT STANDARD TITLE PAGE

1. REPORT NO.	2. GOVERNMENT ACCESSION NO.	3. RECIPIENT'S CATALOG NO.

4. TITLE AND SUBTITLE
Characterization and Modeling of Radiation Effects on NASA/MSFC Semiconductor Devices

5. REPORT DATE
December 1978

6. PERFORMING ORGANIZATION CODE

7. AUTHOR(S)
David V. Kerns, Jr., and Koy B. Cook, Jr.

8. PERFORMING ORGANIZATION REPORT #

9. PERFORMING ORGANIZATION NAME AND ADDRESS
Department of Electrical Engineering
Auburn University
Auburn, AL 36830

10. WORK UNIT NO.

11. CONTRACT OR GRANT NO.
NAS8-32634

12. SPONSORING AGENCY NAME AND ADDRESS
National Aeronautics and Space Administration
Washington, DC 20546

13. TYPE OF REPORT & PERIOD COVERED
Final Report

14. SPONSORING AGENCY CODE

15. SUPPLEMENTARY NOTES
Prepared by Auburn University for the George C. Marshall Space Flight Center, Marshall Space Flight Center, AL.

16. ABSTRACT

This work consisted of two phases. The first phase involved a detailed review of the literature on space radiation environments; the study was directed toward understanding the nature of radiation environments likely to be encountered on space missions and on ways of simulating such an environment in the laboratory. Justification was developed for the use of 2MEV protons as the radiation source.

The second phase of this work was experimental, and involved irradiating CMOS devices with protons and recording their performance degradation. Three device technologies were evaluated, bulk silicon CMOS fabricated at RCA, bulk silicon CMOS fabricated at NASA/MSFC, and CMOS-SOS fabricated at RCA. Data is presented and summarized, and recommendations for improved hardness made. This study is unique in that 2MEV protons were used as the radiation source.

17. KEY WORDS	18. DISTRIBUTION STATEMENT
Radiation Effects Proton Irradiation CMOS Integrated Circuits	

19. SECURITY CLASSIF. (of this report)	20. SECURITY CLASSIF. (of this page)	21. NO. OF PAGES	22. PRICE

MSFC - Form 3292 (Rev December 1972)

For sale by National Technical Information Service, Springfield, Virginia 22151

TABLE OF CONTENTS

LIST OF ILLUSTRATIONS

DEFINITION OF SYMBOLS

Symbol	Definition
A	Area
AMV_c	Atomic mass unit
BeV	Billion electron volts
C'_{ox}	Oxide capacitance per unit area
E	Energy
e	Electron Charge
ϵ_j	Weight fraction of element j
Φ	Radiation fluence
ϕ_{ms}	Metal-Semiconductor work function
ϕ_p	Voltage drop in p-type material
g	Grams
KeV	Kilo-electron volts
K_R	Recombination damage constant
m	Electron mass
MeV	Million electron volts
μ	Carrier mobility
n	Proton fluence
Na	Acceptor concentration
N_D	Total number of defects
N_O	Total number of preirradiation defects
Q'_{ss}	Interface charge per unit area

R	Carrier recombination rate
ρ	Oxide charge distribution
S	Stopping power
σ	Conductivity
τ	Minority carrier lifetime
V	Projectile velocity
V_B	Body or substrate voltage
V_C	Channel voltage
V_{FB}	Flat-band voltage
V_T	Threshold Voltage
X_{ox}	Oxide thickness
Z	Atomic number

CONTRACTOR REPORT

Final Report

Characterization and Modeling of Radiation Effects on NASA/MSFC Semiconductor Devices

SUMMARY

This work consisted of two phases. The first phase involved a detailed review of the literature on space radiation environments; the study was directed toward understanding the nature of radiation environments likely to be encountered on space missions and on ways of simulating such an environment in the laboratory. Justification was developed for the use of 2MEV protons as the radiation source.

The second phase of this work was experimental, and involved irradiating CMOS devices with protons and recording their performance degradation. Three device technologies were evaluated, bulk silicon CMOS fabricated at RCA, bulk silicon CMOS fabricated at NASA/MSFC, and CMOS-SOS fabricated at RCA. Data is presented and summarized, and recommendations for improved hardness made. This study is unique in that 2MEV protons were used as the radiation source.

I. INTRODUCTION

This program involves the study of the space radiation environment, and its simulation in the laboratory to assess the radiation hardness of various CMOS structures and processes. The radiation environments examined in the first phase of this work are the near earth trapped radiation of the Van Allen Radiation Belts, the radiation environment within our solar system resulting from the solar wind, and the cosmic radiation levels of deep space.

It was determined that a reasonable simulation of space radiation, particularly the earth orbital environment, could be achieved in the laboratory by proton bombardment. The Dynamitron 3 MeV proton accelerator located at Auburn University was used to proton irradiate CMOS integrated circuits fabricated by three different processes.

The three types were bulk silicon CMOS inverter arrays fabricated by RCA (RCA 4007), Silicon on Sapphire CMOS inverter arrays fabricated by RCA (RCA TCS-071), and a bulk silicon CMOS inverter IC fabricated by NASA/Marshall Space Flight Center at Huntsville (MSFC-C-015).

Samples of these circuits were biased during irradiation in one of three configurations, gate tied to +V (input high), gate tied to ground (input low), or all terminals grounded (passive). The +V power supply was set at +10 volts in all cases. Active bias during irradiation was applied because there is considerable evidence that the extent of radiation induced damage is bias dependent, and this work reexamined this postulate. The data recorded consisted of the drain (supply) current and output

voltage for each inverter as the input voltage was swept from zero to ten volts after each successive irradiation. From this data pertinent device parameters can be extracted. Probable damage mechanisms are discussed, and recommendations for improved radiation hardness suggested.

Because of the large amount of data required in characterizing each inverter after each of several irradiations, the device population used was not large. While this is typical of most radiation damage studies, it does not represent a limitation of this type approach. This will be discussed in a later section.

II. SURVEY OF SPACE RADIATION ENVIRONMENTS

A. Background

With the launch of the Explorer I satellite on January 31, 1958, and its sensing of radiation by an on-board Geiger counter developed by Professor Van Allen of Iowa, the notion that space can pose a radiation hazard was born. The processing of the initial data from this experiment lead Ernie Ray of Van Allen's laboratory to make his classic remark, "My God, space is radioactive."

Subsequent Explorer satellite probes helped map the bands of trapped radiation encircling the earth, which have come to be known as the Van Allen Radiation Belts.

There are other sources of radiation to be dealt with in space. Within our solar system there is a constant stream of radiation emanating from the sun and diverging radially from it. This radiation stream, known as the solar wind can represent a significant radiation exposure over time intervals required for interplanatary travel. Within deep space, the cosmic radiation measured has indicated the presence of radiation of very high energy, but relatively low fluence levels.

B. The Van Allen Belts

The most serious radiation threat to electronics in earth orbit is the trapped radiation of the Van Allen Radiation Belts. The early Explorer satellites, followed by the Pioneer Spacecrafts, began the task of mapping the nature of these bands of radiation encircling the earth.

The Pioneer III Spacecraft, intended to be a lunar probe, carried two Gieger counters. Part of its mission was to further characterize the trapped radiation discovered on Explorer I. By combining the data from Explorer IV and Pioneer III, the first complete map of the trapped radiation was produced. (See Figure 1). This early picture lead to the concept of inner and outer radiation zones - a concept useful qualitatively, but of limited merit [2].

We now have a fairly complete picture of these radiation belts, as a result of years of effort and numerous satellite radiation mapping programs. The belts are composed of charged particles, almost exclusively protons and electrons trapped in toroidal shaped bands about the earth by the earth's magnetic field.

The high intensity "inner" belt is now known to be composed of high energy protons. A density map of these high energy protons (Ep > 30 MeV) is shown in Figure 2. Complete mappings of the proton fluxes, and energies of the inner belt have been compiled by Vette [3].

The outer zone is more complex is actually composed of a superposition of lower energy protons and electrons. A toroid of protons in the 1.0 to 5.0 MeV range at fluxes as large as $10^8/cm^2$-sec are illustrated in Figure 3 [4].

Electron fluxes are much less for electron energies greater than 1.6 MeV, showing maximums in the $10^4/cm^2$-sec, as shown in Figure 4. There is a fairly large flux of low energy electrons indicated by Figure 5 where flux density of electrons with energies greater than 40 KeV are mapped.

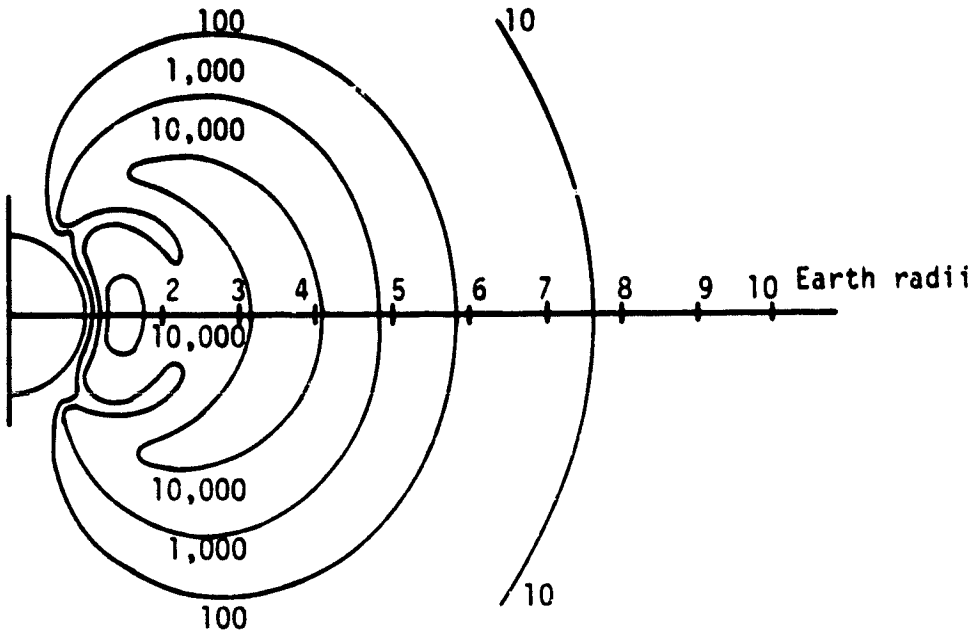

Figure 1. Van Allen's First Map of the Radiation Belts showing relative radiation in density in arbitrary units. (after Hess)

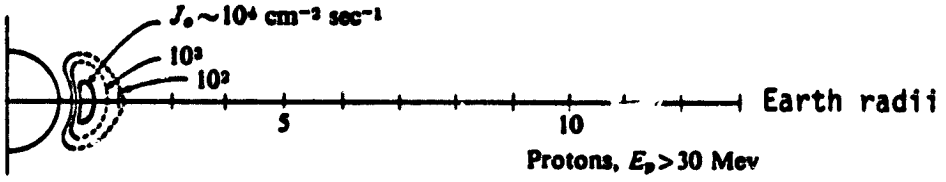

Figure 2. Spatial Distribution of Trapped Proton Flux With Energy Greater Than 30 MeV. (after Hess)

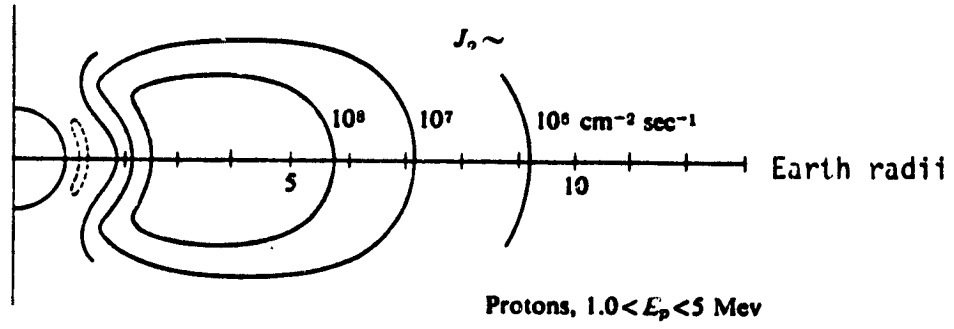

Figure 3. Spatial Distribution of Trapped Proton Flux With Energy Between 1 MeV and 5 MeV. (after Hess)

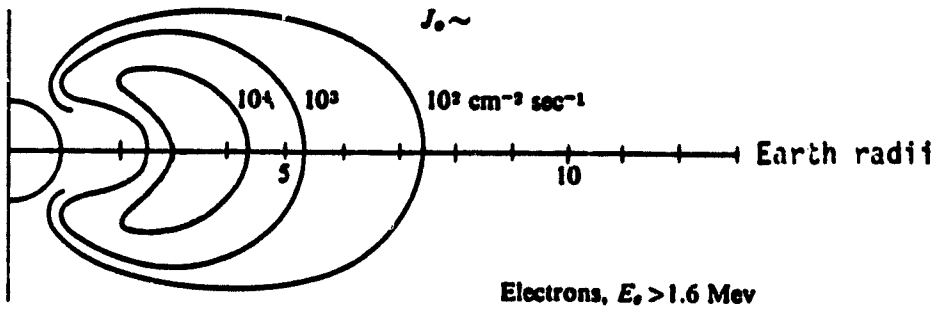

Figure 4. Spatial Distribution of Trapped Electron Flux of Energy Greater than 1.6 MeV. (after Hess)

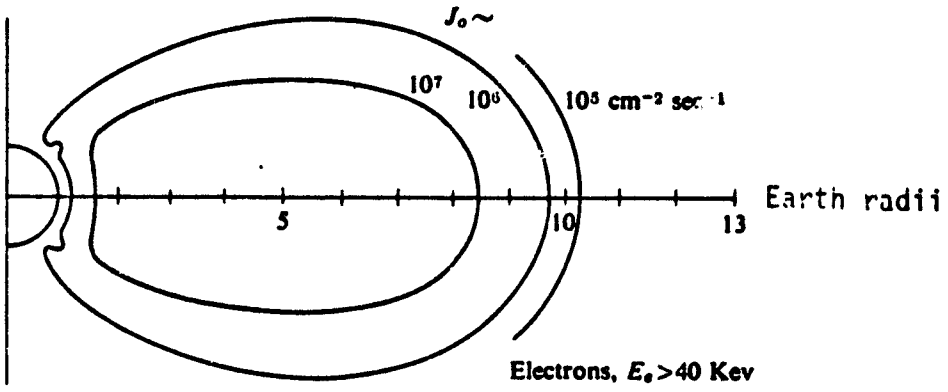

Figure 5. Spatial Distribution of Trapped Electron Flux of Energy Greater than 40 KeV. (after Hess)

Preceding the discovery of the natural radiation belts various laboratories suggested that charged particles could be artificially injected and trapped in the earth's magnetic field. After Van Allen's discovery, experiments were devised to further study this idea, such as the Project Argus nuclear explosions in 1958, and the Starfish and similar explosions by the Soviet Union in 1962 [5].

The 1.4 megaton Starfish explosion increased the number and average energy of trapped electrons by several orders of magnitude. [6]. These electrons did not fully decay to the natural levels until approximately 1970 [7]. Thus, the flux and energy distributions of particles within the Van Allen Belts are dynamic quantities, changing with time, and often influenced by solar activity or nuclear events.

One natural mechanism for the generation of Van Allen Belt particles involves the interaction of high-energy cosmic protons with the earth's upper atmosphere. The protons collide with the nuclei of atmospheric oxygen and nitrogen. The resultant neutrons decay into protons and electrons in approximately 1000 seconds [5].

When any charged particle enters a uniform magnetic field, it spirals. The radius of curvature of the resultant helix is directly proportional to the momentum of the particle and inversely proportional to the strength of the magnetic field [8]. Therefore if the radius is very large or small, the particles will not remain in the earth's curved field for long. Only at intermediate energies will the particles become trapped (i.e., have long lifetimes) and help form the Van Allen Belts.

Any planet possessing a magnetic field therefore captures charged

particles of particular energy ranges. The field acts as a leaky bucket whereby particles are continually entering and escaping [5].

The intensity of the particles depends on the strength of the field. For example, in late 1973, Pioneer 10 found that Jupiter has a magnetic field some twelve times stronger than Earth's at cloud top levels [9]. On Pioneer 10's mission it was found that the flux of electrons (E > 3 MeV) was 5 x 10^8/cm-sec, and the flux of protons (E > 30 MeV) was 4 x 10^6/cm-sec [10]. In contrast the maximum electron (E > 3 MeV) flux in the earth's Van Allen Belts is on the order of 10^5/cm-sec and the maximum flux of protons (E > 30 MeV) is on the order of 5 x 10^4/cm-sec [6]. Therefore the Pioneer flyby registered particle encounters some one hundred times the maximum intensities found about the earth.

C. Solar Wind

The sun is an emitter of both particle and electromagnetic radiation. Solar electron magnetic radiation wavelengths vary from the low millimeter range (radio waves) down to below 1A° (gamma rays) [11]. Particle radiation manifests itself as solar wind (supersonic electrons and protons) and solar flare protons.

Solar wind particle energies are low - proton energies typically 1 keV - and electron energies much less with intensities on the order of 1-2 x 10^8/cm-sec [5,8] in the vicinity of the earth's orbit. Solar proton events (solar flares) typically last a few days with particle energies up to 100 MeV or greater and with intensities as high as 5 x 10^5/cm-sec. (E > 300 keV). [5.8].

The sun has also followed an eleven-year cycle whereby its magnetic

field reverses polarity [11]. This results in a periodicity in its activity. Variations occur in solar wind intensity as well as in the magnitude and frequency of solar proton events [5].

During solar maximum (to occur again in 1980 or 1981) solar wind intensity may increase twofold. Solar proton events may typically occur two, three or more times per year and produce high proton intensities (discussed earlier) [11].

D. Cosmic Radiation

The composition of cosmic particle radiation is primarily high-energy protons (90%) and alpha particles (10%). Energies typically range from one to ten billion electron volts (1 BeV < E < 10 BeV) [12] with intensities ranging from 1.5/cm-sec during solar maximum to 4/cm-sec during solar minimum [5]. Variations in intensities result from scattering of cosmic particles by the variations in the solar magnetic field strength. The solar magnetic field, effectively carried by the solar wind, acts as a downstream "current" which the cosmic particles must "swim" against. This typically results in a smaller (i.e., 1.5/cm-sec) cosmic flux [5, 8].

E. Summary

A comparative summary of the various particle radiation environments is illustrated in Table I. The table compares some representative particle counts and their respective energy spectra. A complete model of these radiation environments is difficult to achieve for several reasons.

First is the degree of complexity of the environments. For example, the particle count about the earth varies with position, time, particle

energy, and particle type [4, 13, 14]. Particle counts at higher geomagnetic latitudes versus equatorial fluxes may differ substantially. Likewise proton counts may dominate in one region, electron counts in another. At the same time attempts to describe intensities without also defining the particle energies as well is meaningless; low-energy particles may be in abundance and high-energy particles relatively scarce. Furthermore, the particle counts often fluctuate dramatically with time. Periods of high solar activity thermally expand the earth's upper atmosphere. Low altitude Van Allen particle encounters with the intruding atmosphere increases, thus decreasing the population of charged particles. Moreover the time of day influences the shape of the belts, causing a shift in the isoflux contours [15]. Despite these complexities, detailed models of the Van Allen Belts have been devised [13], which provide the spacecraft designer with a reasonable approximation of the radiation expected to be encountered for a given orbit. This model has been computerized so that orbital information can be input directly and radiation parameters received as output.

Outside the Van Allen Belts, little radiation information is available. For example, Jupiter's radiation belts are relatively unexplored.

Table 1. Space Particle Radiation Environment

- A Comparative Summary

Particles	Type	(particles/cm^2 s) Flux	Energies	Notes
(1) Magnetically Trapped				
(a) Van Allen Belts	protons	5×10^4	E > 30 MeV	typical maximum fluxes;
		10^8	1 MeV < E < 5 MeV	Large fluxes of low
	electrons	~ 10^5	E > 3 MeV	energy particles also exist
(b) Jupiter	protons	4×10^6	E > 30 MeV	encountered by Pioneer 10
	electrons	5×10^8	E > 3 MeV	at Jupiter's cloudtops
(2) Solar				
(a) solar wind	protons	$10^8 \rightarrow 3 \times 10^8$	~ 1 keV	typical intensities at earth's orbit at solar minimum (circa 1962)
	electrons	$10^8 \rightarrow 3 \times 10^8$	~ 1 eV	
(b) solar flares	protons	5×10^5	10 MeV < E < 2 BeV	typical maximum flux; event duration typically a few days
(3) Cosmic	protons and α-particles	1.5	1 BeV < E < 10 BeV	solar maximum
		4	1 BeV < E < 10 BeV	solar minimum

III. RADIATION DAMAGE CONCEPTS

A. Types of Radiation Damage

There are only four principal types of radiation used in the bulk of the studies regarding radiation damage [16]. These four are protons, neutrons, electrons, and gamma rays. The proton and the neutron have almost the same mass but, the proton has a charge of $+1.6 \times 10^{-19}$ coulombs, whereas the neutron, as its name implies, has no charge. The electron has considerably less mass than the proton or neutron, but has a charge equal in magnitude to that of the proton but with the opposite sign. Gamma rays are simply electromagnetic waves of rather high frequency, usually above the frequency of X-rays. The bombardment of any device or material with any of the three particles just mentioned or with gamma rays is termed irradiation.

In discussing radiation-induced damage in solid state devices, it is useful to investigate the effects of this radiation on semiconductor materials, usually either silicon or silicon dioxide. Understanding the nature of the defects produced by the radiation in the material aids in a prediction of the effects on the device [17].

The effects of radiation on semiconductor materials can be divided into two types, ionization damage and displacement damage, although sometimes a third type called surface damage also resulting from ionization is also included [16]. Ionization occurs by the radiation knocking valance electrons from atoms in the semiconductor, forming ions in the material. According to the band theory this would be represented by the

excitation of a valence band electron into the conduction band. This can be a temporary effect, as when the radiation is removed, after some time delay, the liberated electrons will again return to their orbits around the ions. If, however, this ionization occurs in an insulating material (such as silicon dioxide) the time delay involved may be long enough for the effect to be considered permanent. This latter effect is often called surface damage, referred to later. Displacement damage is a permanent type of damage. This is the result of the radiation actually displacing atoms in the semiconductor lattice from their original position to some new position, usually an interstitial position. As this mechanism actually disrupts the normal order of atoms in the semiconductor crystal, this is sometimes called "bulk" damage. In 1949, Seitz [18] presented his work On the Disordering of Solids by Action of Fast Massive Particles, which was the earliest estimate of the energy required to displace an atom by a nuclear collision with a fast particle.

The so-called surface effects referred to earlier are semipermanent changes in the electrical behavior of a device due to ionization near the surface, or charge collection and migration in insulating or passivating layers. These changes can persist for a period of years after the radiation exposure, yet are fundamentally different than the changes as a result of displacement damage. For these reasons it has been suggested that the term "permanent" be avoided when speaking of radiation damage.

B. Effects of Radiation on Semiconductor Devices

Irradiation exposure by gamma rays produces predominantly ionization (and surface) type damage. Most of the literature on radiation effects

on semiconductors utilizes this type of source. The reasons for this are two-fold. First, Cobalt 60 gamma radiation sources are generally more readily available than are neutron sources or particle accelerators. Secondly, much of the radiation damage work has been supported by the military with their primary interest in the area of nuclear explosion effects. A nuclear blast produces large amounts of radiation in the form of gamma rays and neutrons. It should be pointed out that this is a totally different environment than that seen in space radiation - which is principally electrons and protons.

High energy charged particle radiation, electrons and protons can produce both ionization damage and displacement damage. High energy neutrons can also produce both types, but because of the lack of coulombic interaction (uncharged particle) by far the dominant neutron damage effect is displacement damage.

There are two major changes in silicon resulting from displacement damage which effect the electrical characteristics of the semiconductor, namely, the recombination rate and the carrier removal rate.

Consider the first of these, a change in the carrier recombination rate. In an intrinsic semiconductor the valance band and the conduction band are separated by the band gap, an energy interval of 1.11 eV in silicon. Carriers can be excited into the conduction band by thermal agitation, and the rate with which this occurs is called the generation rate. Similarly, electrons can give up energy and return to the valance band at a rate termed the recombination rate.

The irradiation of the silicon creates defects (or defect complexes) in the crystal which introduce energy levels in the "forbidden" gap. These

levels can act as recombination centers, according to the Shockley-Read-Hall theory of hole-electron recombinations [19, 20]. With these recombination centers present, the probability for a carrier recombination is greatly increased, and the observed recombination rate increases accordingly. Recombination can now occur in a two step process, from the conduction band via the trap to the valance band, as illustrated in Figure 6, rather than the less probable band-to-band transistion.

It is generally assumed that in a semiconductor, the number of bulk defects produced by the irradiation is directly proportional to the total radiation exposure, that is:

$$N_D = C_1\Phi + N_o \qquad (3\text{-}1)$$

where

N_D = total number of defects
N_o = total number of pre-irradiation defects
Φ = total radiation exposure
C_1 = constant

This is a reasonable assumption, if the dominant damage mechanism is bulk displacement damage. The total particle radiation exposure, Φ, is termed particle fluence, and represents the total number of particles impinging on the semiconductor surface normal to a unit area. A more detailed description of fluence and fluence measurements will be given in a following section.

Further the recombination rate per carrier (the average number of times a carrier recombines per second) is directly proportional to the

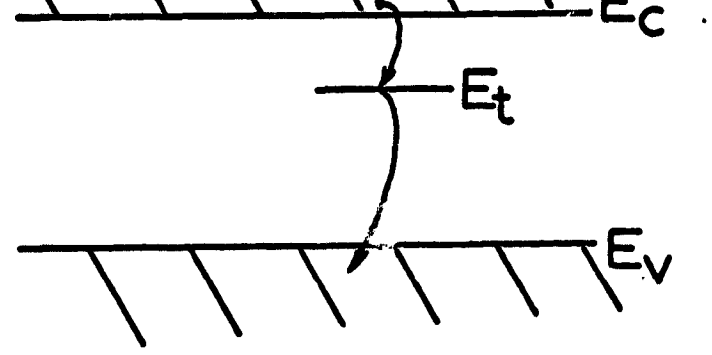

Figure 6. Carrier Reconbination via Reconbination Center. (after Larin)

number of defects in the semiconductor. This can be expressed as

$$R_n = C_2 N_D \qquad (3\text{-}2)$$

where

R_n = electron recombination rate per carrier in p-type material (minority carrier recombination rate).
C_2 = constant

Combining (3-1) and (3-2) we have:

$$R_n = C_2 (C_1 \Phi + N_o)$$

$$R_n = K_R \Phi + R_o \qquad (3\text{-}3)$$

where

$R_o = C_2 N_o$ = pre-irradiation recombination per carrier

K_R = constant = recombination damage constant

Equation (3-3) is often written as:

$$R_n - R_o = K_R \Phi \qquad (3\text{-}4)$$

Similar equations could be written for holes in n-type silicon.

From this latter equation it can be seen that the change in recombination rate is directly proportional to particle fluence, Φ, a characteristic of bulk displacement damage.

The recombination rate per carrier, previously defined as the average number of times a carrier recombines per second, is the inverse of a quantity which expresses the mean time interval between carrier recombination.

This time is called the carrier lifetime τ. In a p-type material the average time an electron spends in the conduction band before recombination is called the minority carrier lifetime, τ_n. τ_p is the same quantity for holes in n-type material. Thus,

$$R_n = \frac{1}{\tau_n} \tag{3-5}$$

From equations (3-4) and (3-5) we obtain

$$\frac{1}{\tau_n} - \frac{1}{\tau_o} = K_R \Phi \tag{3-6}$$

where τ_o = pre-irradiation carrier lifetime.

Therefore, the change in the reciprocal of the minority carrier lifetime is seen to be directly proportional to the radiation exposure, Φ, by a damage constant, K_R. More correctly, this K_R should be called a coefficient, not a constant, as its value does depend upon a number of factors, such as the temperature, type of radiation carrier concentration, etc. Equation (3-6) is of extreme value in studying the effects of displacement radiation on semiconductor devices.

A second important result of the displacement irradiation of silicon is the induced change in carrier concentration. The defects introduced into silicon by irradiation are such that, whether the material is n-type or p-type, it becomes more intrinsic by compensation from the addition of both n and p type defects. The irradiation has the effect of removing carriers or reducing the carrier concentration at a rate called the carrier removal rate. If N is the carrier concentration then:

$$N = N_o - \frac{\Delta N}{\Delta \Phi} \Phi \tag{3-7}$$

where N_o = pre-irradiation carrier density

$\frac{\Delta N}{\Delta \Phi}$ = carrier removal rate

This effect explains the observed changes in the resistivity (or conductivity) of silicon after irradiation. Consider an n-type silicon speciman with an electron concentration of N at room temperature. Then the conductivity, σ, is given by

$$\sigma = N q \mu_n \tag{3-8}$$

where

μ_n is the electron mobility.

Mobility changes as a result of irradiation are of lesser importance, and thus μ_n will be considered a constant [21]. As N is reduced by the radiation according to equation (3-7), the value of σ by equation (3-8) is also reduced.

The radiation thus results in a lowering of the conductivity, or inversely, an increase in the resistivity of the silicon, be it n-type or p-type. This will find application in examining the effect of radiation on the bulk resistances of device structures, and in particular in the change of base resistance in junction bipolar transistors.

Displacement damage in silicon primarily affects the performance of bipolar structures because of its direct affect on altering carrier lifetimes and concentrations. This, however, is not to say that in studying radiation effects on MOS IC's that displacement damage can be ignored.

Most MOS circuits have protection diodes on input gates, and in bulk silicon technologies, junction isolation is standard. These junctions, not to mention the channel region itself, are subject to displacement damage effects and a complete characterization must include these possibilities.

MOS semiconductor devices will undergo a shift in threshold voltage and loss of transconductance due to displacement radiation damage introducing carrier-removal sites [22]. This, however, is secondary to the principle radiation degradation mechanism in MOS devices which is surface damage from ionizing radiation. Ionizing radiation degrades MOS transistor performance by causing a build-up of strongly trapped positive charges in the gate insulator. The result of the positive charge accumulation is a shift in the threshold voltages of both n and p channel MOS transistors toward more negative voltages. To a first approximation this charge build-up can be modeled as directly proportional to the number of ion pairs created in the oxide, which in turn is proportional to the energy deposited in the oxide. (This is measured in units of rads.)

The most generally accepted model of this ionization radiation induced positive charge build-up is that the radiation creates electron-hole pairs in the silicon dioxide. The electrons are mobile and will drift out under the influence of a field (usually resulting from gate bias) until they either recombine with a hole or escape from the oxide at the metal-oxide interface. The holes, on the other hand, are much less mobile and get trapped almost immediately. For each electron that escapes, a trapped hole with positive charge is left locked in the oxide

The larger the electric field in the oxide during irradiation, the more electrons escape, and thus the larger the build-up of positive charge, which occurs primarily at the silicon-silicon dioxide interface. The increased positive charge in the oxide implies a more negative voltage must be applied at the gate to offset it, and consequently a shift in threshold voltage to more negative values results.

It can be seen that controlling charge build-up in the oxide of MOS devices is of critical importance in controlling their radiation hardness; improved rad-hard devices require development of an insulating layer which does not show appreciable charge trapping.

Numerous authors have contributed to the development of theoretical expressions for FET performance based on physical parameters. For example, Muller and Kamins in their book, "Device Electronics for Integrated Circuits", summarize the pertinent FET equations including the following expression for threshold voltage, V_T, for an n channel device

$$V_T = V_{FB} + V_c + 2|\phi_p| + \frac{1}{C'_{ox}}\sqrt{2\,\epsilon_s\, e\, N_a(2|\phi_p| + V_c - V_B)}$$

where $$V_{FB} = \Phi_{MS} - \frac{Q'_{SS}}{C'_{ox}} - \frac{1}{C'_{ox}} \int_0^{X_{ox}} \frac{X}{X_{ox}} \rho(x)dx$$

and

V_c = channel voltage

ϕ_p = voltage drop in p-type material

C'_{ox} = oxide capacitance per unit area

ϵ_s = dielectric permittivity of silicon

V_B = body or substrate voltage

V_{FB} = flat-band voltage

ψ_{MS} = metal semiconductor work function

Q'_{SS} = interface charge per unit area

X_{ox} = oxide thickness

$\rho(x)$ = oxide charge distribution

From these expressions it can be seen that device threshold voltage is theoretically directly proportional to flat-band voltage, V_{FB}. V_{FB} is related to the integral of the oxide charge distribution times the position (depth) of this charge in the oxide. The radiation induces trapped charge in the oxide, and it is this charge distribution, $\rho(x)$, that determines the effect of ionizing radiation on threshold voltage. Since this charge distribution is generally not uniform, and depends on many factors including bias, it is difficult to obtain a meaningful analytical expression.

The displacement damage can also alter the acceptor concentration of the substrate and affect the forth term in the expression for V_T; this however, is generally a much smaller effect than the accumulation of oxide charge.

C. Radiation Terminology and Dosimetry

Previous sections have shown that the radiation environments seen by electronics is generally either electromagnetic radiation or particle

bombardment by either electron, protons or neutrons. In considering the radiation dose delivered by each type of radiation, first a distinction must be made between exposure dose, and absorbed dose. Exposure dose is a measure of the radiation field to which a material is exposed, whereas absorbed dose refers to energy imparted to tne irradiated material [23].

Exposure dose has been defined for gamma radiation fields by the "Roentgen".

ROENTGEN: The amount of electromagnetic radiation which deposits a given quantity of energy into a standard reference material, usually air.

For partial irradiation exposure dose can be measured in terms of the particle flux, particle fluence, and particle energy.

PARTICLE FLUX: The intensity of particle radiation given in encounters per second per square centimeter. (e.g., protons/cm^2-sec)

PARTICLE FLUENCE: The time integral of flux, or the total number of particles per square centimeter from time zero to time T.

$$\text{Fluence} = \int_0^T (\text{flux})\, dt$$

(e.g., protons/cm^2)

PARTICLE ENERGY: The kinetic energy of the particle usually measured in electron volts. Both energy and flux information must be given to characterize the radiation.

The absorbed dose depends on the type of material being irradiated; given the same exposure dose various materials absorb more or less energy. The unit of absorbed dose is generally the Rad.

RAD: The amount of radiation which deposits 100 ergs of energy into one gram of the material under consideration.

The material generally used in semiconductor radiation studies is silicon. It can be seen that in considering ionization damage, where the amount of deposited energy can be related to number of electron-hole pairs created, the Rad is a useful dosage indicator.

For reasons that will be described later protons were selected as the radiation source to be used in these experiments. In order to calculate the Rads (absorbed dose) produced by a particular proton fluence, the following calculation was undertaken.

The stopping power, S, for a given particle traveling through a given target material is defined as the average energy loss per unit path length.

$$S = \frac{dE}{dx}$$

The high energy behavior of the stopping power can be described by the Bethe-formula [24].

$$S = \frac{4\pi e^4 Z_1^2 Z_2}{mV^2} \quad \ell n \left(\frac{2mV^2}{I}\right) + \ell n \left(\frac{1}{1-\beta^2}\right) - \beta^2 - \frac{c}{Z_2}$$

where

Z_1 and Z_2 are atomic numbers of projectile and target respectively

V is a projectile velocity

e is electron charge

m is the mass of electron

$\beta = V/c$ where c is the speed of light

The parameter I is generally estimated by Block's rule as

$$I = (10 \text{ eV})Z_2 \quad .$$

This relation describes the stopping fairly well for particle energies above 1 MeV, however the error increases rapidly for lower energies.

The experiment described in this work utilized 2 MeV protons; this energy is on the useful edge of the validity of the Bethe formula. To avoid the complexity and error of this calculation a compilation of experimentally determined stopping powers for hydrogen (protons) in every element was used [25]. The referenced publication has stopping power plotted as a function of particle energy, as shown in Figure 7 for silicon, Figure 8 for aluminum, and Figure 9 for oxygen.

For these elements the stopping power of 2 MeV protons was calculated as follows:

1) Silicon = 25.8 KeV/micron

2) Aluminum = 30.1 KeV/micron

3) Oxygen = 15.0 KeV/micron

The first two elements above are directly applicable to an MOS device structures, however to determine the stopping power of protons in

----------ENERGY IN KEV----------
SOLID CURVE = (S[LOW]) (S[HIGH]) / (S[LOW] + S[HIGH])

S[LOW] = 4.7 (ENERGY $^{0.45}$)

S[HIGH]= (3329 / ENERGY) LN [1+(550 / ENERGY) + (0.01321 ENERGY)]

ENERGIES BELOW 10 KEV : STOPPING = 4.15 (ENERGY $^{0.5}$)

FOR PRECISION VALUES ABOVE 1000 KEV USE SHELL COEFFICIENTS

PROTON MASS = 1.008 AMU
DEUTERON MASS = 2.014 AMU
TRITON MASS = 3.017 AMU

SI[14]- ATOMIC DENSITY = 4.978E22 ATOMS / CM3
MASS DENSITY = 2.321 GRAMS / CM3

FOR STOPPING [KEV/MICROMETER] MULTIPLY GRAPH BY: 4.978
FOR STOPPING [EV/(MICROGM/CM2)] MULTIPLY GRAPH BY: 21.45

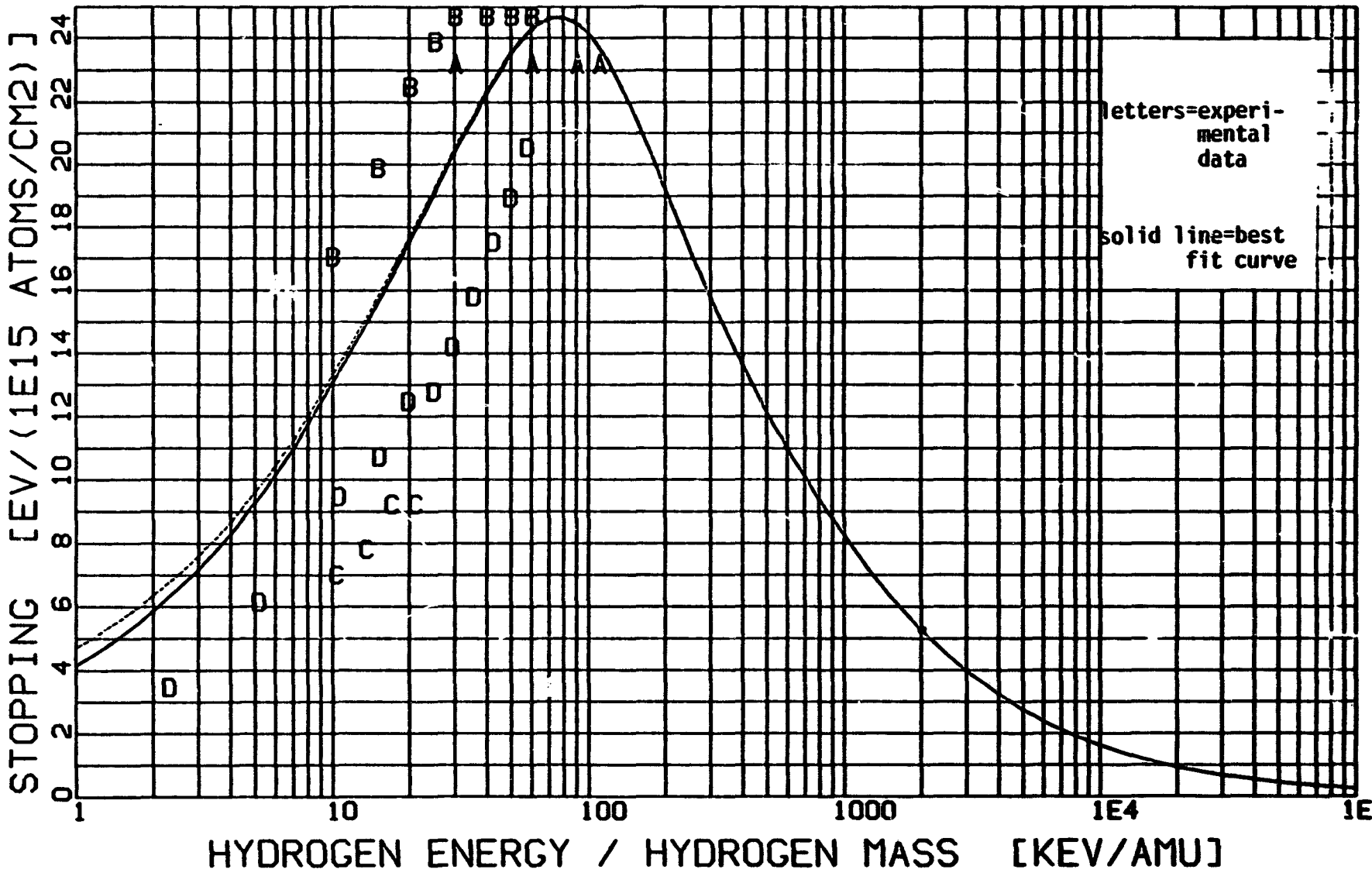

SOLID CURVE IS BEST FIT
DASHED CURVE [LOW ENERGIES] IS SOLID LINE PLUS I .S. NUCLEAR STOPPING

FIG. 7 SILICON STOPPING POWER

SI[14]

AL[13]

----------ENERGY IN KEV----------
SOLID CURVE = (S[LOW]) (S[HIGH]) / (S[LOW] + S[HIGH])
S[LOW] = 4.739 (ENERGY $^{0.45}$)
S[HIGH]= (2766 / ENERGY) LN [1+(164.5 / ENERGY) + (0.02023 ENERGY)]

ENERGIES BELOW 10 KEV : STOPPING = 4.154 (ENERGY $^{0.5}$)
FOR PRECISION VALUES ABOVE 1000 KEV USE SHELL COEFFICIENTS

PROTON MASS = 1.008 AMU
DEUTERON MASS = 2.014 AMU
TRITON MASS = 3.017 AMU
AL[13]- ATOMIC DENSITY = 6.023E22 ATOMS / CM3
MASS DENSITY = 2.698 GRAMS / CM3

FOR STOPPING [KEV/MICROMETER] MULTIPLY GRAPH BY: 6.023
FOR STOPPING [EV/(MICROGM/CM2)] MULTIPLY GRAPH BY: 22.33

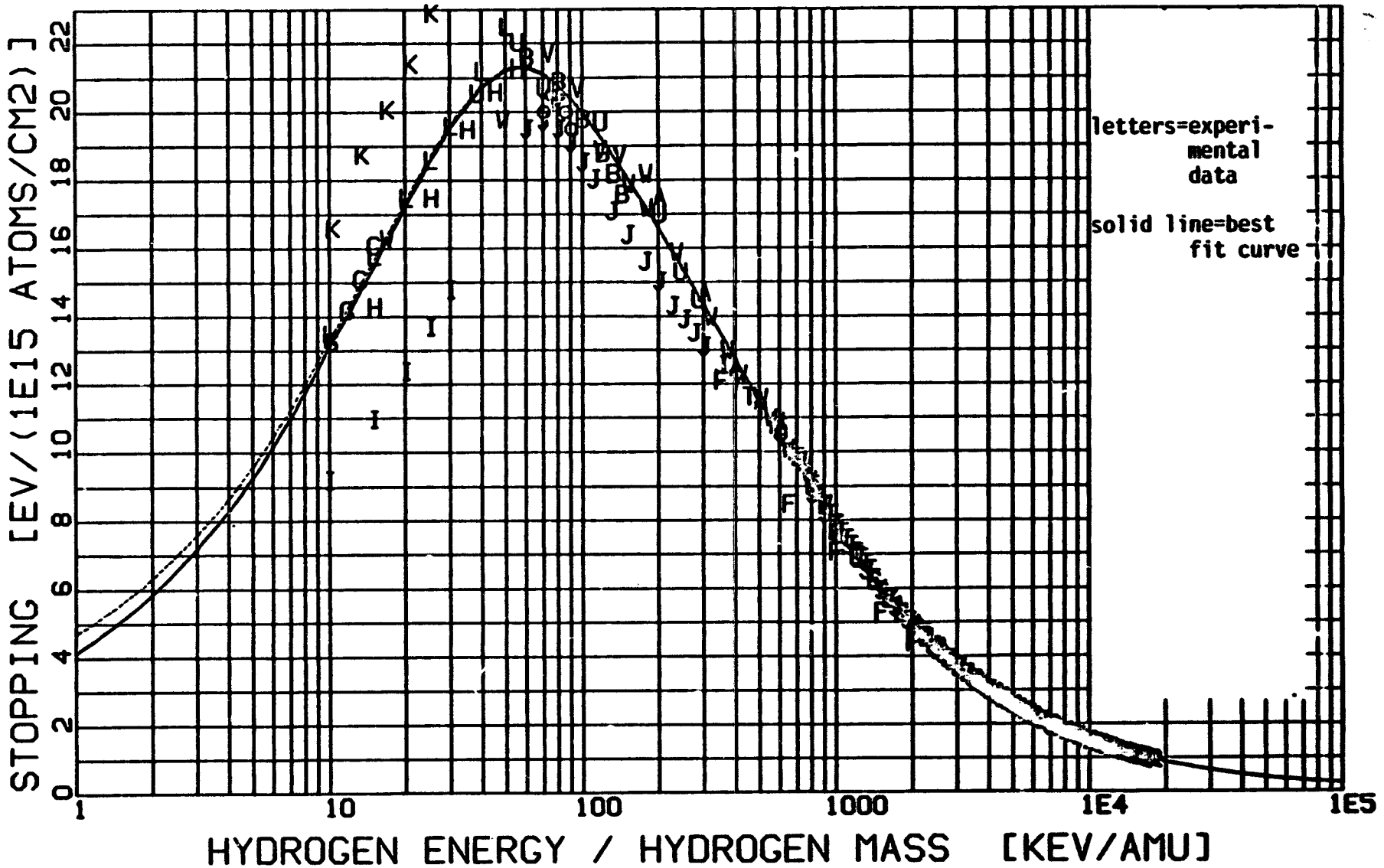

SOLID CURVE IS BEST FIT
DASHED CURVE [LOW ENERGIES] IS SOLID LINE PLUS L.S.S. NUCLEAR STOPPING

AL[13]

FIG. 8. ALUMINUM STOPPING POWER

28

O[8]

----------ENERGY IN KEV----------
SOLID CURVE = (S[LOW]) (S[HIGH]) / (S[LOW] + S[HIGH])

S[LOW]= 3 (ENERGY $^{0.45}$)
S[HIGH]= (1920 / ENERGY) LN [1+(2000 / ENERGY) + (0.0223 ENERGY)]

PROTON MASS = 1.008 AMU
DEUTERON MASS = 2.014 AMU
TRITON MASS = 3.017 AMU
O[8]- ATOMIC DENSITY = 4.302E22 ATOMS / CM3
MASS DENSITY = 1.143 GRAMS / CM3

ENERGIES BELOW 10 KEV : STOPPING = 2.652 (ENERGY $^{0.5}$)
FOR PRECISION VALUES ABOVE 1000 KEV USE SHELL COEFFICIENTS

FOR STOPPING [KEV/MICROMETER] MULTIPLY GRAPH BY: 4.302
FOR STOPPING [EV/(MICROGM/CM2)] MULTIPLY GRAPH BY: 37.66

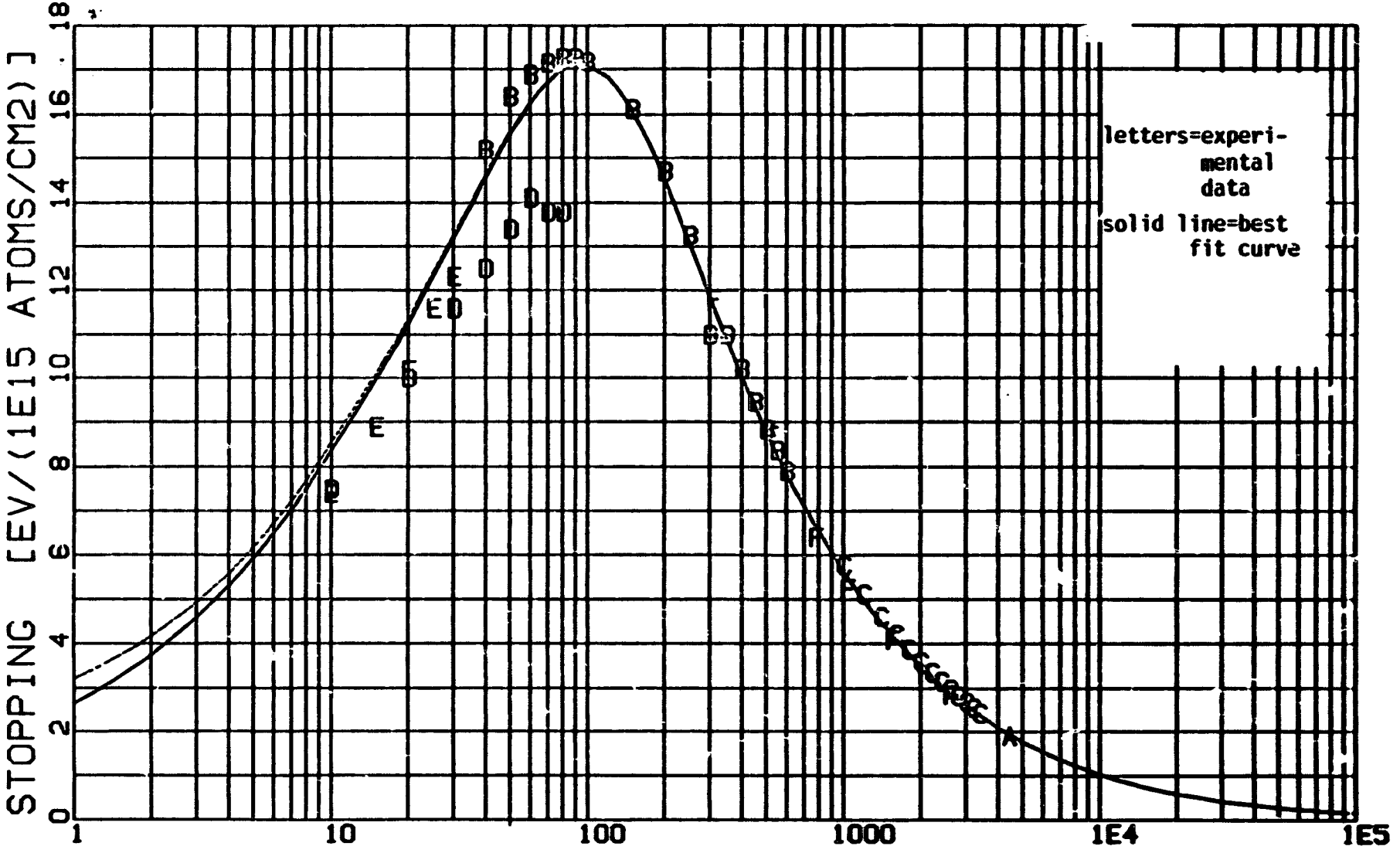

62

SOLID CURVE IS BEST FIT
DASHED CURVE [LOW ENERGIES] IS SOLID LINE PLUS L.S.S. NUCLEAR STOPPING

FIG 9. OXYGEN STOPPING POWER

O[8]

silicon dioxide, Braggs activity rule for compounds can be used to first approximation [26]

$$\frac{dE}{dx} = \sum_j \epsilon_j \left.\frac{dE}{dx}\right|_j$$

where ϵ_j is the weight fraction of element j in the compound.

Thus

Silicon dioxide = (.533) 15 keV/micron + (.466) 25.8 keV/micron

= 20.0 keV/micron

The materials of interest all have similar stopping powers ranging from 20 to 30 keV/micron.

The MOS devices fabricated in the NASA/MSFC laboratory have a cross section drawn to scale as shown in Figure 10 [27]. Notice that the entire active device structure is in the top 2 or 3 microns of the device structure. If the rate of energy loss for an incoming 2 MeV particle is only 20 - 30 keV/micron, it is a reasonable approximation to assume 2 MeV particles suffer a negligible energy loss and thus dE/dx is constant as a particle passes through the active device region. This simplifies the following calculation.

Let n equal proton fluence (protons/cm^2) that impinge on an area, A, of silicon surface. Assume a depth, x, small enough so that the above approximation is valid, and now it is possible to compute the energy deposited in the volume, V = Ax, of silicon

$$\text{Energy deposited} = n\left(\frac{\text{protons}}{cm^2}\right) A(cm^2) \left(\frac{25 \text{ keV}}{10^{-4} \text{ cm-protons}}\right) x \text{ (cm)}$$

$$= 2.5 \times 10^5 \text{ nA x keV}$$

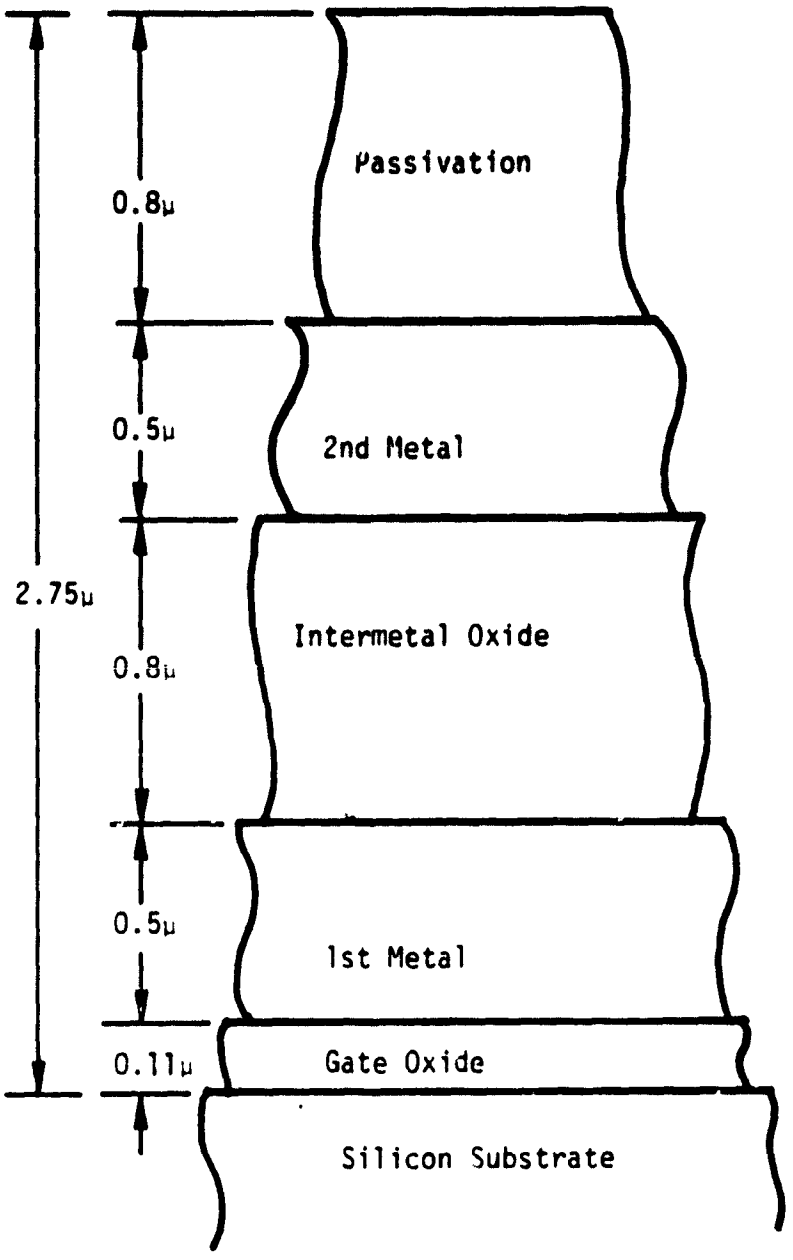

μ = micron

Figure 10. Cross-Section of NASA/HSFC C-015 MOS Device

$$\text{Dose (Rads Silicon)} = \frac{\text{Energy deposited}}{\text{mass}}$$

Assuming the density of silicon = $2.4 g/cm^3$

$$\text{Dose (Rads Silicon)} = (1.67 \times 10^{-6}) \times n(\text{protons}/cm^2)$$

or

$$n(\text{protons}/cm^2) = (6.0 \times 10^{5}) \times \text{Dose (Rads Silicon)}$$

These conversions can be employed to relate proton irradiation exposure in protons/cm^2 to absorbed radiation dosage in rads silicon.

IV. SIMULATION OF THE SPACE RADIATION ENVIRONMENT

The radiation environment of space is very complex, as described in Section II. It varies substantially with position, time, and in addition, there is a wide spectrum of particle energies present. To simulate all those conditions in the laboratory would be impossible, and thus simplifying assumptions based on sound engineering judgment are called for.

Referring again to Section II, it can be seen that the cosmic radiation, although high in energy, is of such low flux as to relegate it to a position of lesser importance. Electron and proton damage are the principle sources to be dealt with in space.

The Figures of Section II show that within the Van Allen belts the higher energy electron flux (Ee > 1.6 MeV) is at a relatively low level of about $10^4/cm^2$-sec maximum, and the higher electron flux occurs at low energies; these electrons are fairly easily shielded. The proton flux, on the other hand, is intense, and of high energy, requiring much more shielding to achieve the same equivalent radiation of flux level. Thus it becomes apparent that proton radiation is the limiting radiation factor in spacecraft design.

This conclusion has been supported by other researchers. For example, a study of the radiation belts by the Explorer 51 satellite revealed that the radiation dosage in rads is dominated by proton damage for an aluminum shield thickness of anything over about 50 mils thickness. The total dosage obtained during one year in orbit as a function of aluminum shield

thickness is shown in Figure 11 [28]. A similar result was obtained on Explorer 55, which shows in Figure 12 the total radiation dosage obtained using various thicknesses of aluminum shields after 139 days in orbit [29]. Again there is a strong domination of proton damage over most of the curve.

Proton damage has been shown to be the radiation source to the reckoned with in space. It is interesting, therefore that most radiation effects on MOS semiconductor studies use gamma irradiation as the source. The assumption implicity made in these studies is that the dominant degradation mechanism is ionization damage, which can be imparted by either gamma irradiation or protons. This is probably a valid assumption in most cases, and it is true in these cases that it makes little difference whether the rad is delivered by a photon or a proton. There is a physical difference, however, in that the proton is also capable of doing displacement damage in the silicon crystal, and this is to be expected in space. If displacement damage effects become significant for a particular device structure, it would never be detected using a Cobalt 60 gamma radiation source. In this work, however, proton irradiation was selected, and this is thought to more accurately represent the environment seen by the electronics of a spacecraft.

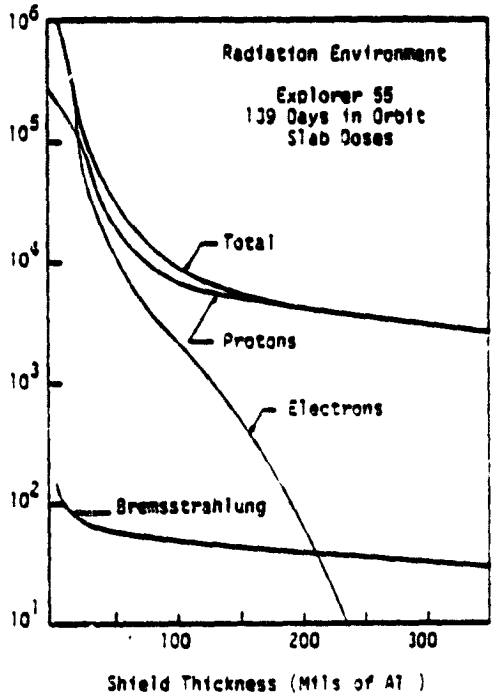

Figure 11. Contribution of Electrons, Protons, and Bremsstrahlung to the Total Dose-depth Curve for Explorer 55 Satellite

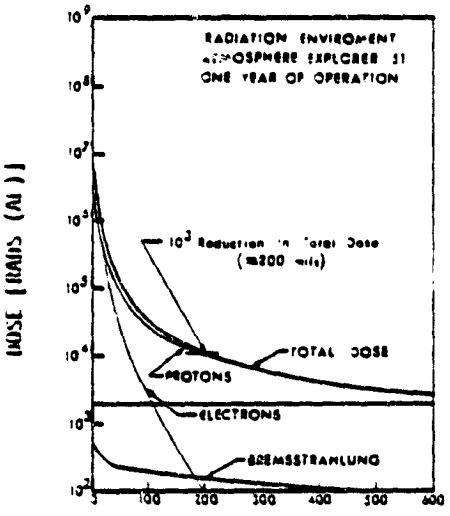

Figure 12. Ionization Dose versus Shielding Thickness of Aluminum for Radiation Environment of the Atmosphere Explorer 51 Satellite.

V. DESCRIPTION OF EXPERIMENT

A. Irradiation Facility and Fixture

The proton irradiations for the experimental phase of this project were done at the Leach Nuclear Science Center on the campus of Auburn University. This facility houses a 3-million volt Dynamitron particle accelerator (shown in Figure 13) configured for proton acceleration. The target chamber is shown in Figure 14, and is large enough to house a rotatable disk shown in Figure 15. This disk was a special fixture designed for holding up to 9 CMOS devices under proper bias, and allowing each one to be successively rotated under the proton beam for irradiation without breaking vacuum.

The three types of CMOS inverters characterized were the RCA 4007 A, bulk silicon device, the RCA TCS-071 SOS device, and the MSFC C-015, bulk silicon device. For each of these device types, three bias schemes were used during irradiation, input high, input low and no bias, as shown in Figures 16 - 18.

The effect of gate bias on radiation sensitivity has been alluded to earlier. The logic state (high or low) of the input determines the nature of the field seen by the gate oxide in both the n channel and p channel devices. As shown by Poch [30], the "on" device has gate field lines terminating in the channel and uniform from source to drain. The fields in the gate insulator of the "off" device are not uniform across the channel, and contain a strong lateral component. These fields are responsible for the positive charge migration and accumulation that

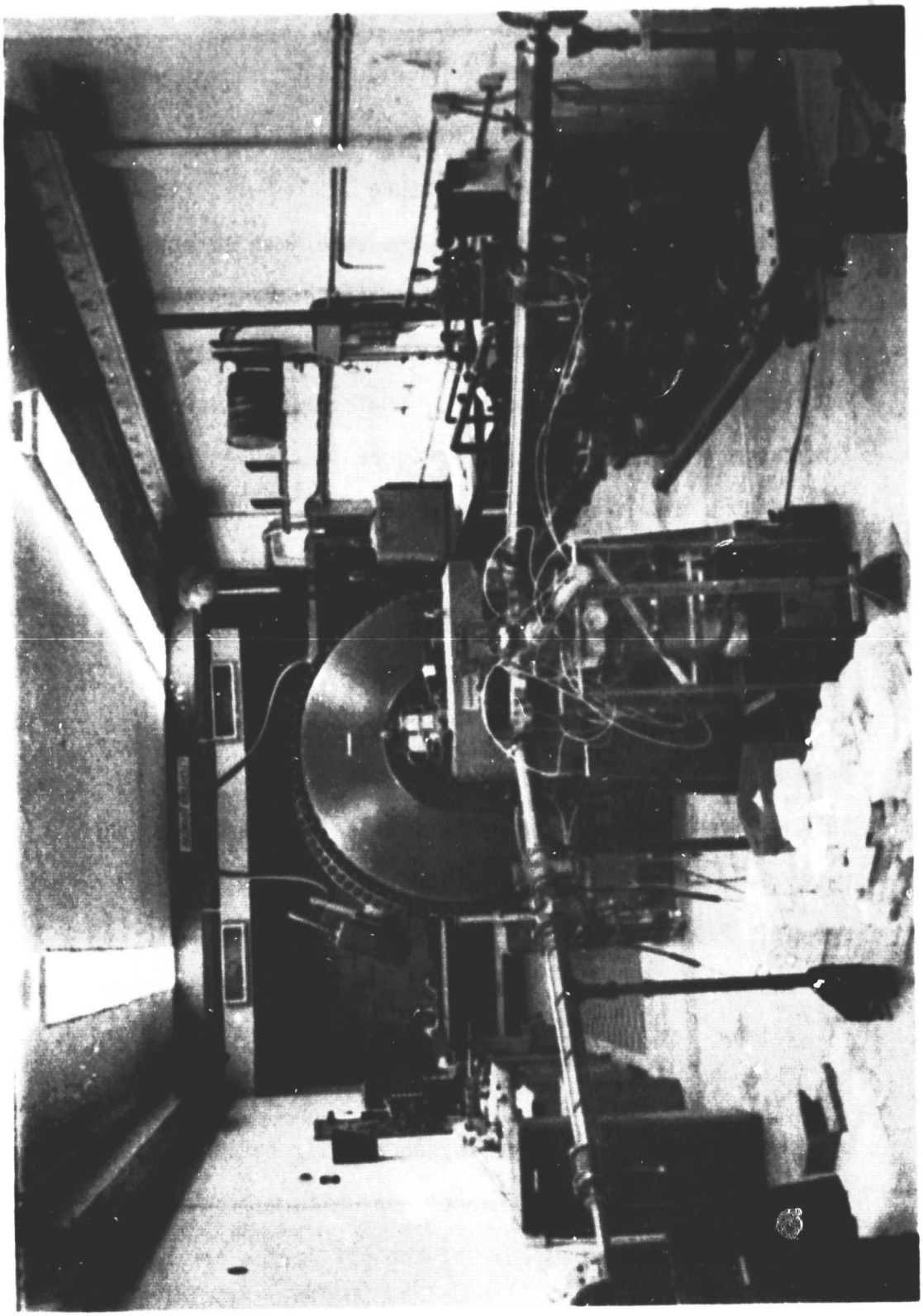

Figure 13. Dynamitron Proton Accelerator

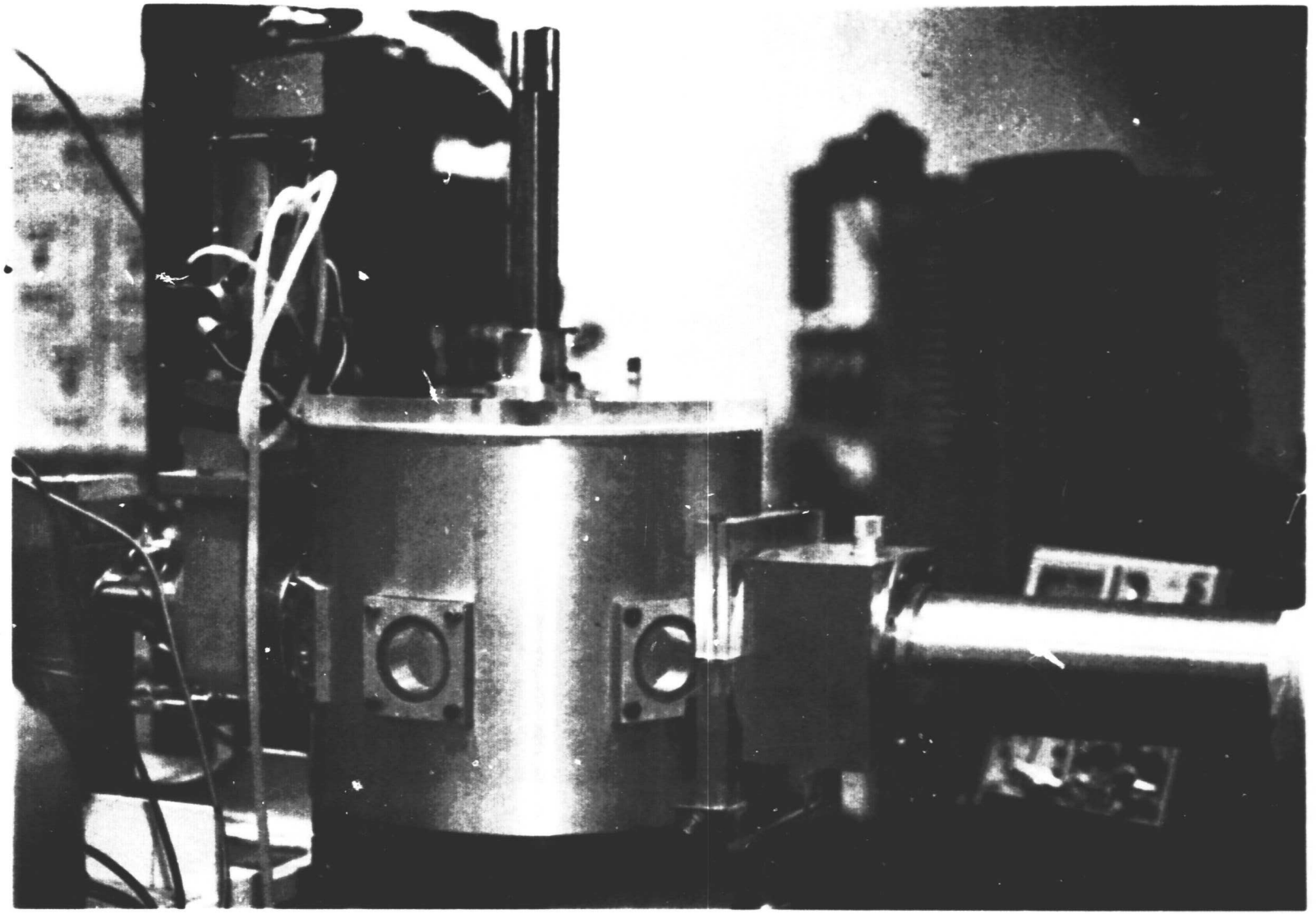

Figure 14. Target Chamber

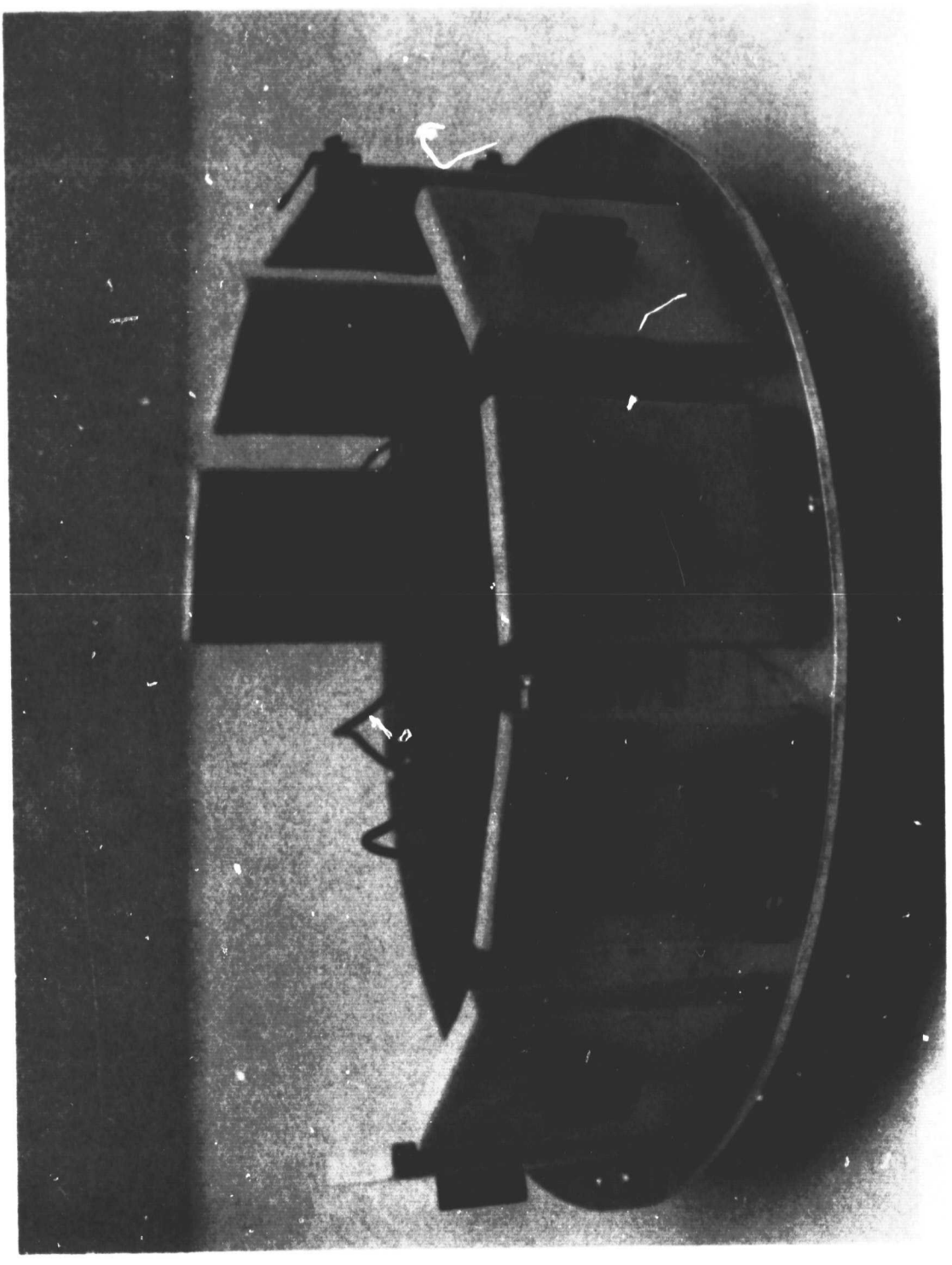

Figure 15. Device Irradiation Fixture

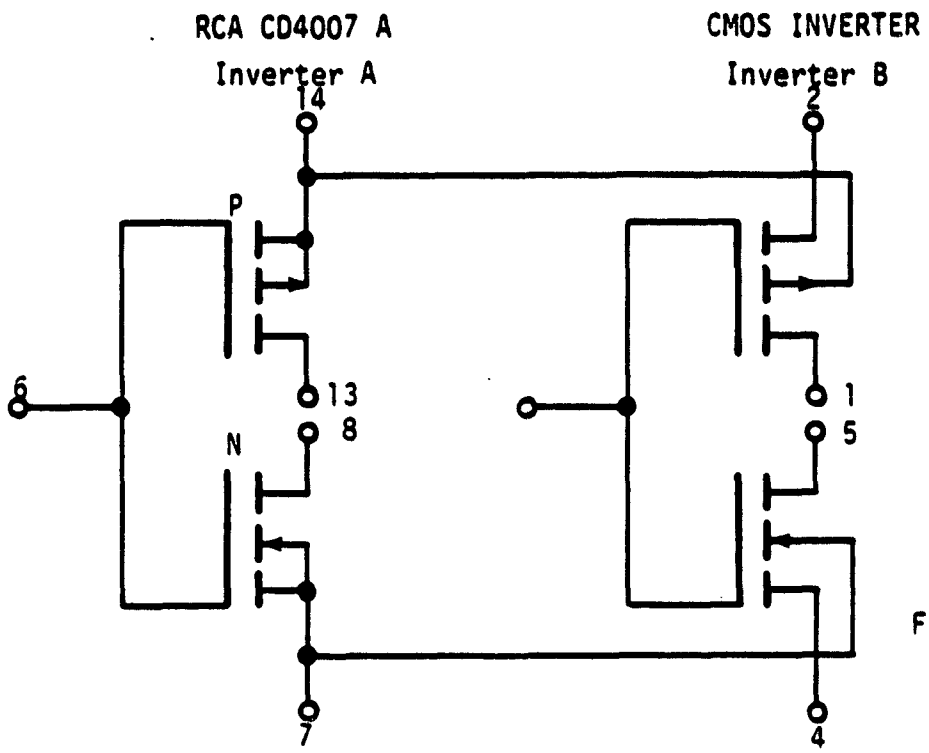

Figure 16. RCA CD4007 Inverter

Bias Scheme

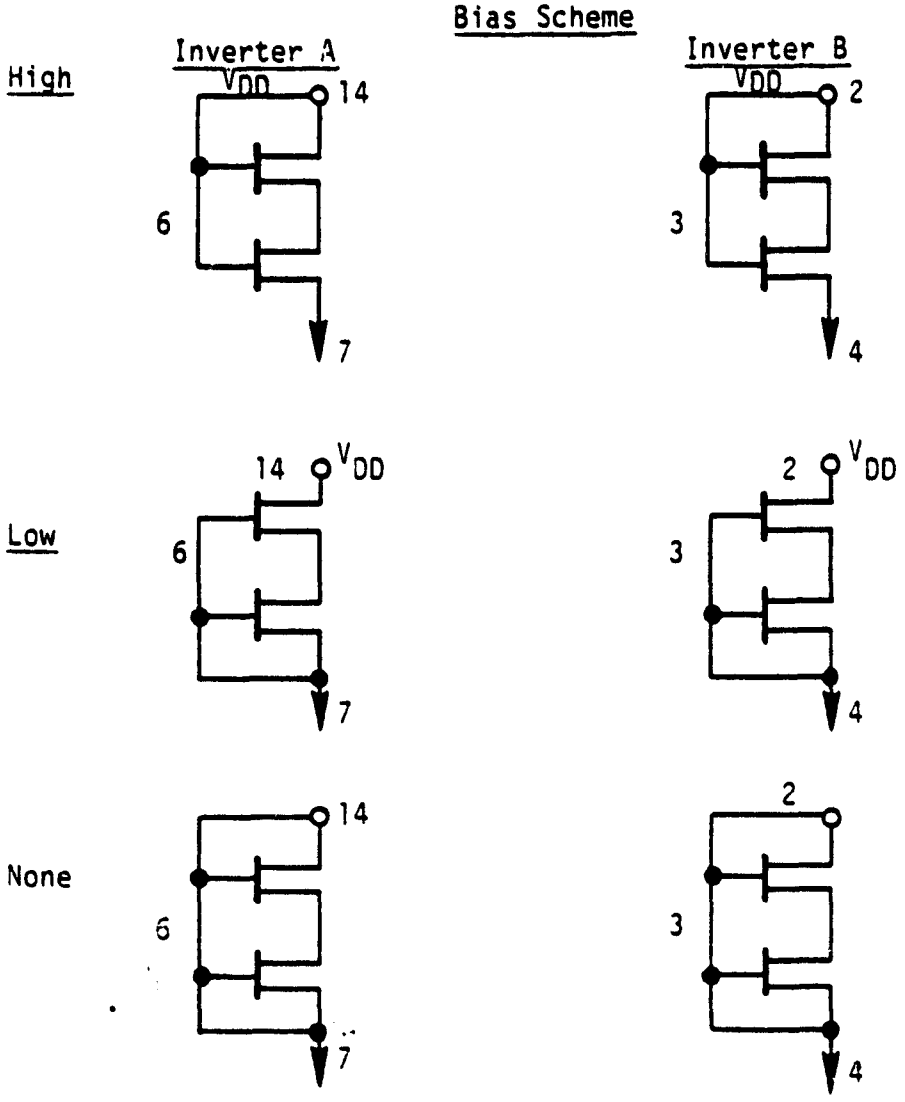

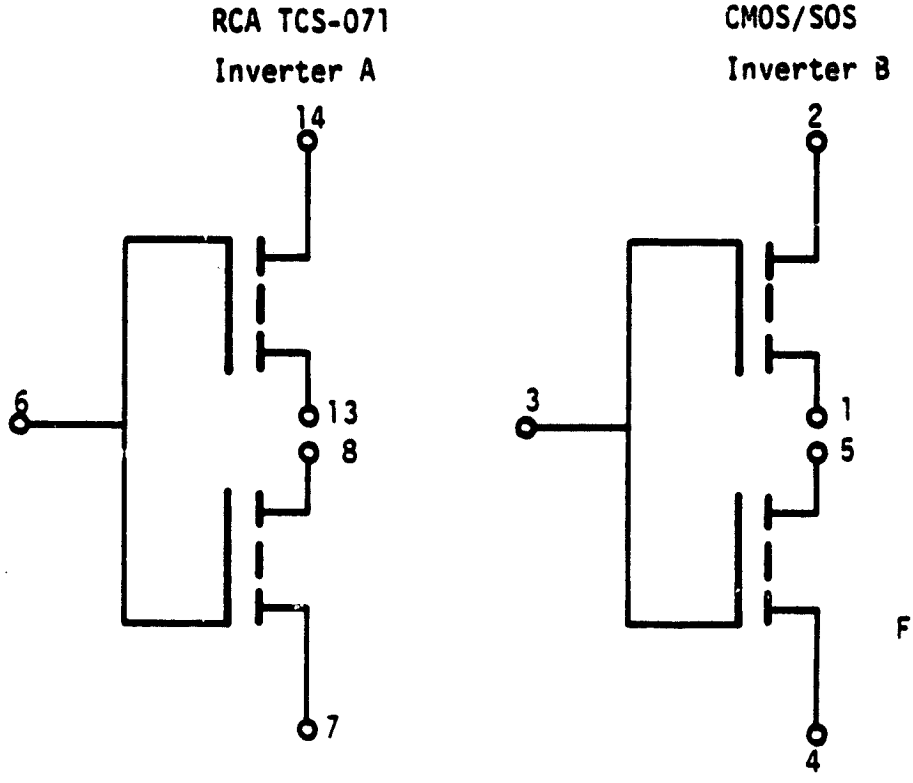

Figure 17. RCA TCS-071 Inverter

Bias Scheme

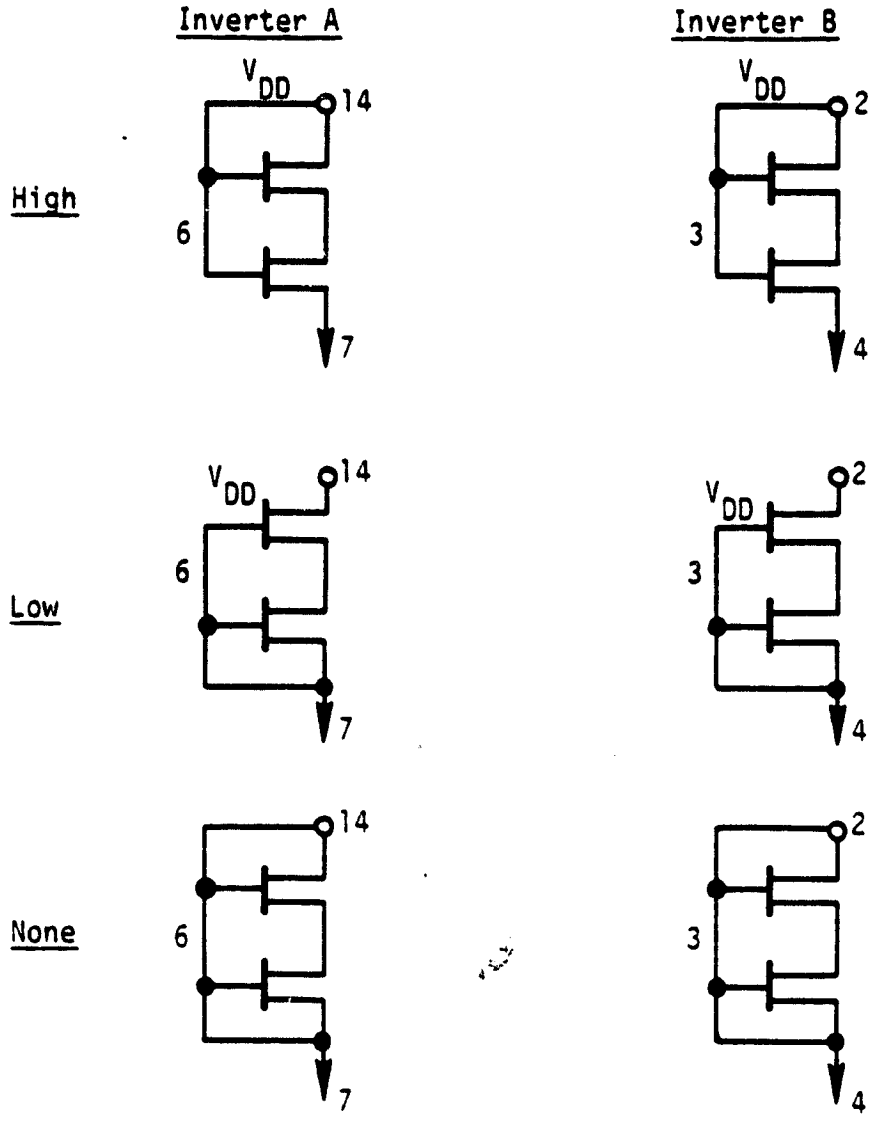

MSFC C-015
bulk silicon substrate

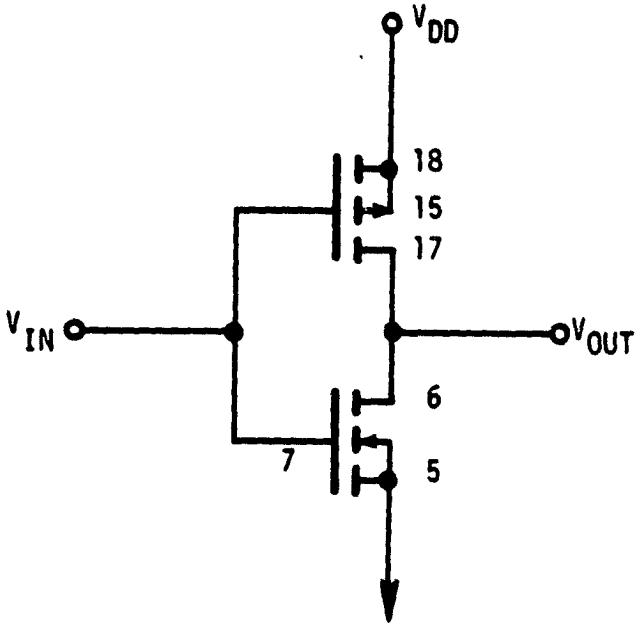

Figure 18 NASA/MSFC C-015
Inverter

Bias Scheme

I. bias high

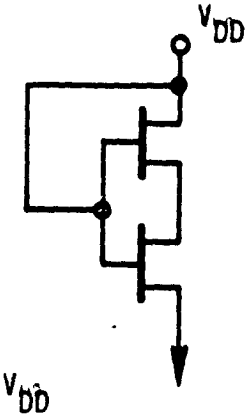

II. bias low

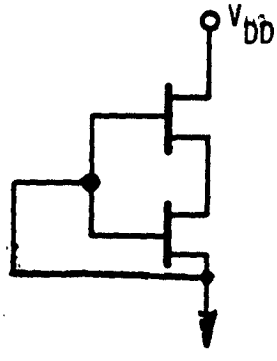

III. unbias

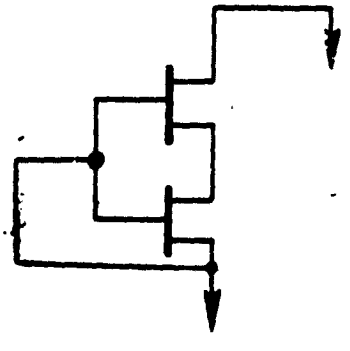

causes the threshold voltage shifts; thus the resulting damage would be expected to depend on the nature of these bias fields. The exact nature of this dependence is difficult to predict and remains a subject of continued study and interest. The following general observations, however, can be made. For positive gate bias, threshold shifts are larger, indicating an increased positive charge build-up; the opposite is true for negative gate bias.

All irradiations were done at a proton energy of 2 MeV, and at or near minimum beam current. This was to ensure that thermal heating of the device would be minimized, and not a factor in the resulting device degradation.

B. Characterization Fixture and Method

The devices were characterized before irradiation and after each succeeding radiation exposure. The device characterization fixture provided the capability for sweeping the input voltage from zero to ten volts, and monitoring the supply current and output voltage. The schematic of this system is shown in Figure 19. These measurements enabled plots to be made of the square root of drain current versus input voltage (from this type plot threshold voltages can be extracted), and the voltage transfer curves.

A typical example of this type graph is illustrated in Figure 20. On this plot the extraction of the n channel threshold voltage, p channel threshold voltage, and peak current are demonstrated.

Test Circuit

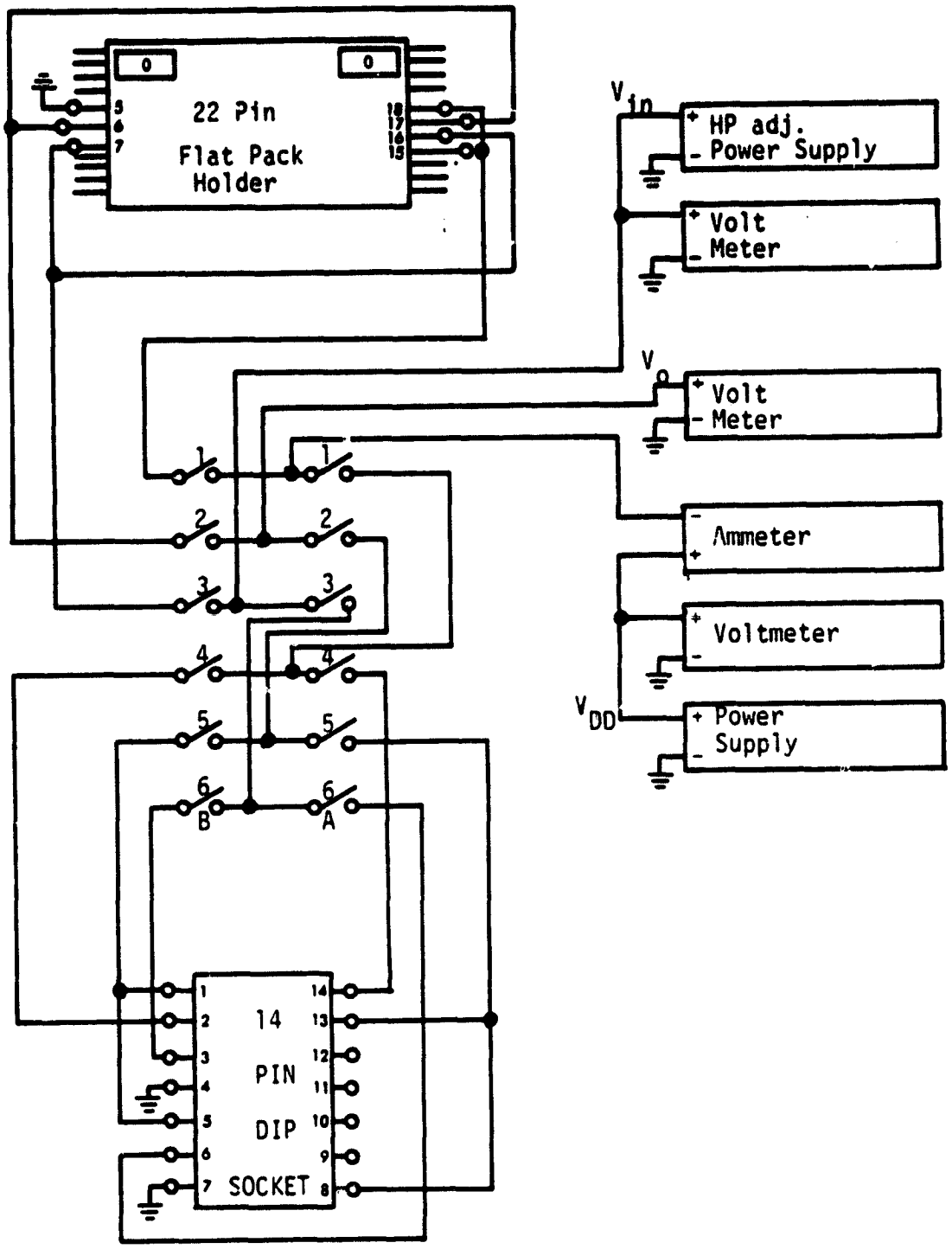

Figure 19. Inverter Characterization Fixture

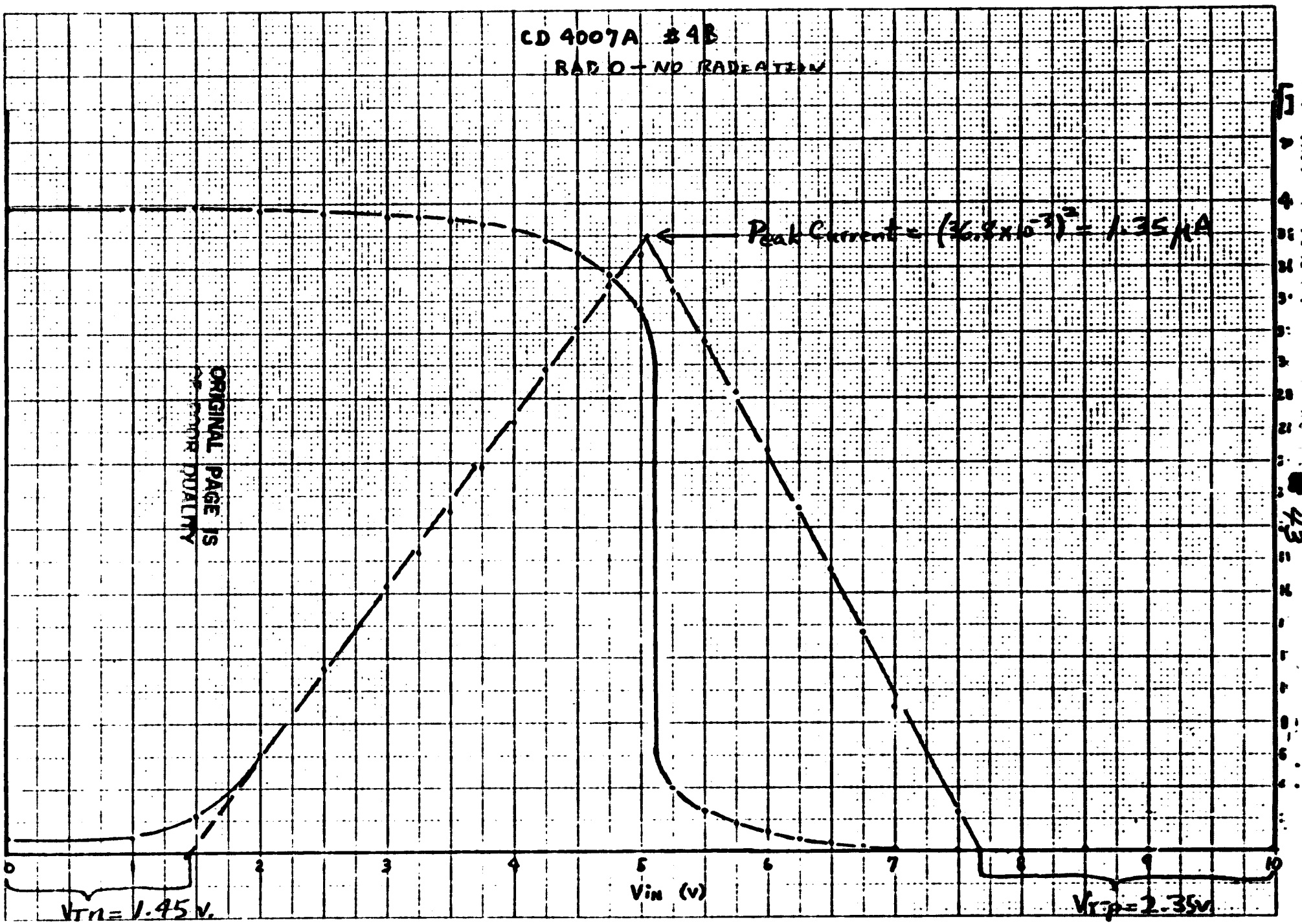

FIG 20. SAMPLE TRANSFER AND CURRENT DATA.

VI. EXPERIMENTAL RESULTS

Using the experimental apparatus and procedures described in the previous section, data was recorded before the first radiation exposure and after each irradiation. As previously stated, this data consisted of supply current, and output voltage for each inverter; the plots of this data are given in the Appendix. From these curves both n and p channel threshold voltages, as well as peak supply current were extracted.

Figure 21 summarizes the threshold voltage data for the RCA CA4007 bulk silicon devices. Two inverters (labeled A and B) on each of three chips are characterized in this Figure. Notice the p channel device threshold voltage shows an average increase in magnitude of 15% at a radiation dose of 5×10^5 RADS; the n-channel device threshold voltage decreases an average of 24% for the same exposure. The effects of low, high and no gate bias during irradiation do not seem significant in these results. An interesting observation is that the B inverter on each chip shows a relatively large shift in p channel threshold voltage (average of 0.52 volts) compared with the A inverter (average of 0.23 volts). The n-channel threshold shifts are comparable on both A and B inverters. The overall average change in threshold voltage resulting from 5×10^5 RADS proton irradiation is 0.38 volts for the p-channel device and 0.31 volts for the n-channel device. The value of the peak current remains approximately constant throughout the radiation exposure, indicating the n and p channel thresholds are shifting approximately at the same rate. If the p-channel threshold shifts faster than the n-channel threshold, the

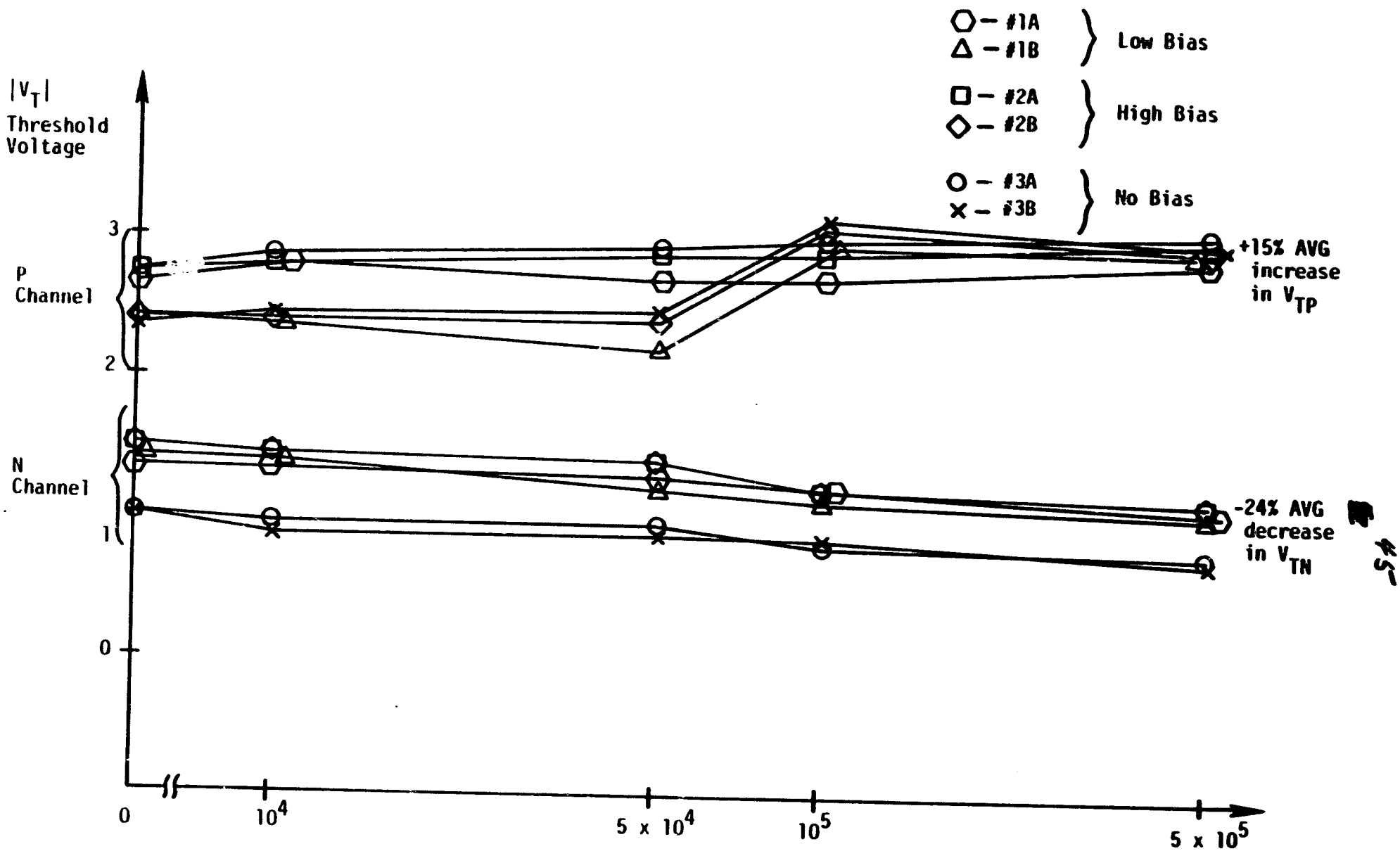

Figure 21. CD4007A - RCA Bulk Silicon

peak current will increase with radiation exposure, assuming the transconductance does not change appreciably. The converse of this is also true.

Figure 22 summarizes the threshold voltage data obtained from measurements on RCA TCS-071 silicon or sapphire devices. Again two inverters on each of three chips were characterized. The observed increase in magnitude of the p-channel threshold voltage resulting from a radiation dose of 5×10^5 RADS is an average of 9%; the corresponding decrease in n-channel threshold voltage is seen to be 17%. The RCA silicon-on-sapphire technology appears to offer an improvement in proton radiation hardness over the RCA bulk silicon technology by a factor of about 1.5. The average change in n-channel threshold voltage for these devices at 5×10^5 RADS is 0.20 volts, and for the p-channel device, 0.11 volts. The peak supply current for these SOS inverters was approximately constant during the radiation exposure, but about 3 times the magnitude of that for the CD4007. Again, the bias condition during irradiation appeared to have negligible effect.

The C-015 devices fabricated by NASA/MSFC using a bulk silicon process showed less radiation hardness compared to the RCA devices, but this was not unexpected, as these devices were never designed with the intention of utilization in a radiation environment. Two C-015 chips were irradiated and characterized as shown in Figure 23. The p-channel devices at 5×10^5 RADS showed an average increase in magnitude of threshold voltage of 296%; the n-channel threshold decreased by 78% at the same radiation dosage. The average shift in n-channel threshold was 1.80 volts, and 4.15 volts for the p-channel device. Other researchers

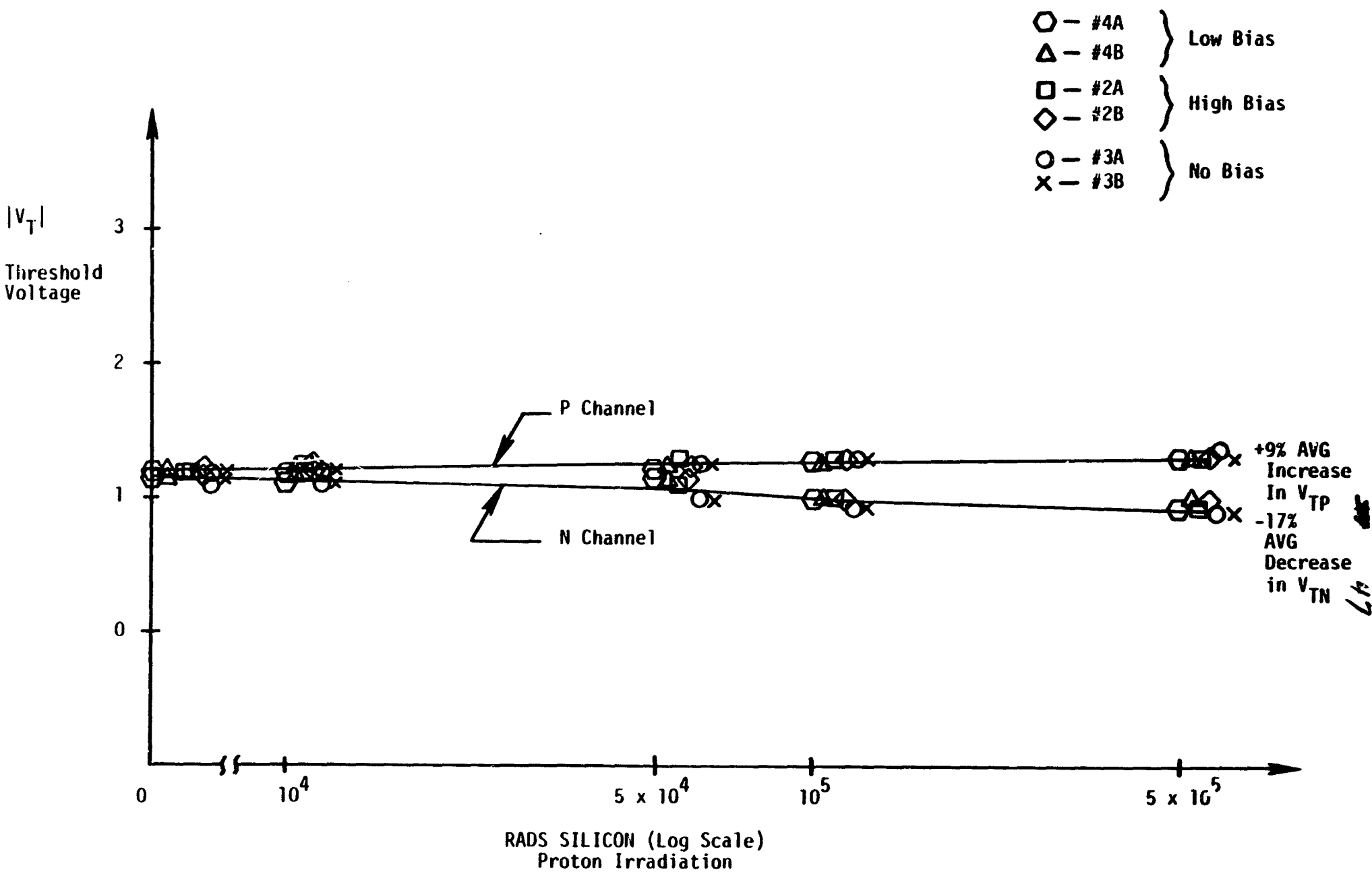

Figure 22. TCS-071-RCA-S05

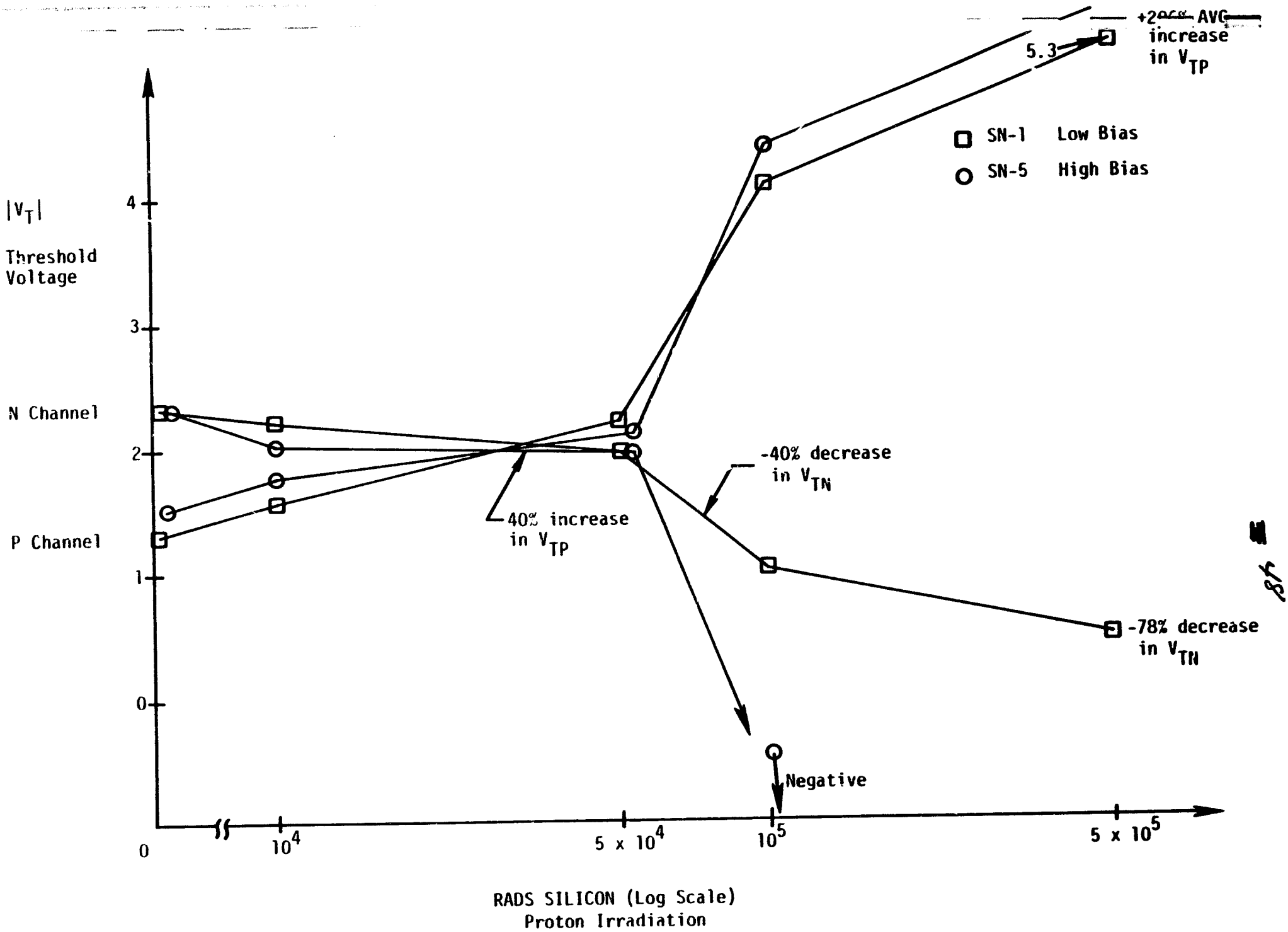

Figure 23. C-105-MSFC-Bulk Silicon

have used the criteria that a shift in threshold voltage of 40% represents failure of the circuit. Using this guideline, these C-015 circuits failed at a total radiation dose of about 5×10^4 RADS.

The average n and p channel threshold voltage shifts for each device type at 5×10^5 RADS are summarized in Figure 24. The peak supply current is plotted as a function of radiation dose for a number of inverters in Figure 25; the negative slope of the curve for the C-015 indicates the p-channel threshold voltage is changing more rapidly with radiation than is the n-channel threshold.

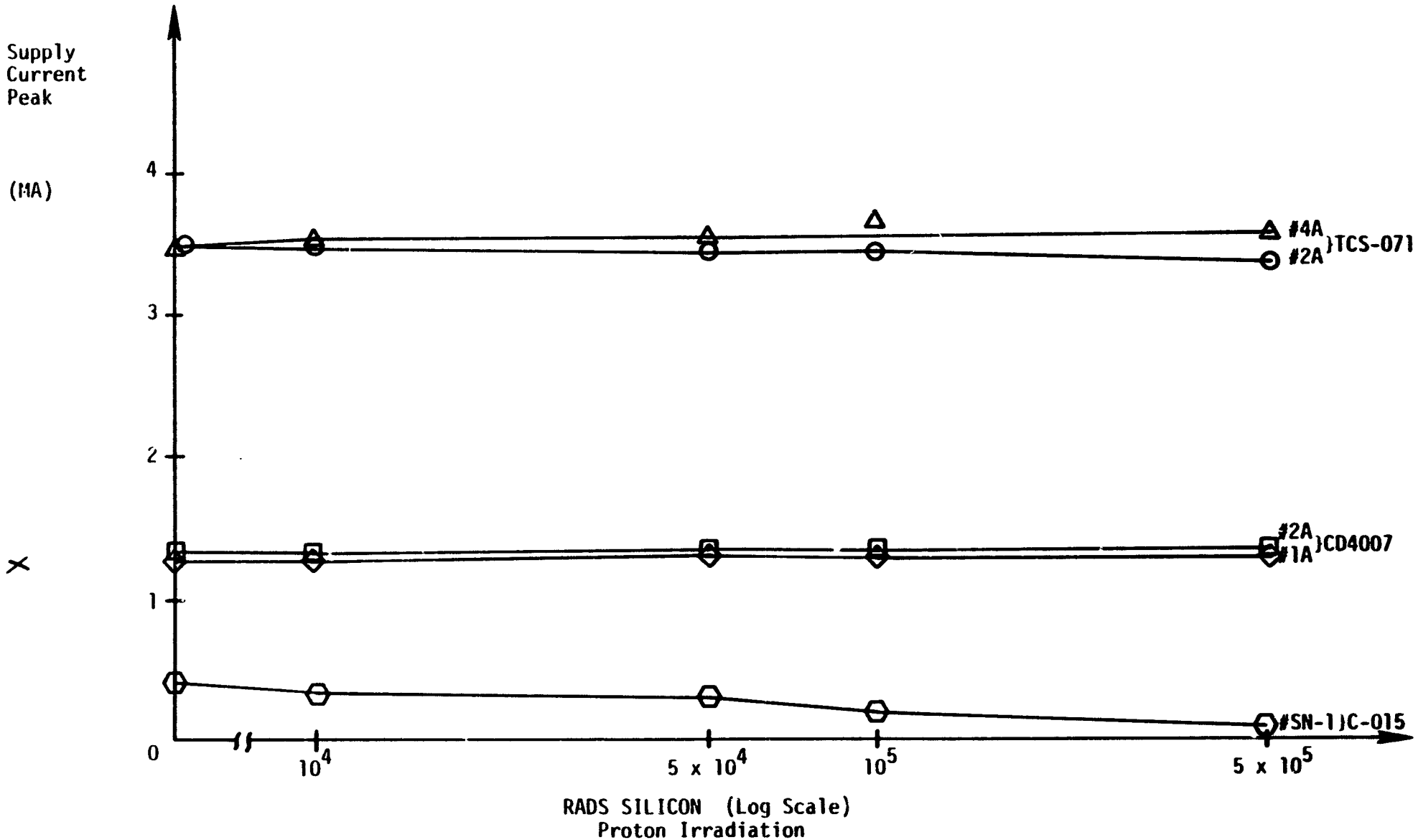

Figure 25. Peak Supply Current vs Radiation Dose

	ΔV_{TN}	ΔV_{TP}
CD4007	- .31	+ .38
TCS-071	- .20	+ .11
C-015	-1.80	+4.15

Figure 24. Average Threshold Voltage Change For 5×10^5 RADS Proton Radiation

VII. CONCLUSIONS AND RECOMMENDATIONS

The various radiation environments of space were examined, including the Van Allen Belts, the solar wind, cosmic radiation of deep space, and the trapped radiation of Jupiter. It was shown that proton radiation is the dominant type of radiation to be dealt with in space (assuming minimal shielding to reduce electron flux), and the limiting radiation factor in spacecraft design.

The Dynamitron proton accelerator at Auburn University was used to produce a 2 MeV proton radiation environment. Three types of CMOS inverters were characterized after irradiation,the RCA CD4007, RCA TCS 071, and NASA/MSFC C-015.

The RCA TCS-071 SOS technology offered about a factor of 1.5 improvement in radiation resistance to proton damage over the RCA bulk silicon process used for the CD4007. At a proton exposure dose of 5×10^5 RADS the average threshold voltage shifts for the n and p channel devices for the CD4007 were 24% and 15% respectively; 17% and 9% for the TCS-071. These threshold shifts were not enough to render the inverter inoperative and extrapolation would indicate both these devices would operate well into the 10^6 RAD range.

The NASA C-015 device, however, showed substantially less radiation tolerance. The same exposure dose of 5×10^5 RADS yielded an average p channel threshold voltage shift of 296%. These inverters were judged inoperative at a radiation dose of about 5×10^4 RADS. Even with 100 mils of aluminum shielding, this represents the proton dose that would

have been received by the electronics in the Explorer 51 satellite after only one year. Clearly, the NASA/MSFC C-015 devices characterized are not adequately proton radiation resistant, and are not suited for prolonged space flight missions. It is recommended that an effort be undertaken to improve the rad-hardness of these devices. A study of the literature has revealed that certain processing changes can produce more radiation tolerant CMOS structures, such as

1) Making the gate oxide thin [31]
2) Cleanliness and contamination control [32]
3) Using dry oxide [31]
4) Chrome doping of oxide [33]
5) Control of high temperature processes [31]

as well as others.

The present NASA/MSFC process, as detailed in NASA Technical Memorandum 78188 entitled "The MSFC Complementary Metal Oxide Semiconductor Process Handbook," was evaluated for steps inconsistent with radiation hardness. The step considered a principle candidate for improving the radiation hardness of these devices was determined to be the gate oxidation.

As mentioned above, gate oxide thickness is a major contributor to radiation susceptibility. It has been shown (31) that the radiation degradation is proportional to the cube of the oxide thickness.

Therefore the following specific process modifications are proposed in an attempt to improve the rad hardness of the MSFC devices:

a) Under section G, number 4, decrease gate oxide thickness from 1100Å to 800Å. A value of 800Å is about the minimum thickness consistent with a 15 volt breakdown requirement.

b) The gate oxidation should be changed to one of the following two alternatives:

i) Grow oxide in dry oxygen at 1000°C in a tube cleaned in HCl.

or ii) Use existing oxidation process except lower temperature to 850°C.

It is recommended that confirmation of the value of these processing changes be determined by proton irradiation in the laboratory and device characterization.

The structure of CMOS devices designed for rad hardness should include guardrings. The circuit design of CMOS devices for rad hard applications is generally not different from that for normal applications.

APPENDIX I

In order to enhance the evaluation of the radiation tolerance of the NASA/MSFC devices additional data was taken. Nine additional C-015 integrated circuits were irradiated with protons and key device parameters measured. The change in the n-channel MOS device threshold voltage and p channel threshold voltage was evaluated and compared to the previous measurements (data shown in Figure 23). The change in n-channel threshold voltage versus radiation for these additional chips for the cases of no bias, low bias, and high bias conditions are shown in Figure I-A. Notice that the previous data indicated a decrease in n channel threshold voltage of 78% at 5×10^5 RADS whereas the average reduction in n channel threshold voltage for this new lot is minus 74% for the case of low bias. The change in threshold voltage for the case of no bias is minus 81% and for high bias minus 100%. These changes are very similar to those values obtained previously and shown in Figure 23.

The changes in p channel threshold voltage with radiation were measured on the same 9 C-015 chips and this data is shown in Figure I-B. For the case of low bias the p channel threshold voltage increased 227%; for the case of no bias the increase was 155%, and for the case of high bias positive 154%. Again these values are comparable to those shown in Figure 23.

The p channel devices showed leakage currents less than 0.1 microampere all the way through 5×10^5 RADS. The n channel devices however showed substantial leakage beginning at 10^5 RADS due to the threshold voltages nearing zero. These data for the 9 additional chips are shown in Figure I-C.

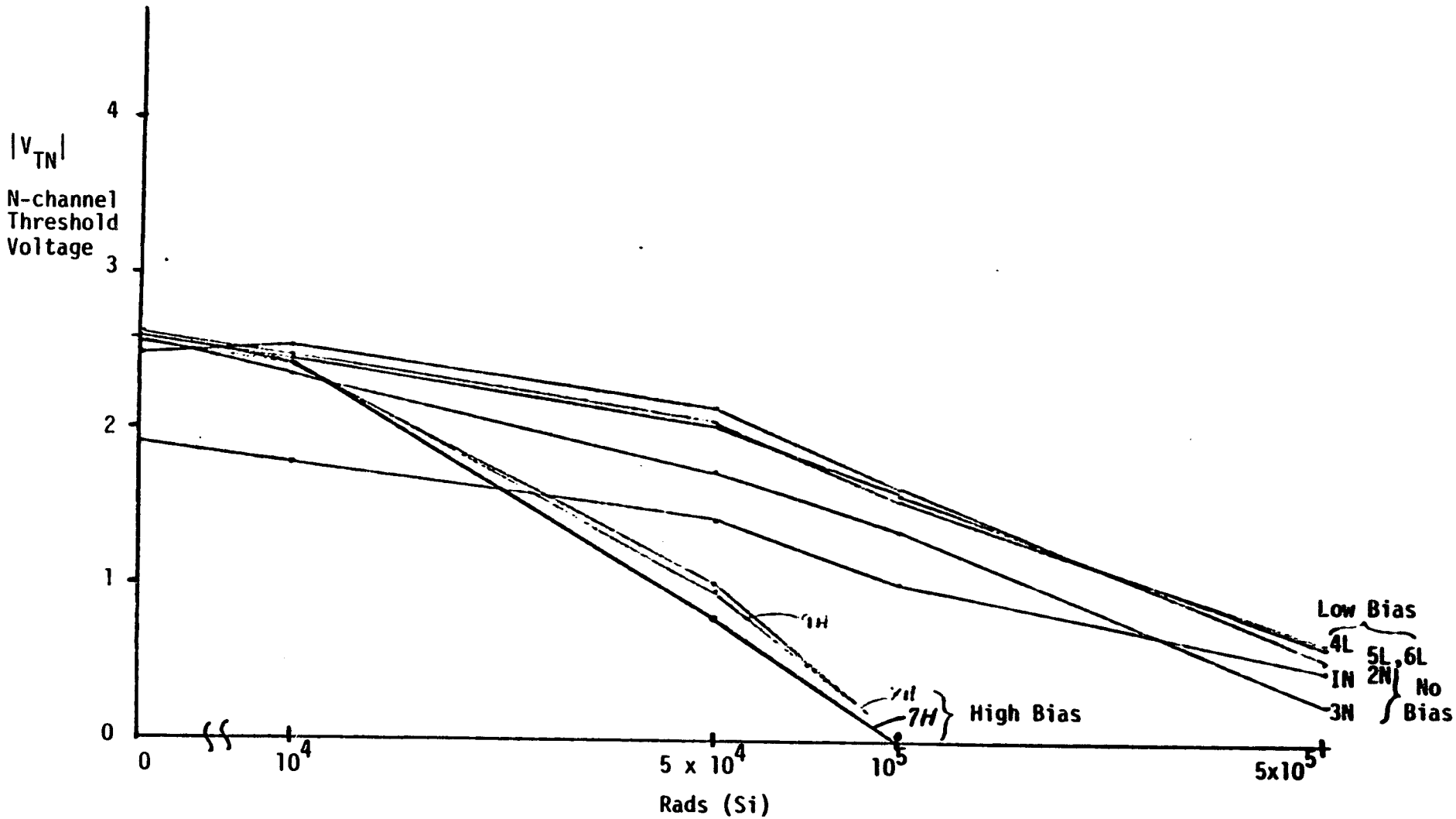

Figure I-A. Proton Irradiation Effects on C-015 n-channel Device Thresholds.

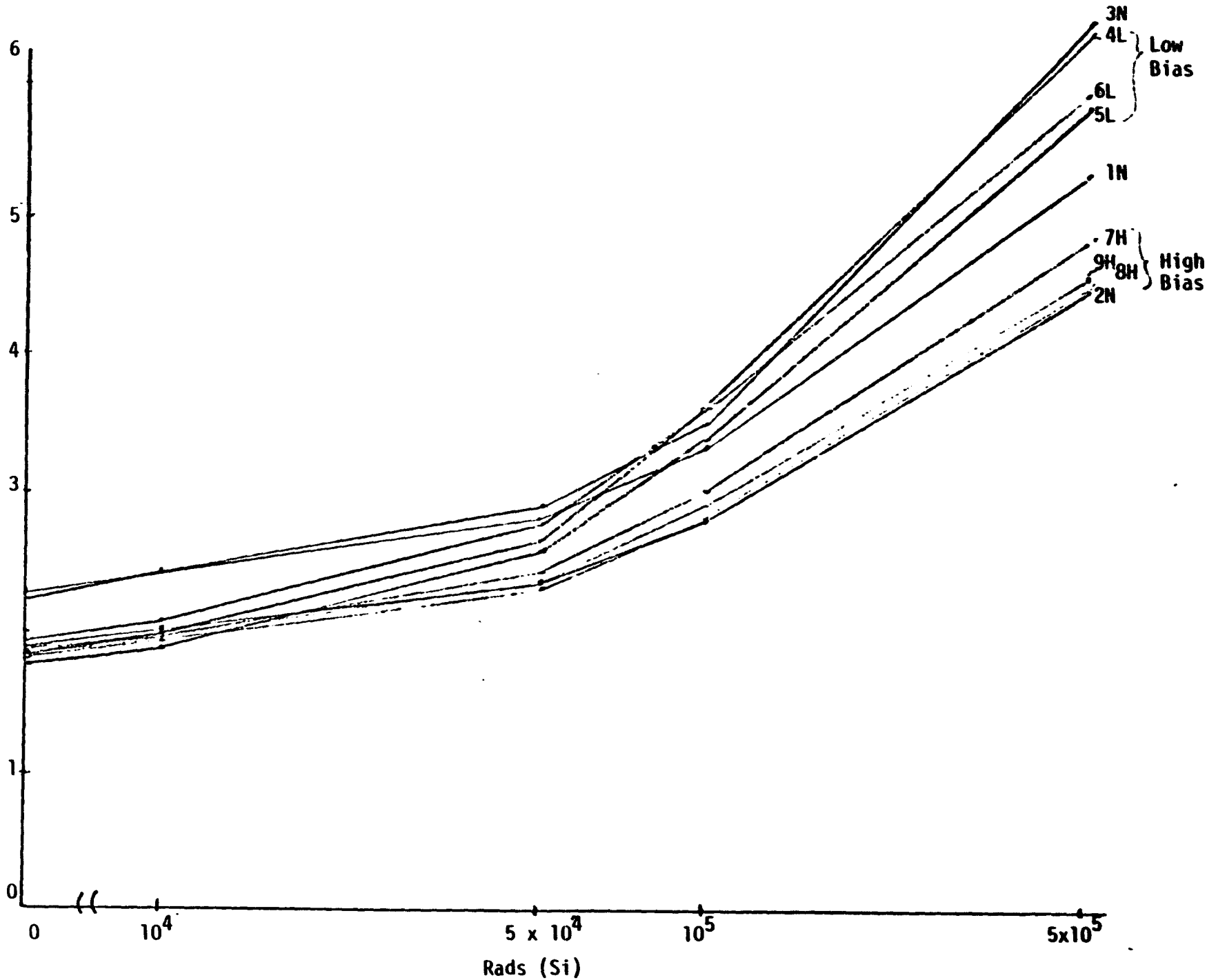

Figure I-B. Proton Irradiation Effects on C-015 p-Channel Device Thresholds.

	Device #	Radiation (RADS Si) 10^5	5×10^5
No Bias	1N	<.1μA	.5μA
	2N	<.1μA	.5μA
	3N	<.1μA	1.2μA
Low Bias	4L	<.1μA	.4μA
	5L	<.1μA	.8μA
	6L	<.1μA	.7μA
High Bias	7H	160μA	5400μA
	8H	89μA	3980μA
	9H	127μA	4290μA

N-CHANNEL LEAKAGE CURRENT VS RADIATION

Figure I-C

APPENDIX II

CD 4007A #2A
RAD-10⁴RADS Bias-11.4
I_{TP}=1.35 mA
V_{TP}=2.8
V_{TN}=1.45
V_{IN} (V)
I_D (mA)

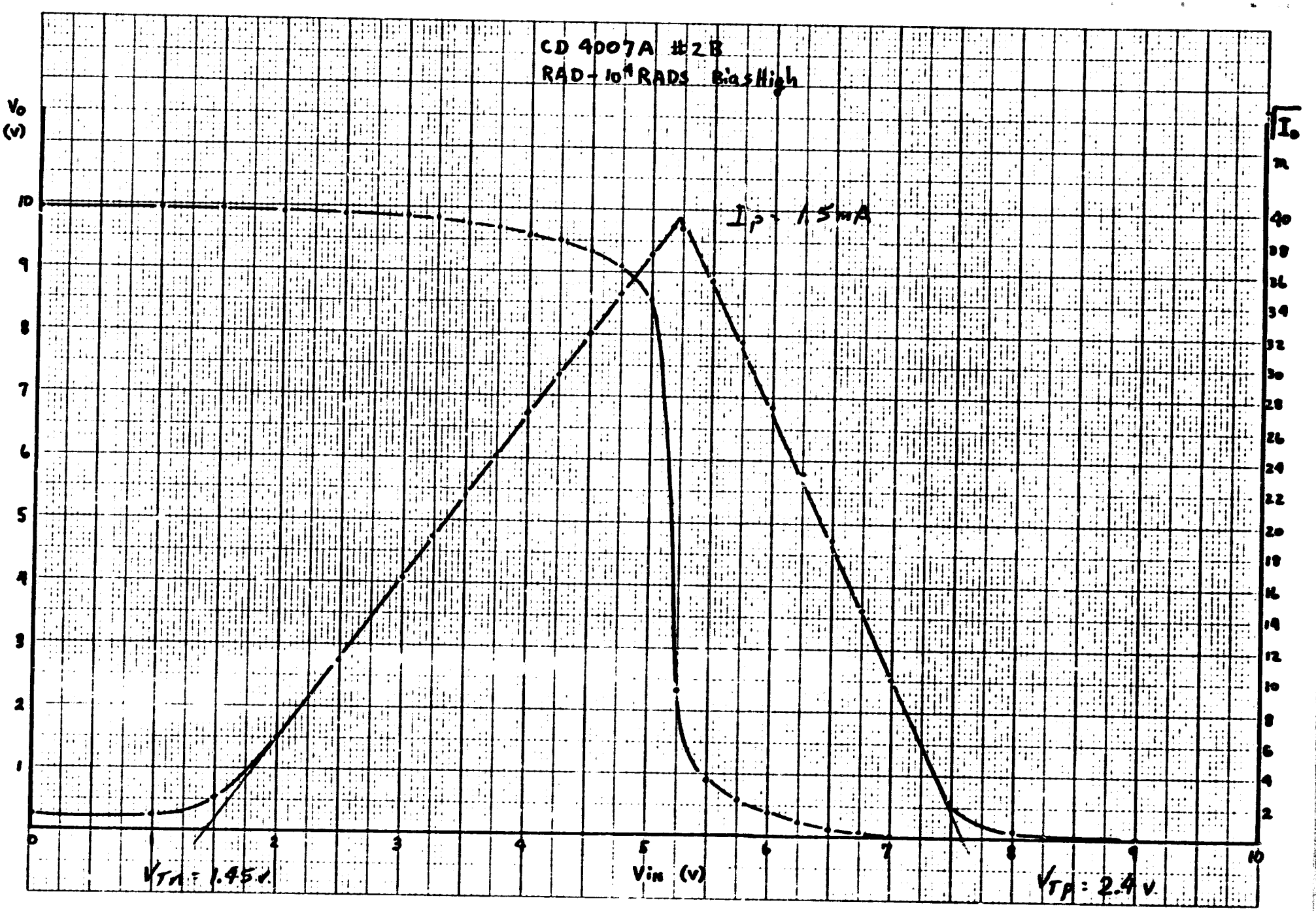
CD 4007A #2B
RAD - 10^4 RADS Bias High
V_o (v)
$\sqrt{I_o}$
$I_p = 1.5$ mA
$V_{TN} = 1.45$ v.
V_{in} (v)
$V_{TP} = 2.4$ v.

KEUFFEL & ESSER CO.
MADE IN U.S.A.
10 X 10 TO 7 INCH
46 1320

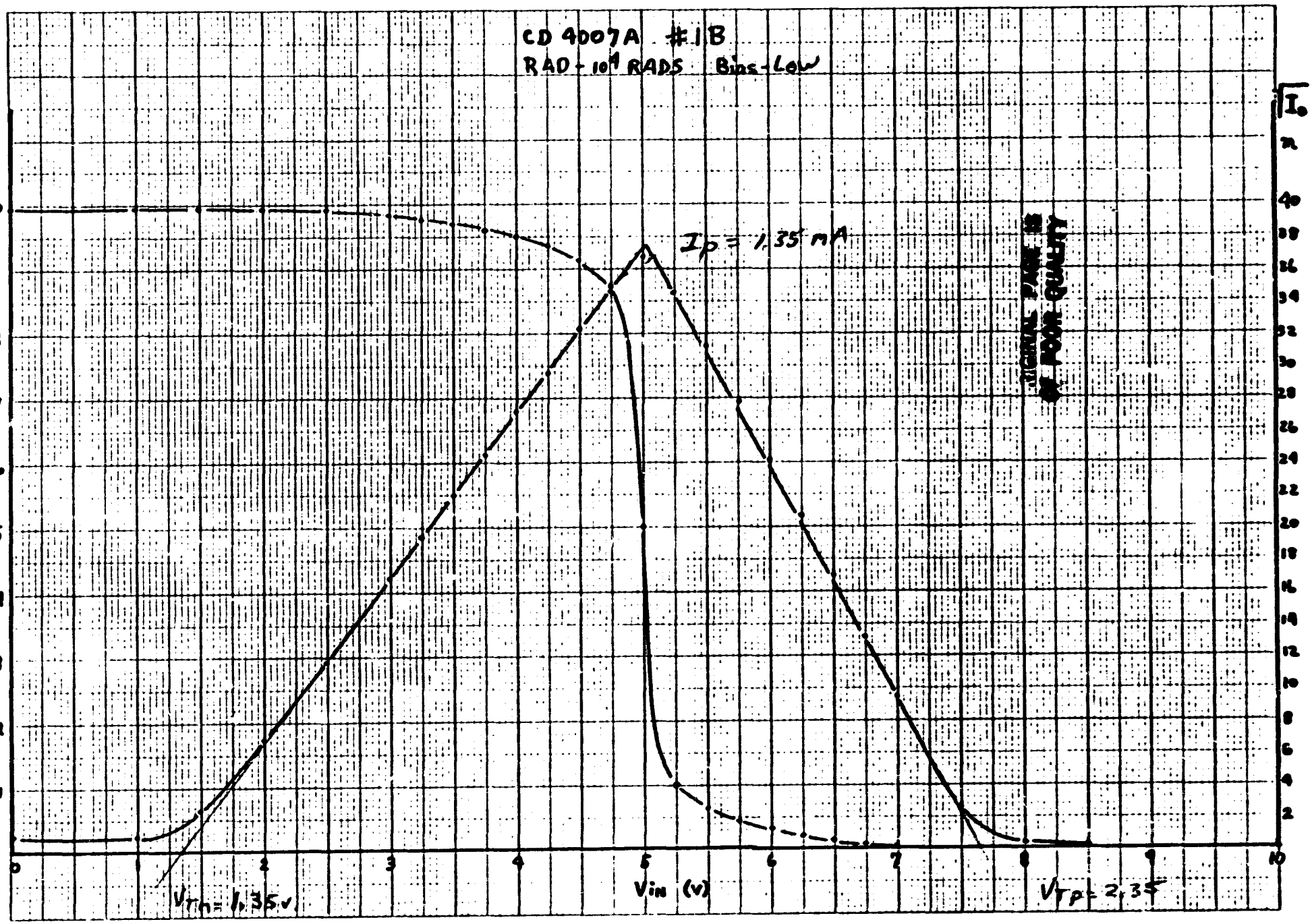

72

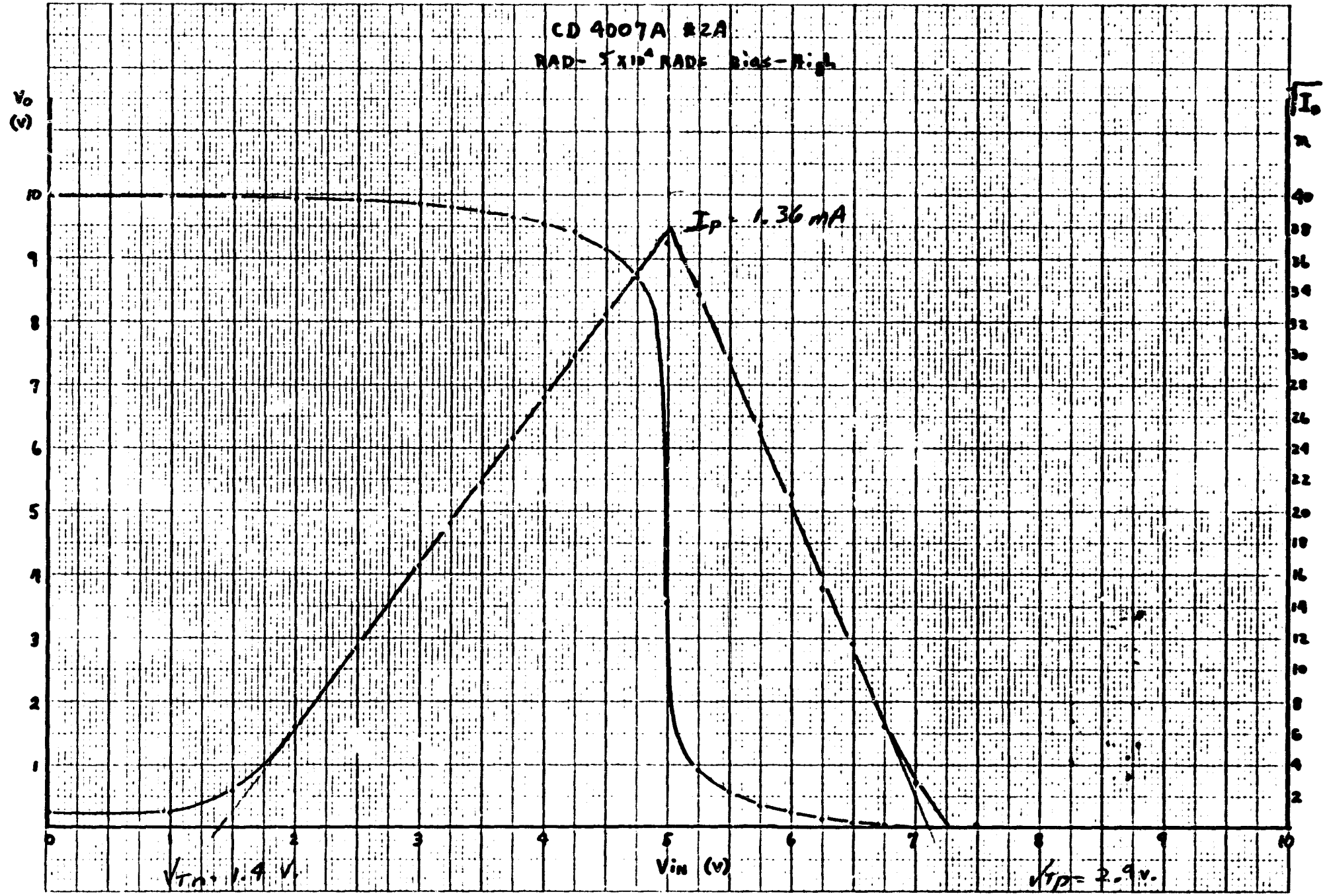
CD 4007A #2A
RAD- 5 X 10^4 RADS Bias - High
V_o (V)
I_o
I_p = 1.36 mA
V_{Tn} = 1.4 V
V_{in} (V)
V_{Tp} = -2.9 V.

73

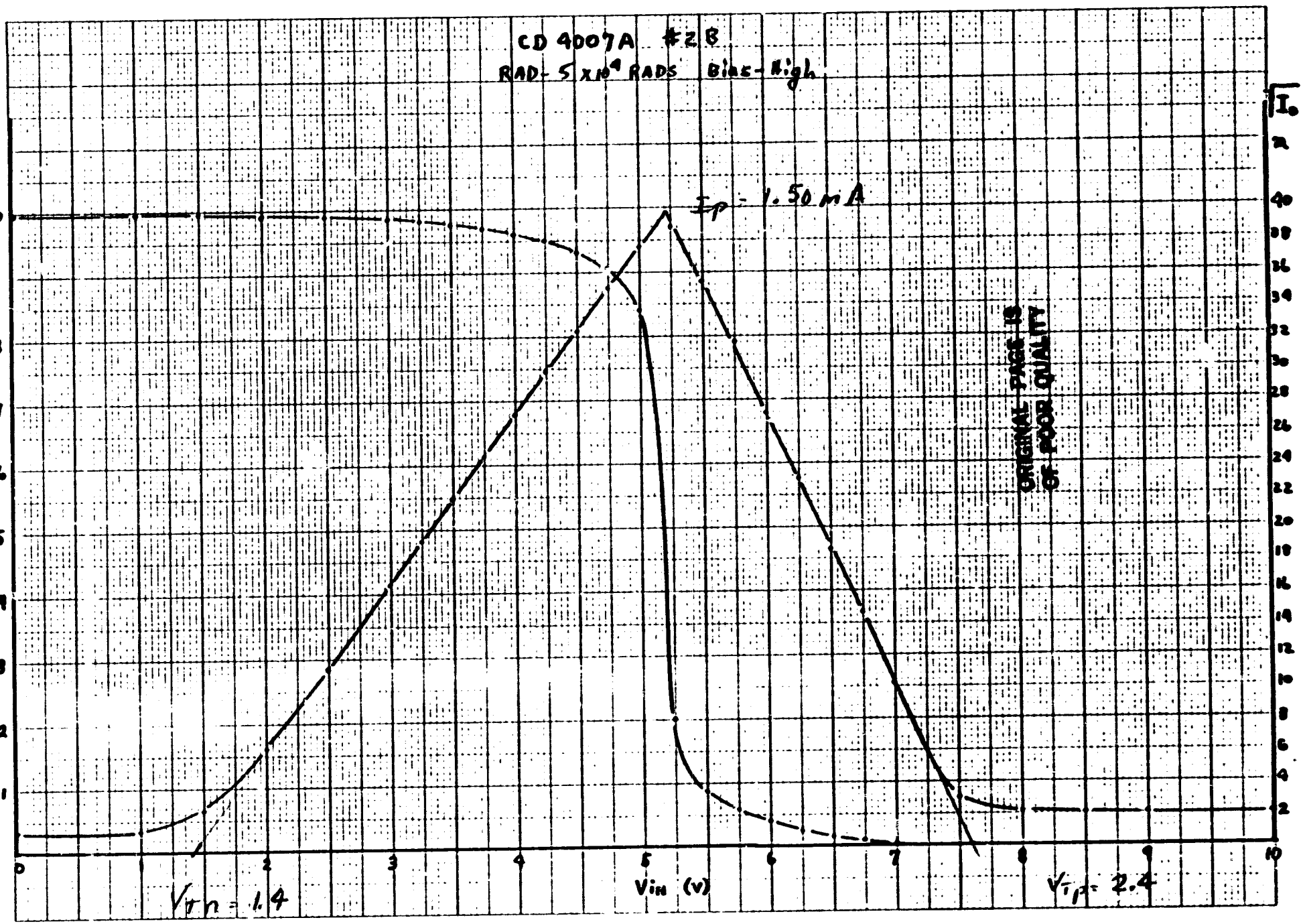

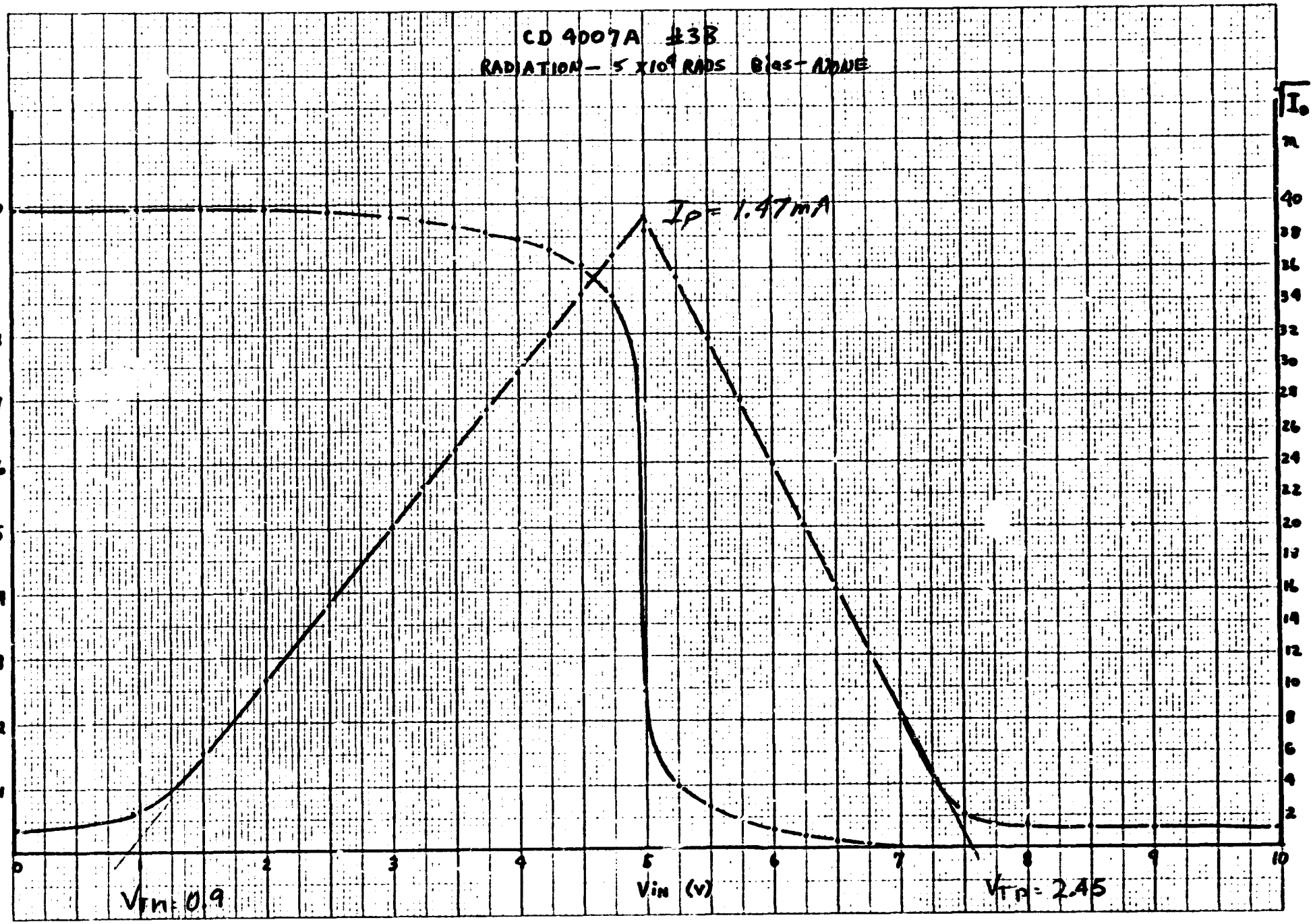

76

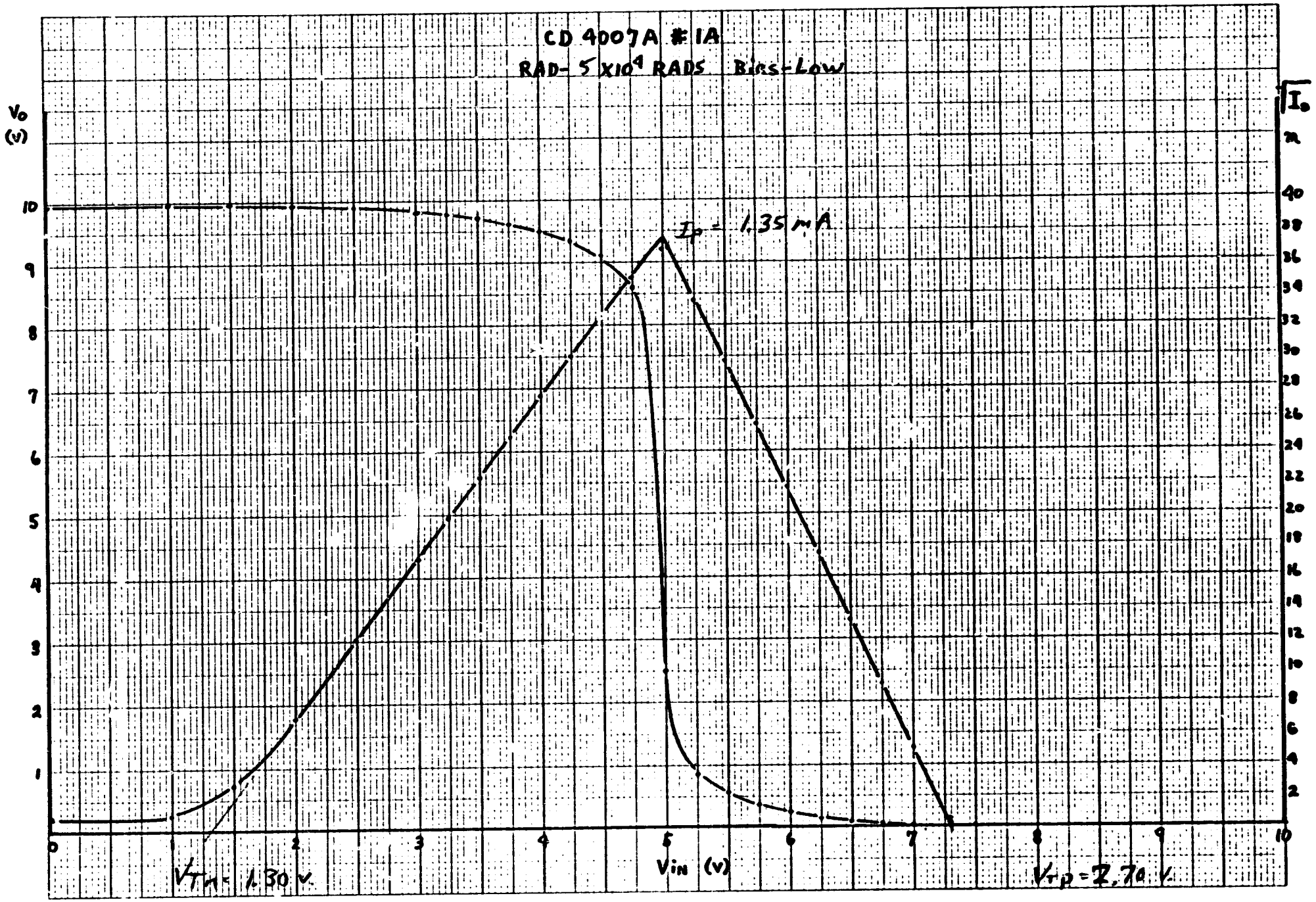

77

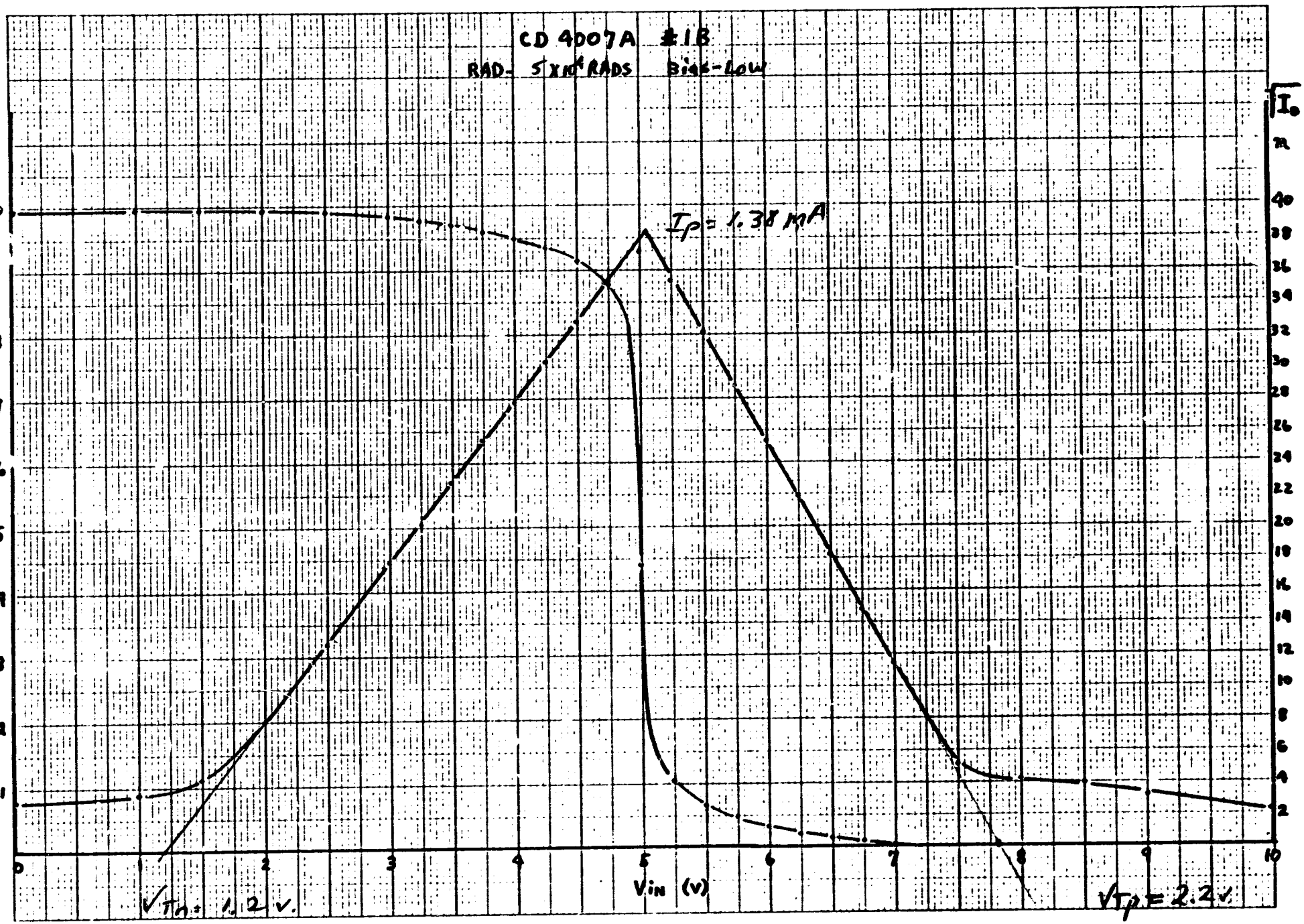
CD 4007A #1B
RAD- 5 X 10^4 RADS Bias-Low
V_O (V)
I_D m
I_P = 1.38 mA
V_{IN} (V)
V_{Tn} = 1.2 V.
V_{Tp} = 2.2 V

46 1320

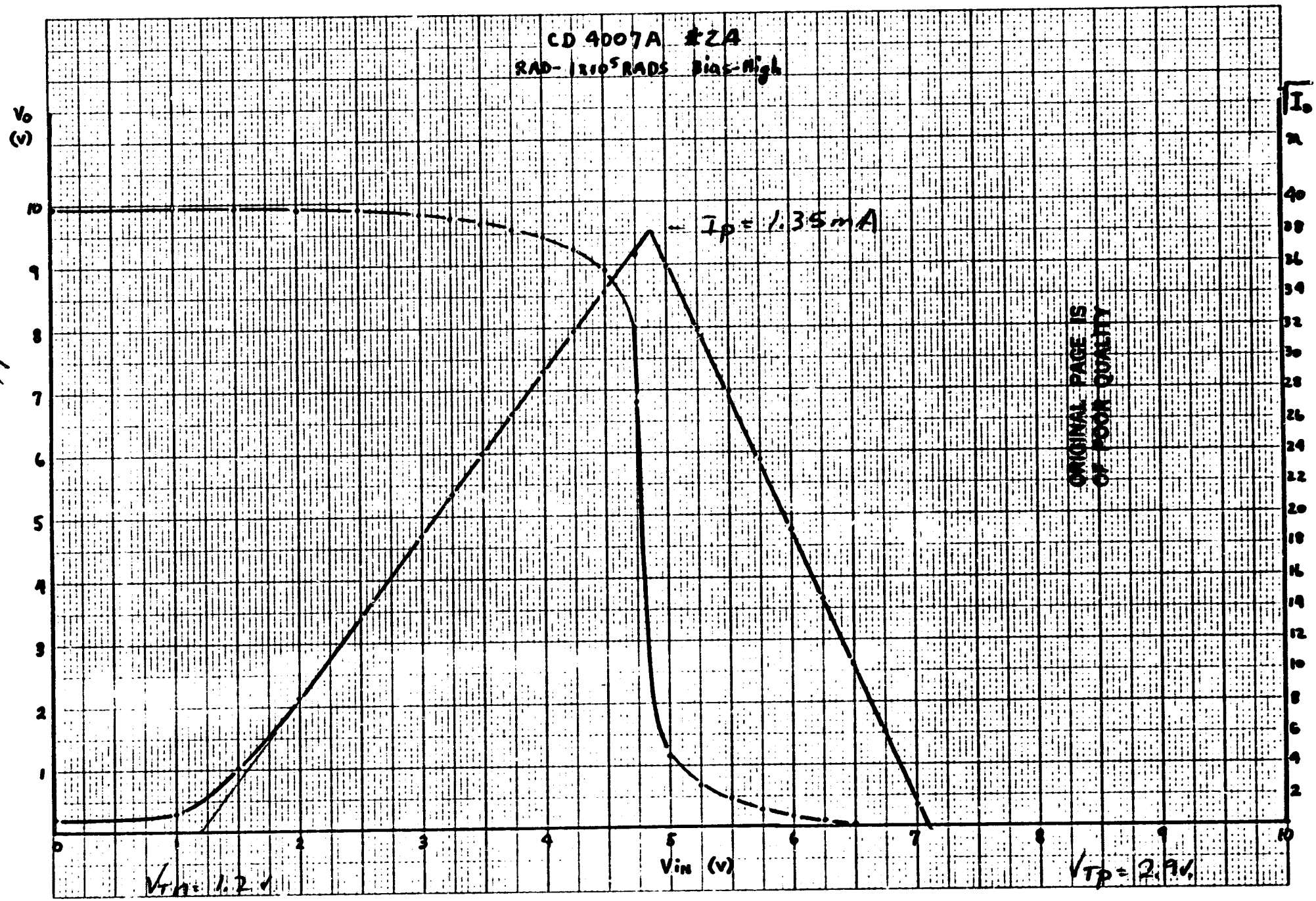
CD 4007A #Z4
RAD- 1x10^5 RADS Bias-High
V_o (V)
$\sqrt{I_o}$
$I_p = 1.35mA$
V_{in} (V)
$V_{Th} = 1.2V$
$V_{Tp} = 2.9V$
ORIGINAL PAGE IS OF POOR QUALITY

79

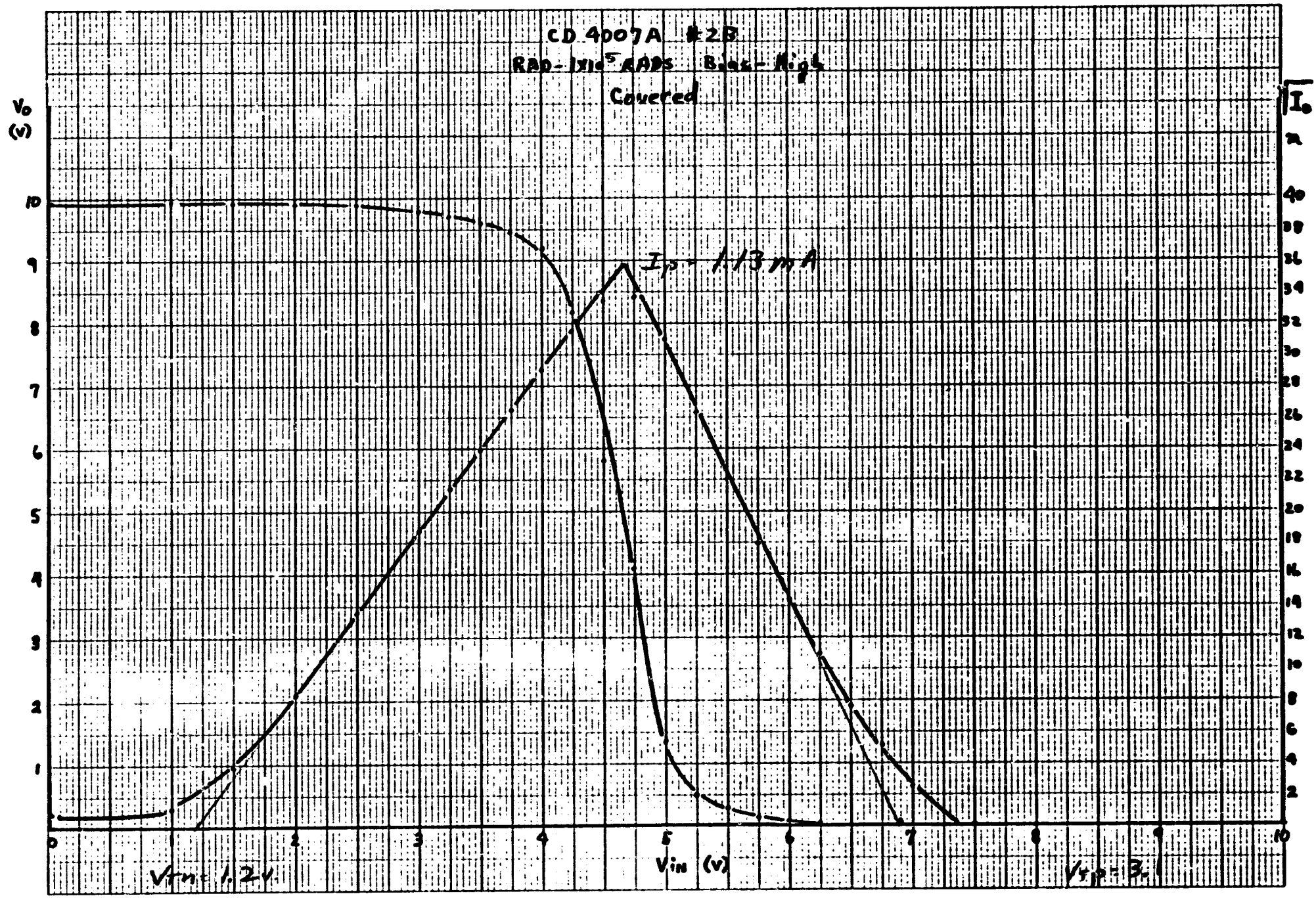

80

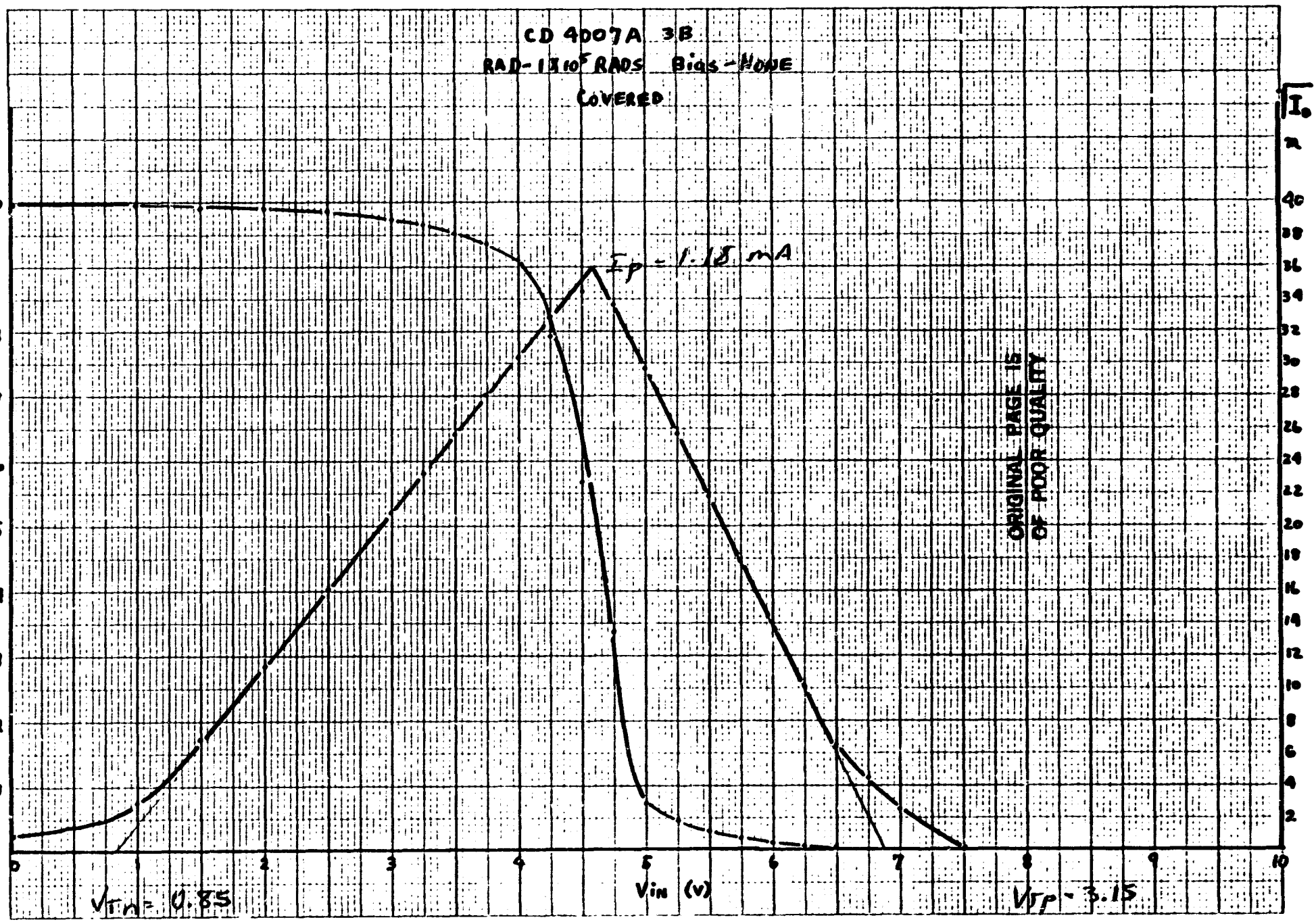

82

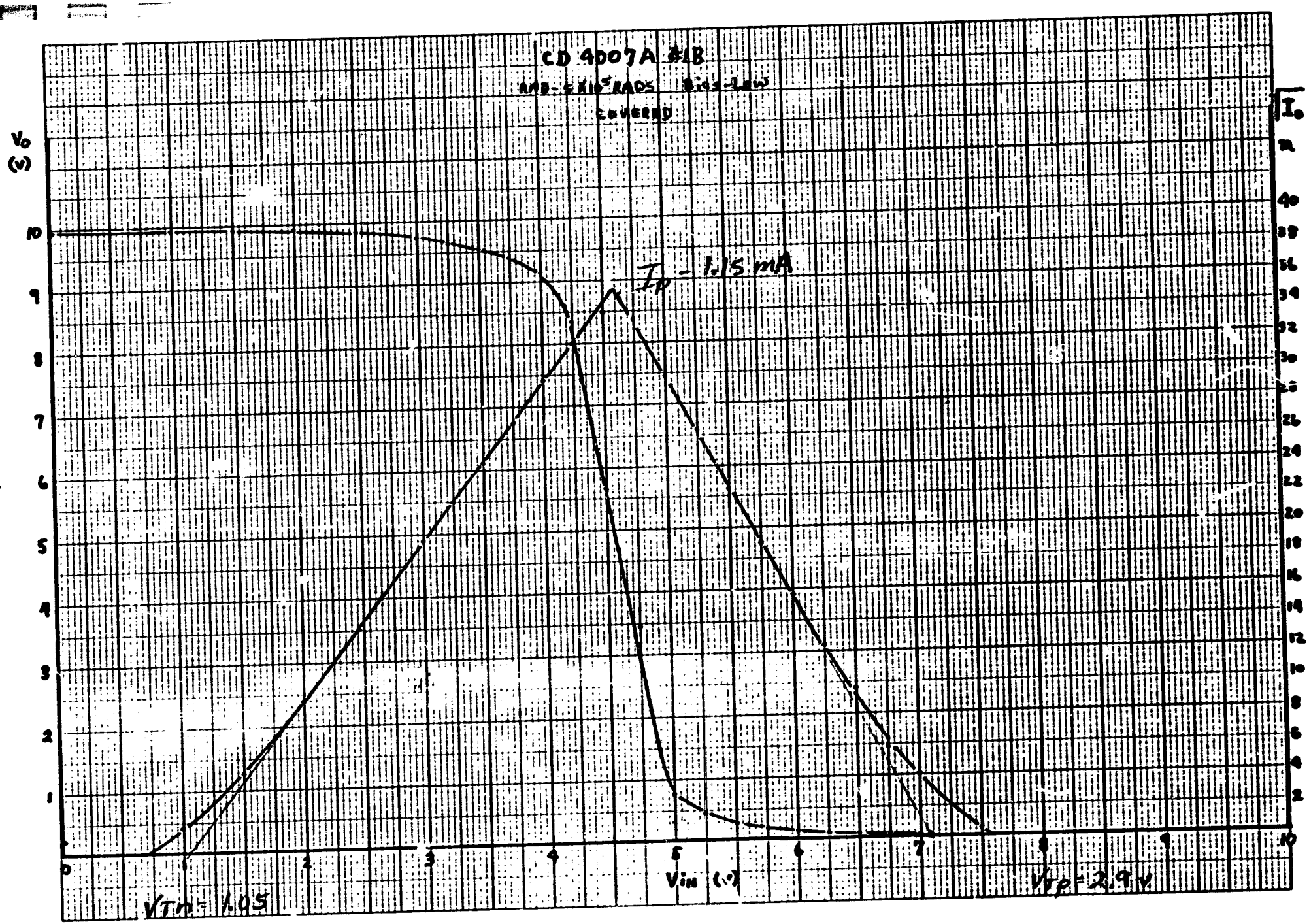

90

TCS-071 #4A
RAD 0
I_D = 3.44 mA
V_{DD} = 11.2 V
V_{SS} = 11.5 V
V_{in} (V)
V_o (V)
I_D (mA)
10 X 10 TO 1 INCH
KEUFFEL & ESSER CO
46 1320

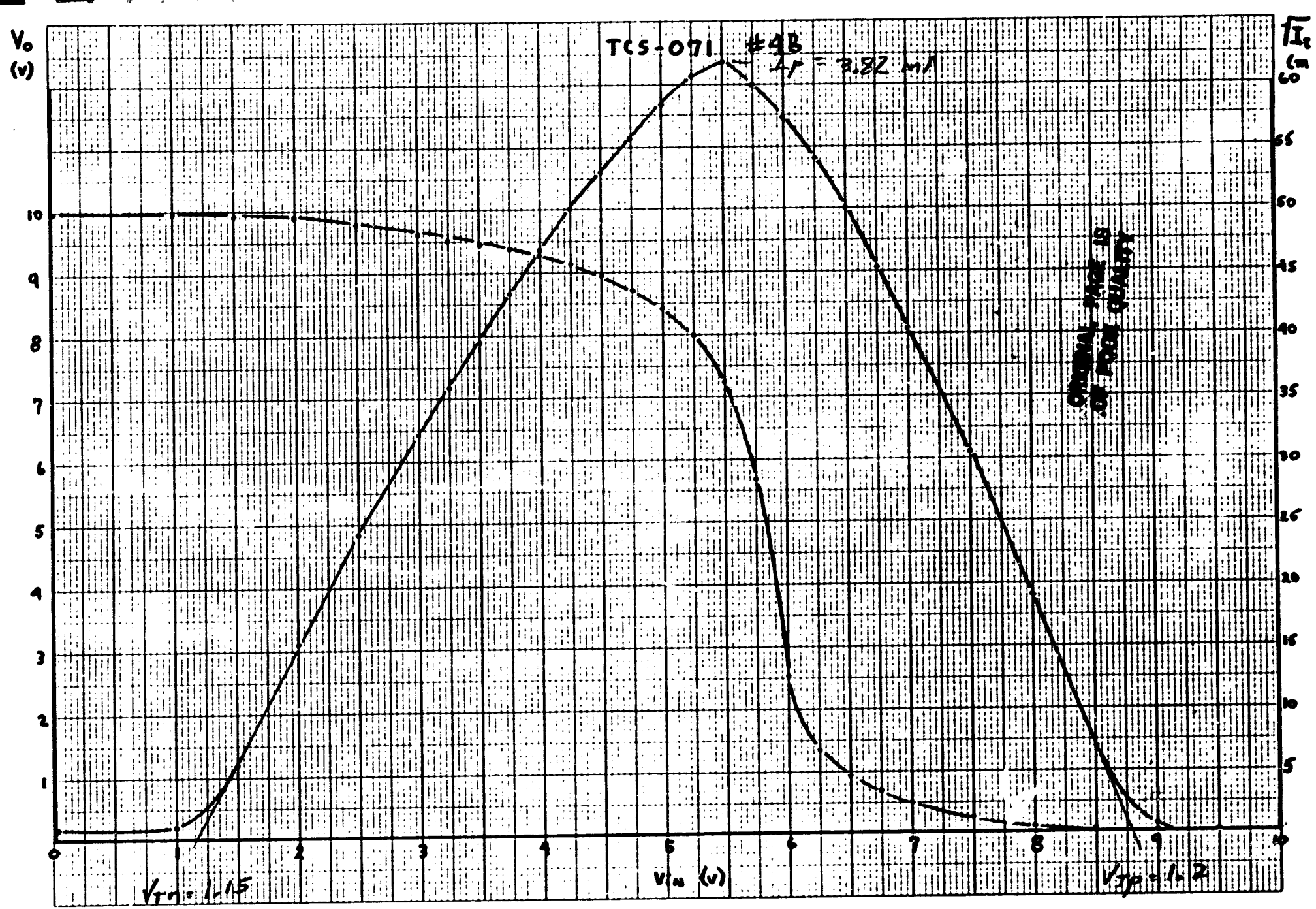
TCS-071 #4B
I_T = 3.82 mA
V_o (v)
I_T (mA)
V_{in} (v)
V_{TH} = 1.15
V_{TP} = 4.2
ORIGINAL PAGE IS
OF POOR QUALITY

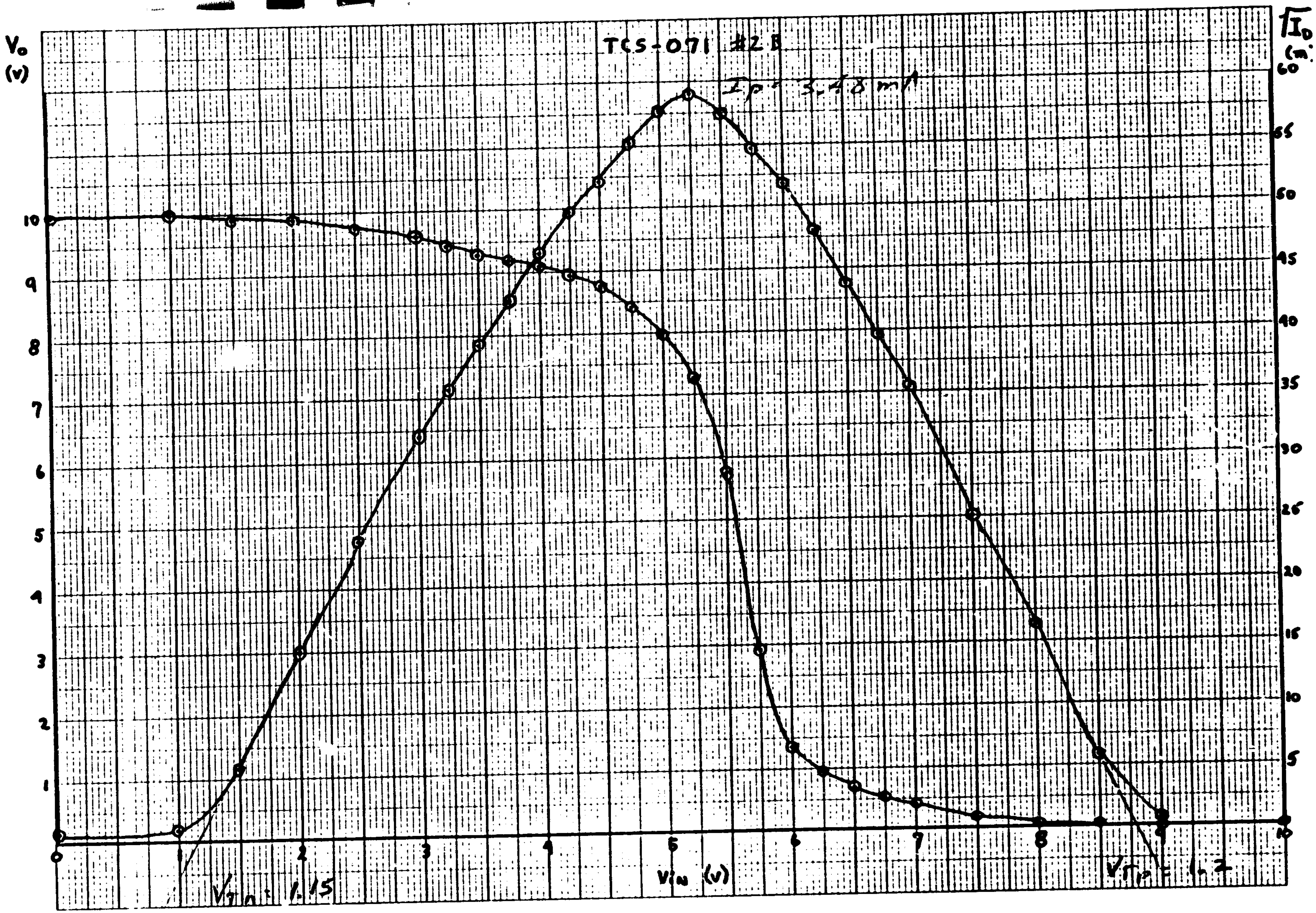

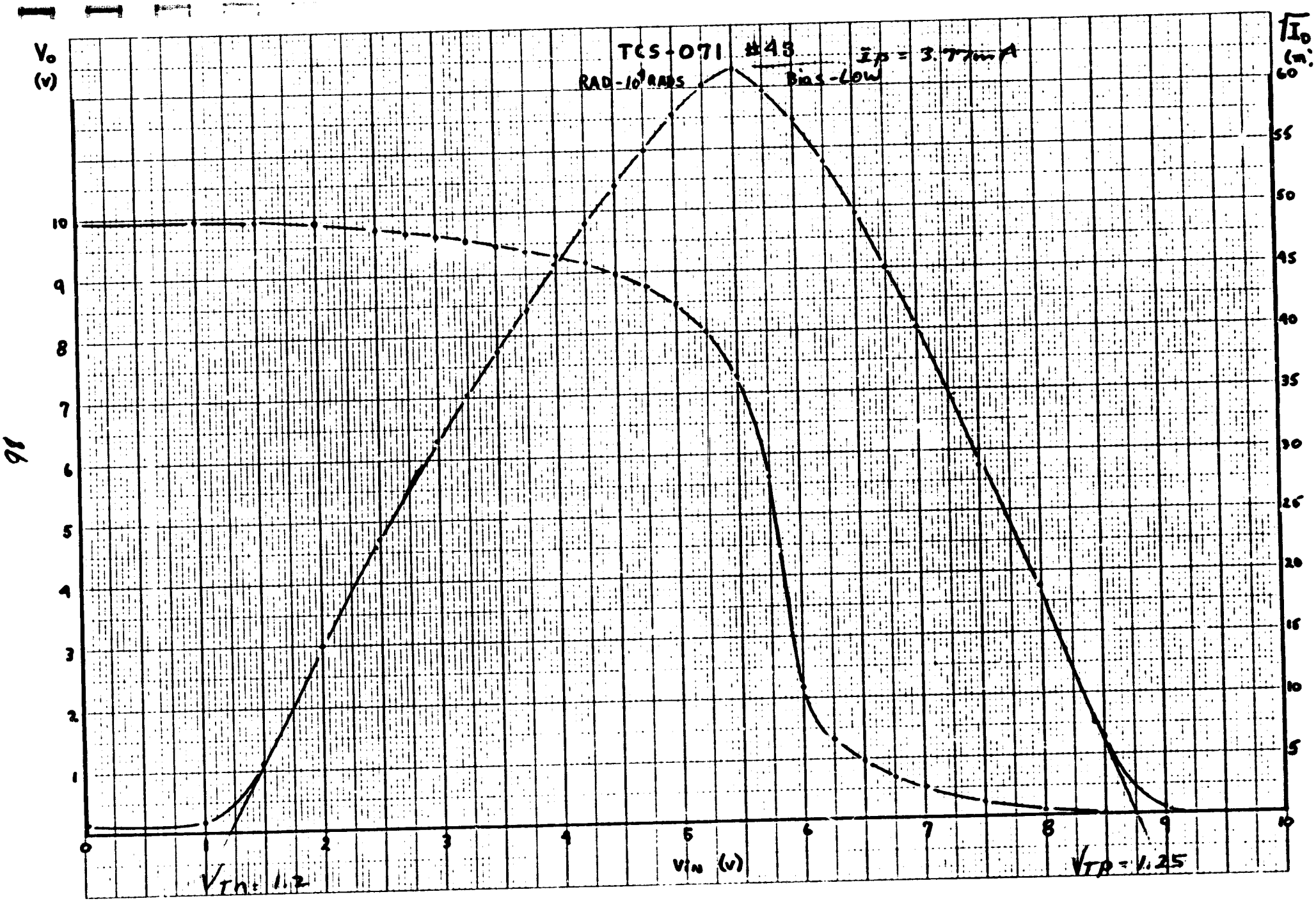
TCS-071 #43
I_p = 3.77mA
RAD-10^4 RADS
Bias-Low
V_o (v)
$\sqrt{I_D}$ (m)
V_{IN} (v)
V_{TH} = 1.2
V_{TP} = 1.25

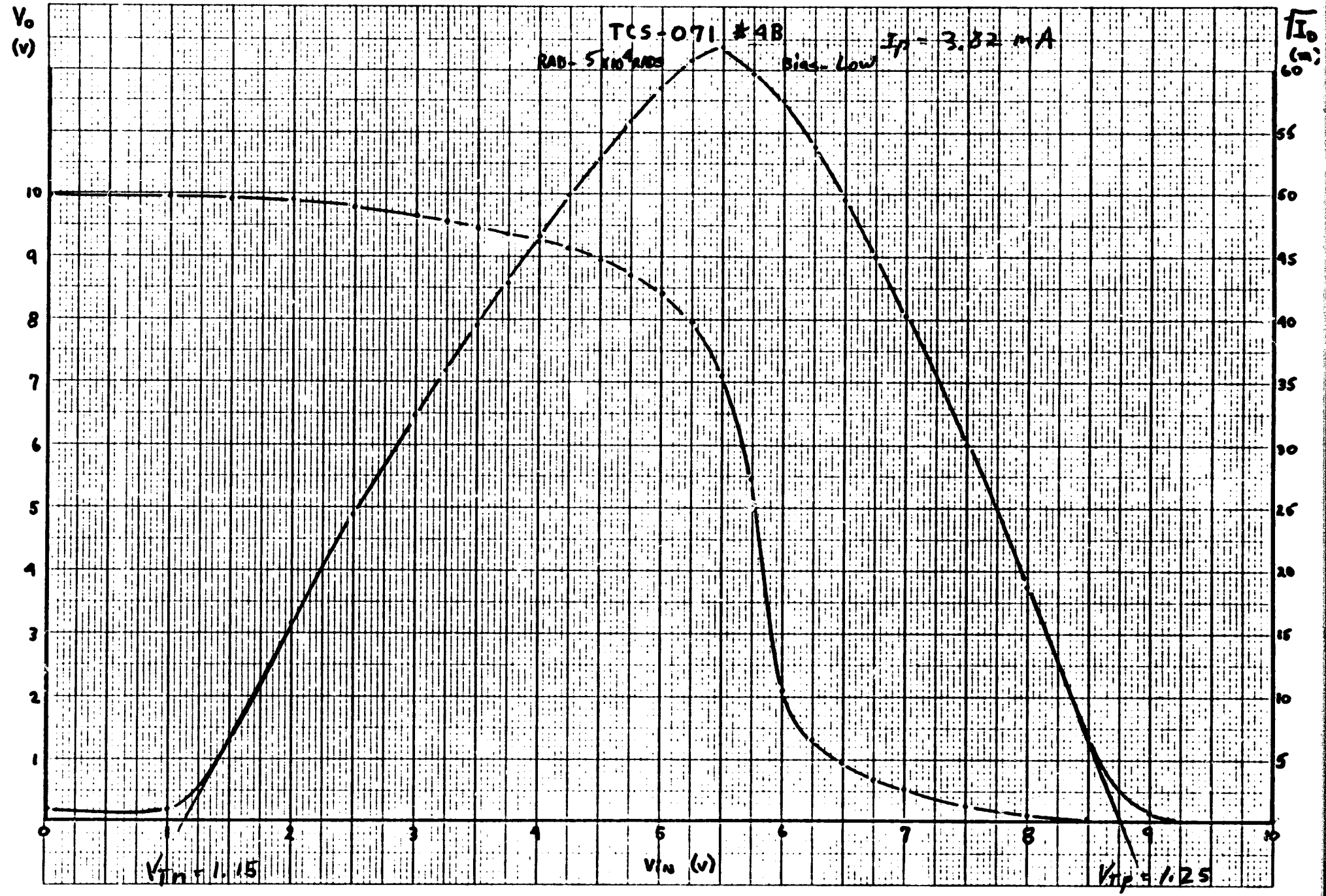
TCS-071 #4B
RAD- 5 KRADS
Bias- Low
I_p = 3.32 mA
V_o (v)
$\sqrt{I_o}$ (m)
V_{IN} (v)
V_{Tn} = 1.15
V_{Tp} = 1.25

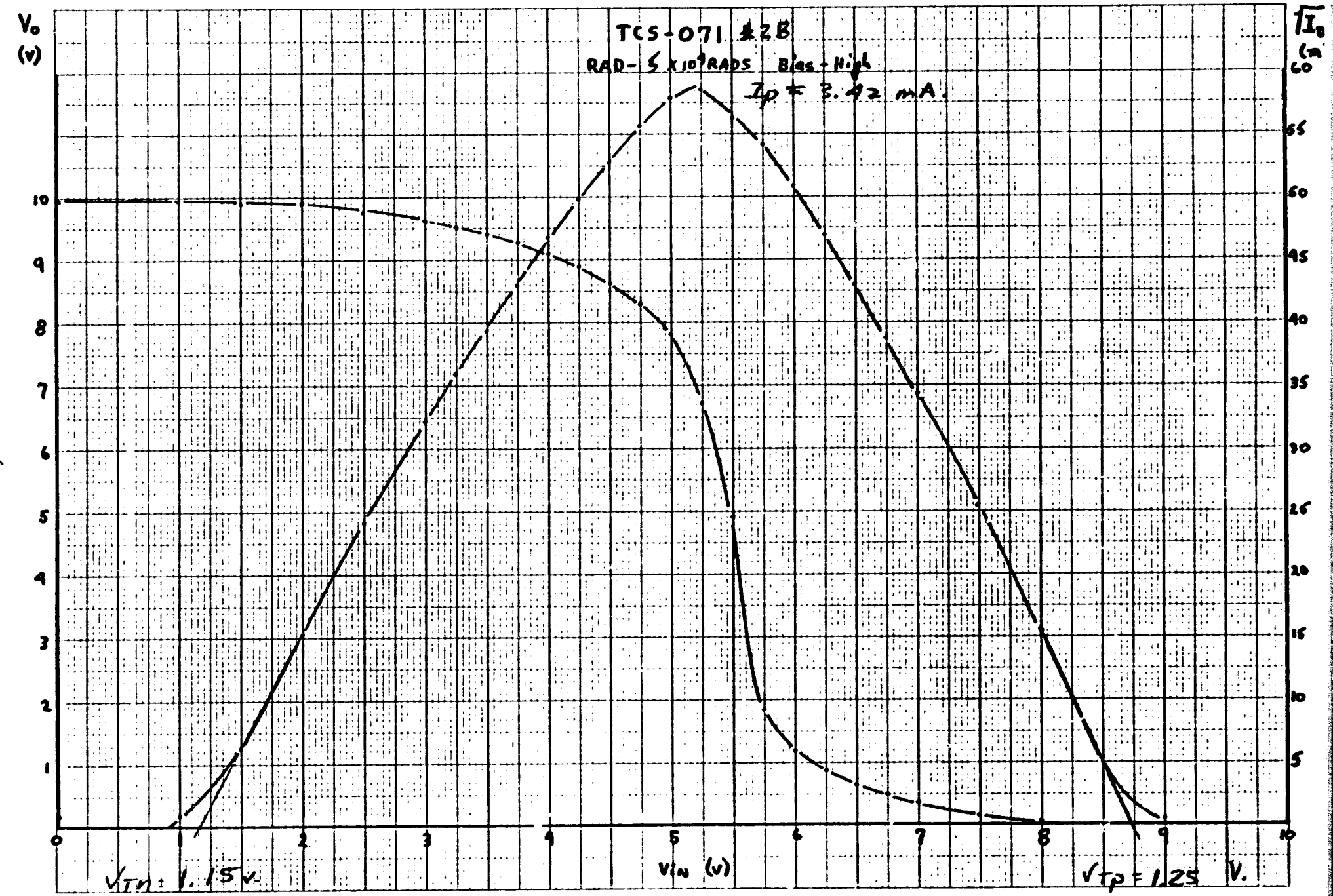

106

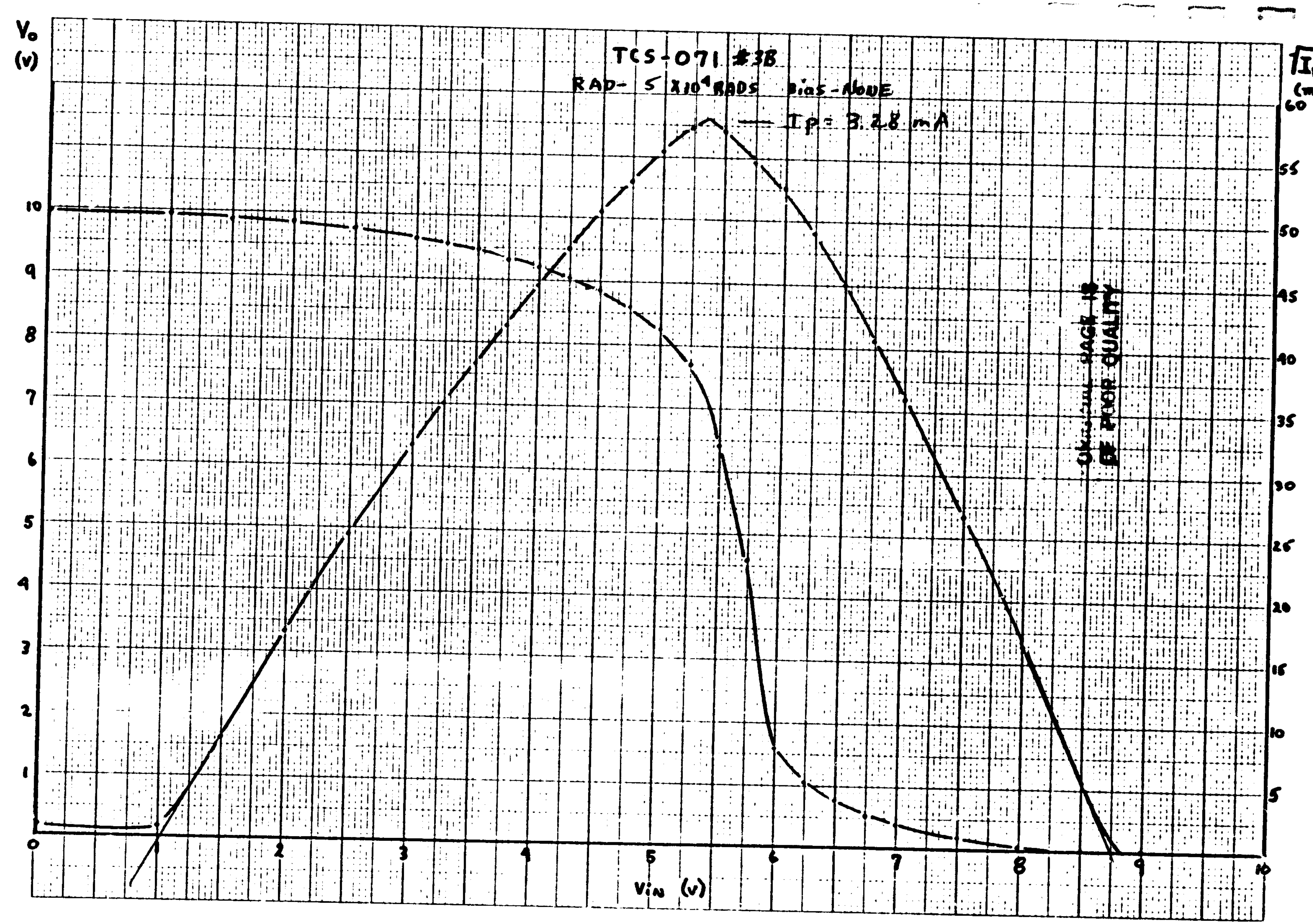

TCS-071 #4A
RAD-1X10^5 RADS
Bias-Low
I_D = 3.63mA
V_{in} = 12V
V_{in} = 10V
V_o (v)
I_o (m)
V_{in} (v)

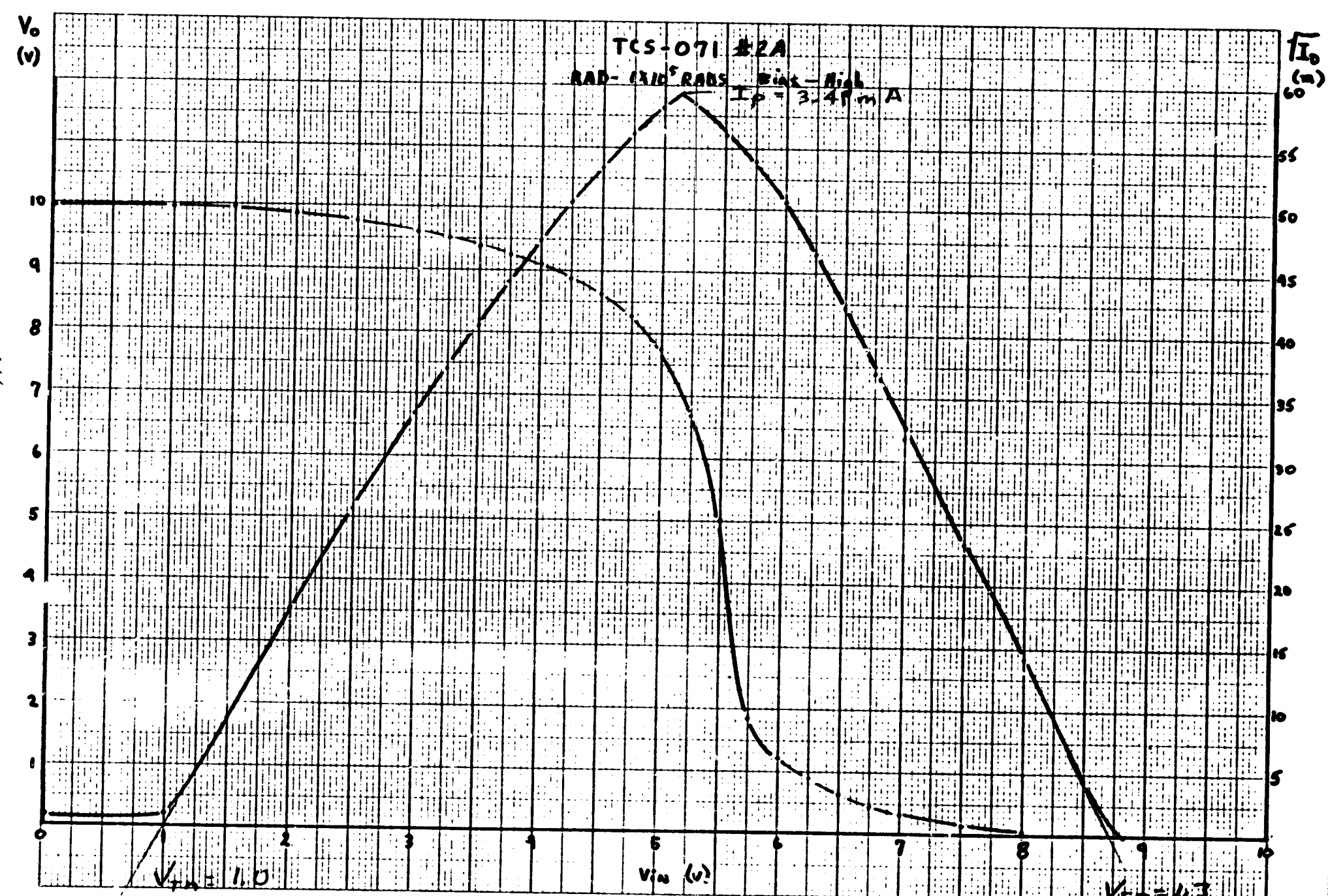

K-E 10 X 10 TO ½ INCH KEUFFEL & ESSER CO

46 1320

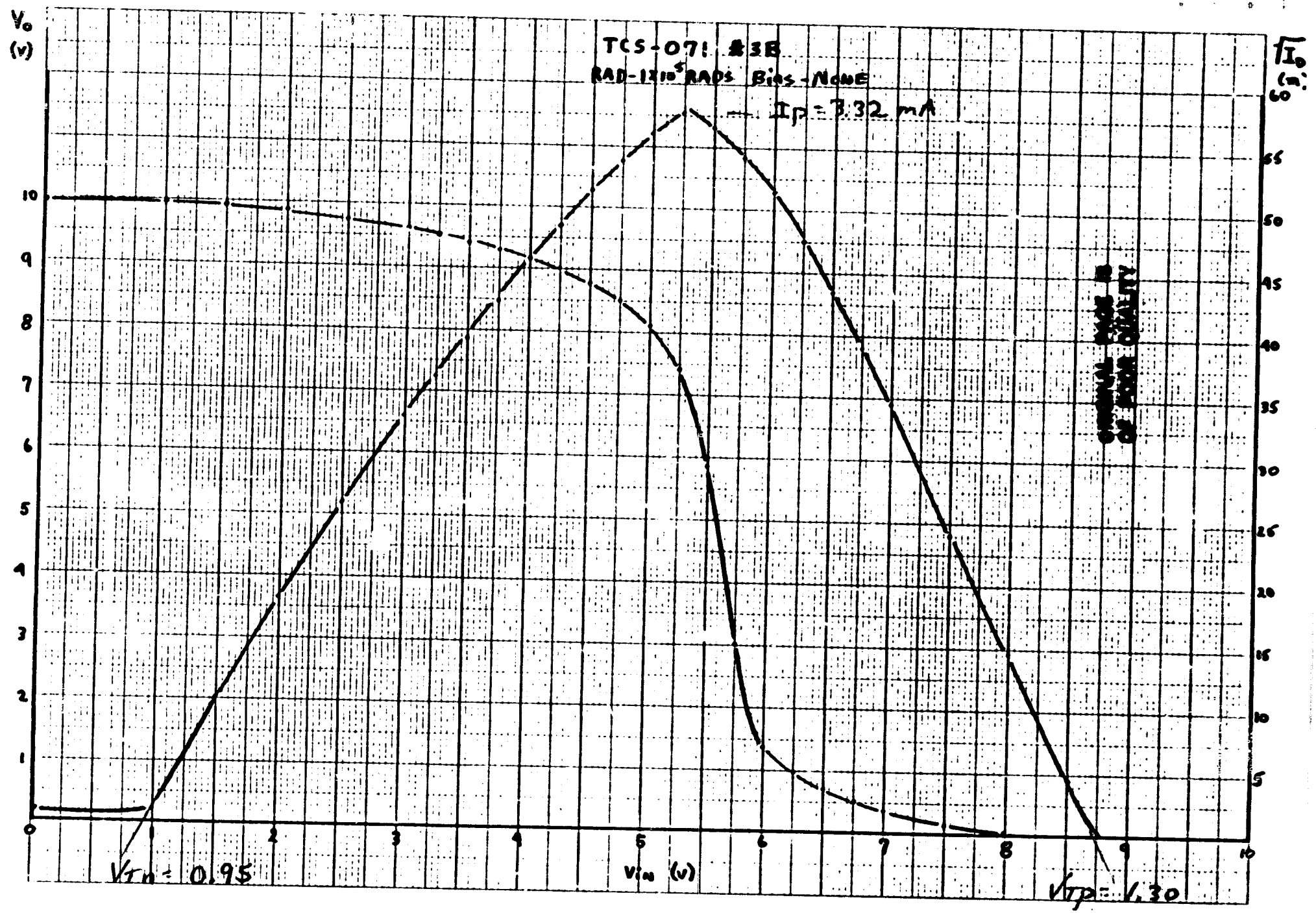

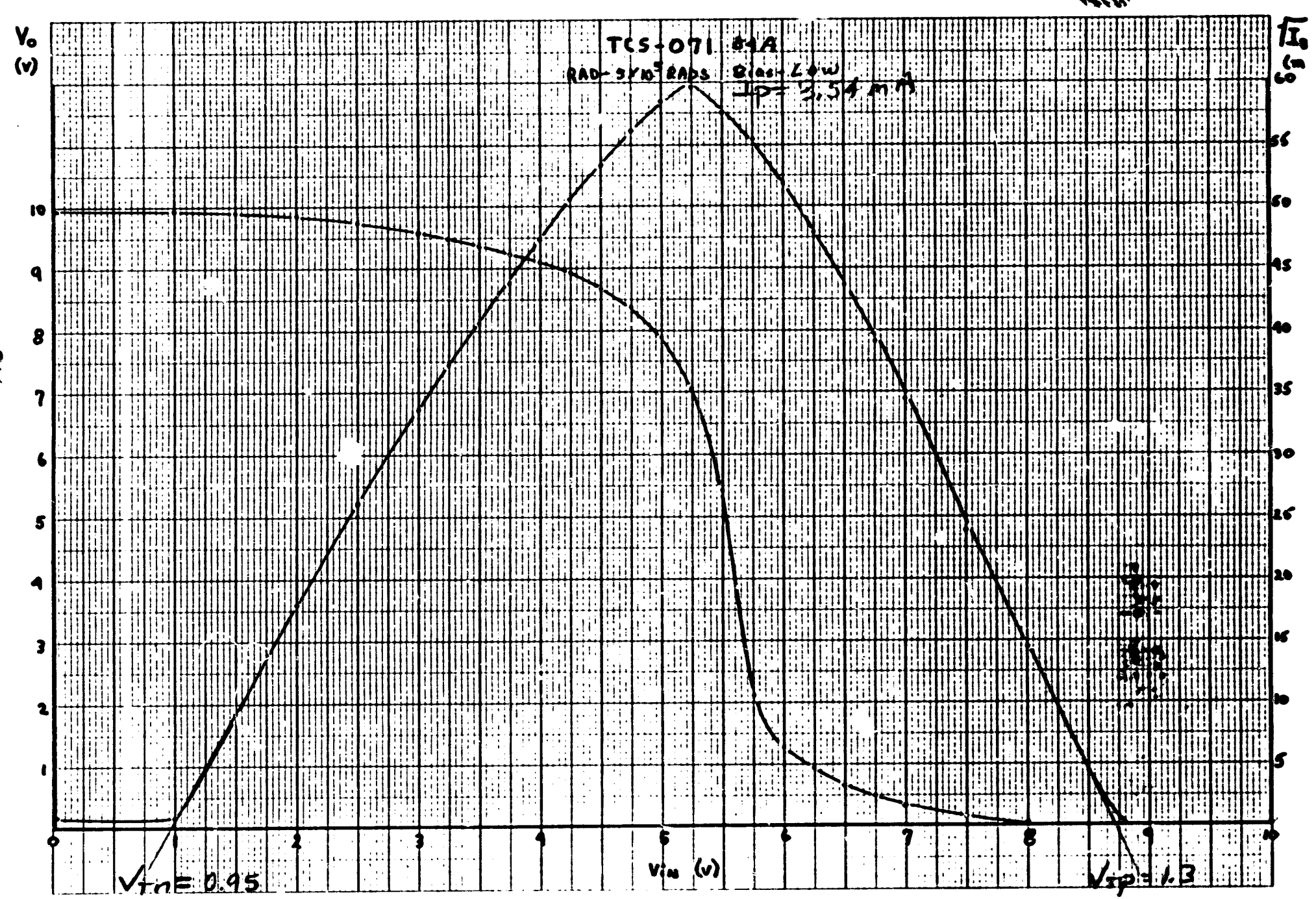
TCS-071 #1A
RAD-3X10³ RADS
Bias-Low
Ip= 3.54 mA
Vo (v)
√Id (m
Vin (v)
Vtn= 0.95
Vtp= 1.3

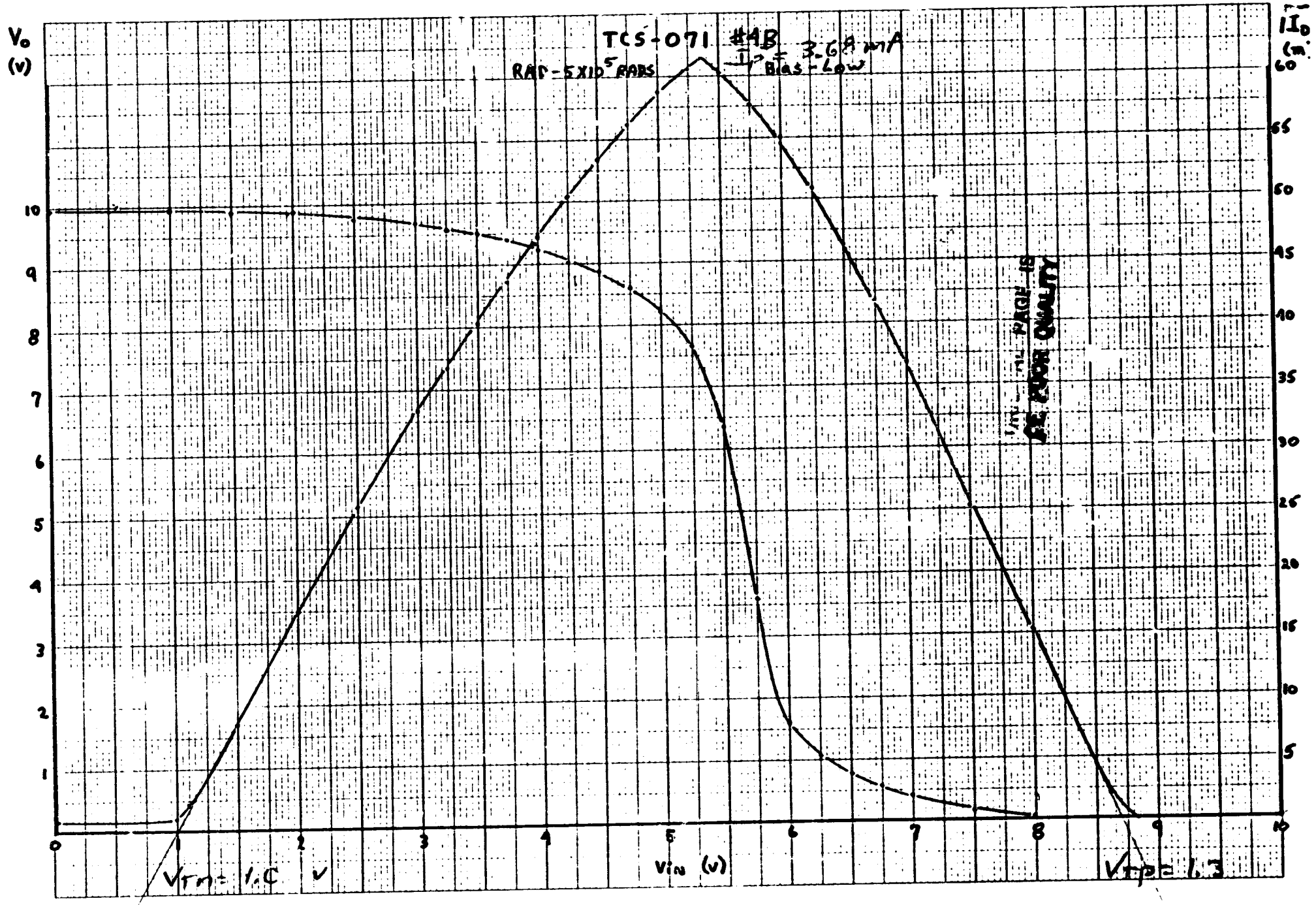

K&E 10 X 10 TO ½ INCH 7 X 10 INCHES
KEUFFEL & ESSER CO MADE IN U.S.A.

46 1320

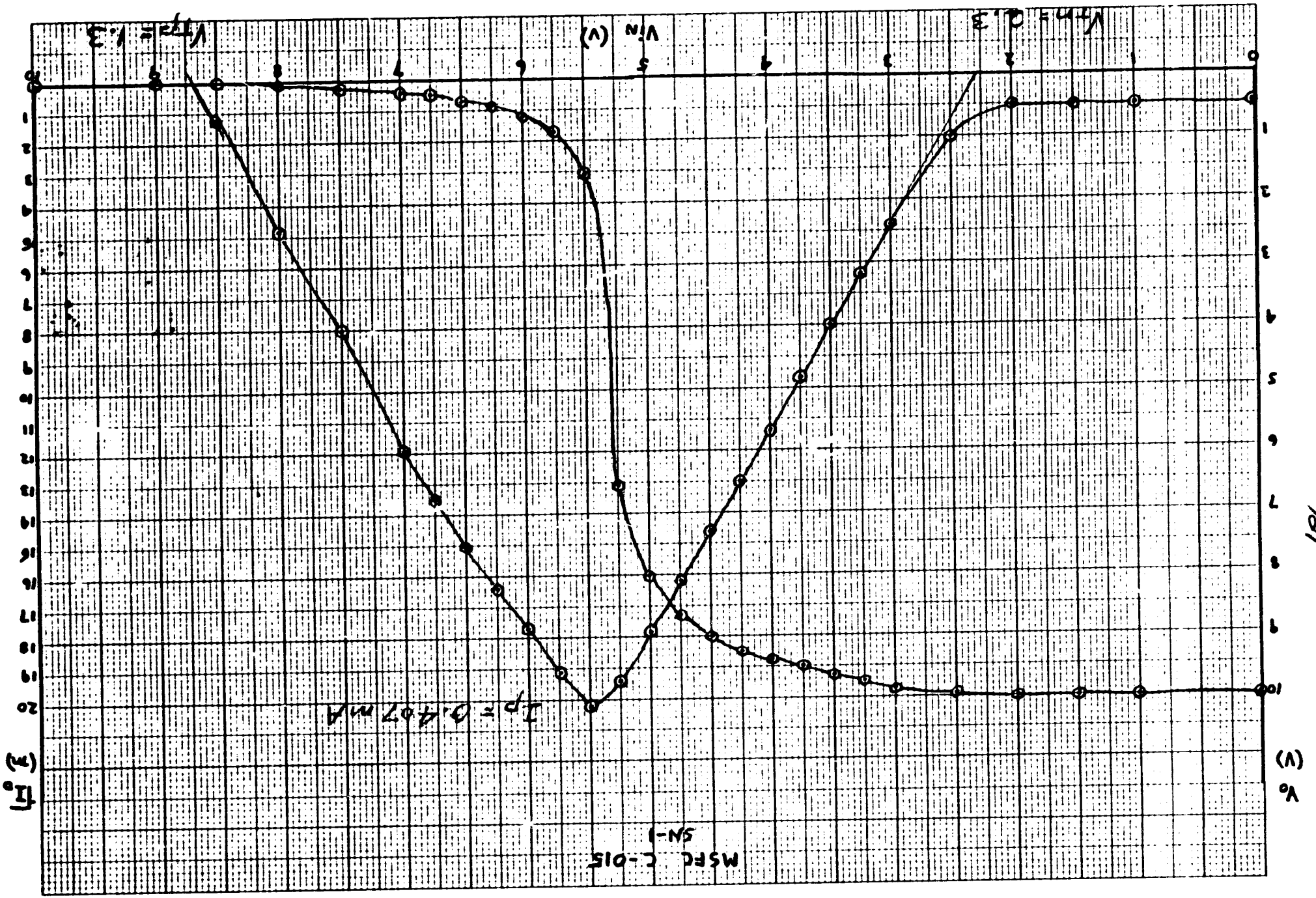

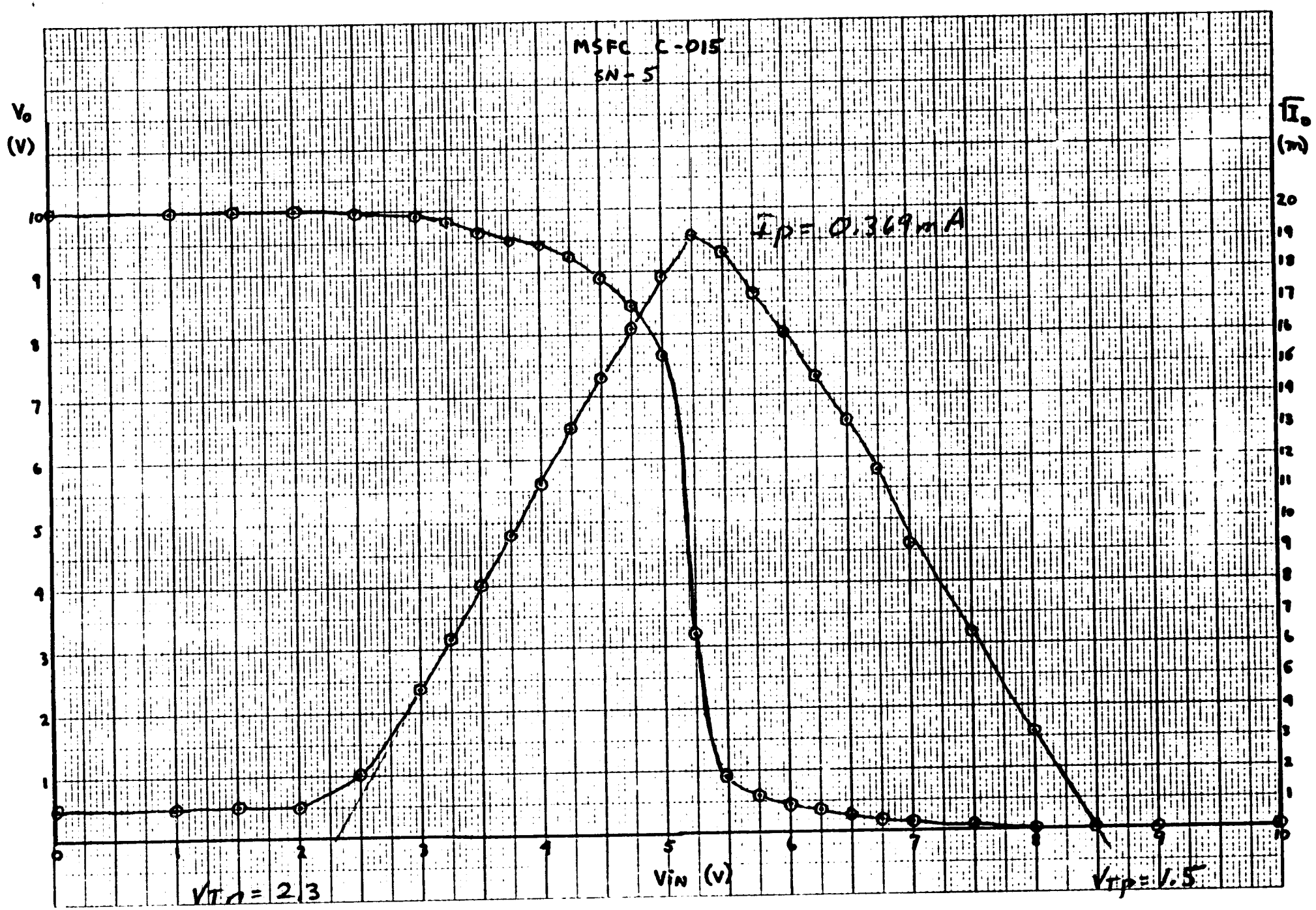
MSFC C-015
SN-5
V_o (V)
$\sqrt{I_o}$ (mA)
$I_{DP} = 0.369$ mA
V_{IN} (V)
$V_{TP} = 1.5$
$V_{TP} = 2.3$
/2d

MSFC C-015 SN-1
RAD-5x10⁴RADS Bias-Low
I_D = 0.325 mA
V_{th} = 1.95 V
V_{th} = 1.64 V
V_{in} (V)
V_o (V)
KE
10 X 10 TO ½ INCH 7 X 10 INCHES
KEUFFEL & ESSER CO
46 1320

Fig. 3

MSFC E-015 SN-5
RAD-1X10^5 RADs Bias-High

V_{th} (V)

V_N (V)

V_o (V)

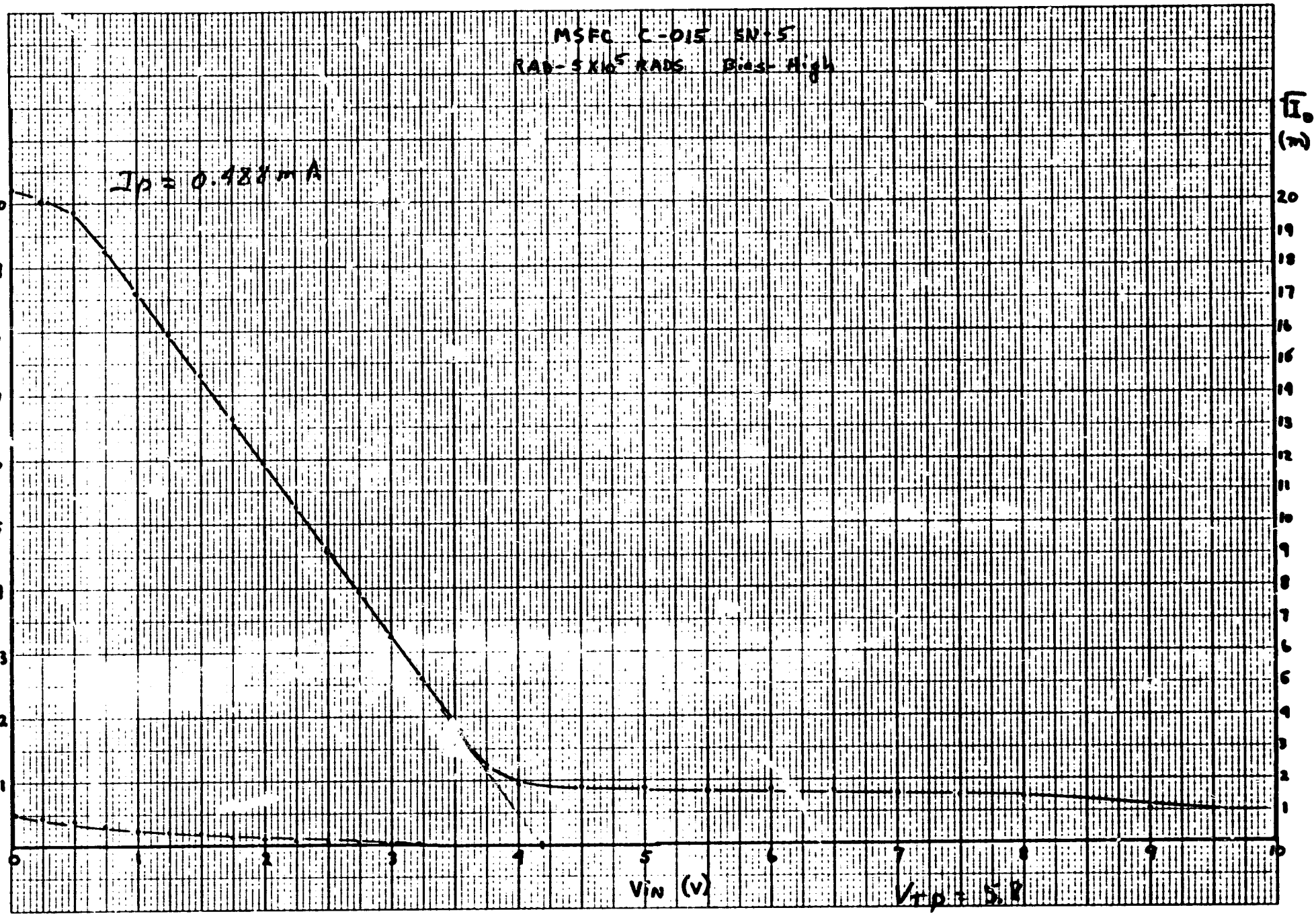

130

REFERENCES

[1] J. A. Van Allen, L. A. Frank, "Radiation Measurements to 658,300 Km With Pioneer IV," Nature, 184, 219 (1959).

[2] W. N. Hess, "The Radiation Belt and Magnetosphere," Blaisdell Publishing Co., 1968, Weltham, MA

[3] J. I. Vette, "Models of the Trapped Radiation Environment - Volume I: Inner Zone," NASA, SP-3024, 1966.

[4] J. H. King, "Models of the Trapped Radiation Environment - Volume IV: Low Energy Protons,"

[5] W. N. Hess, "Earth's Radiation Environment," Space/Aeronautics, pp. 68-76 (November 1964).

[6] W. E. Price, "The Simulation of Space Radiation Damage to Spacecraft Systems," IEEE Trans. Nuc. Sci., pp. 2-7 (December 1965).

[7] A. J. Brucker, R. S. Ohanian, F. G. Stassinopoulos, "Successful Large-Scale Use of CMOS Devices on Spacecraft Traveling Through Intense Radiation Belts," AES-12, no. 1, pp. 23-2[illegible] (January 1976).

[8] J. A. Van Allen, "Interplanetary Particles and Fields," Scientific American, pp. 161-173 (September 1975).

[9] "Encounters With Jupiter," Astronomy, pp. 4-18 (February 1974).

[10] T. Gehrels, "The Flyby of Jupiter," Sky and Telescope, pp. 76-78 (February 1974).

[11] Pasachoff, "Our Sun," Astronomy, pp. 7-24 (January 1978).

[12] H. H. L. Olesen, "Designing Against Space Radiation - Parl I," Electronics, pp. 61-71, December 28, 1964.

[13] Vette, J. I., Lucero, A. B., and Wright, J. A., Models of the Trapped Radiation Environment, Volume II: Inner and Outer Zone Electrons, NASA SP-3024, 1966.

[14] Lavine, J. P., and Vette, J. I., Models of the Trapped Radiation Environment, Volume VI: High Energy Protons, NASA SP-3024, 1970.

[15] Imhof, W. L., et. al., Models of the Trapped Radiation Environment, Volume VII: Long Term Time Variations, NASA SP-3024, 1971

[16] F. Larin, Radiation Effects in Semiconductor Devices (John Wiley, N.Y., 1968.

[17] J. W. Corbett, Electron Radiation Damage in Semiconductors and Metals (Academic Press, N.Y., 1966).

[18] F. Seitz, Discussions Faraday Soc. 5, 271 (1949).

[19] W. Shockley, W. T. Read, Phys. Rev. 87, 387 (1952).

[20] R. N. Hall, Phys. Rev., 87, 387 (1952).

[21] P. A. Andrews, S. Mayburg, Proc. IEEE, October, 1653 (1957).

[22] K. H. Zaininger, private communication.

[23] C. H. Cheek, V. J. Linnenbom, Proc. AIEE, Dec., 1004 (1960).

[24] U. Fano, Am. Rev. Nucl. Sci., 13, 1 (1963).

[25] H. H. Anderson, J. F. Ziegler, Hydrogen-Stopping Powers and Ranges in Nl Elements, Pergamon Press, New York (1977.

[26] K. R. Kase, W. R. Nelson, Concepts of Radiation Desimetry, Pergamon Press, New York (1978).

[27] CMOS Bulk Si Double Metal Process Sheet, NASA/Marshall Space Flight Center (1977).

[28] G. J. Brucker, R. S. Ohanian, E. G. Stassinopoulos, IEEE Trans. on Aerospace and Electronic Systems, AES-12, No. 1, 23-28 (1976).

[29] R. A. Cliff, et.al., IEEE Trans. on Nuclear Science, NS-23, No. 6, pp. 1781-1788 (1976).

[30] W. J. Poch, A. G. Holmes-Siedle, IEEE Trans. on Nuclear Science, NS-16, pp. 33-40 (1969).

[31] B. L. Gregory, IEEE Trans. on Nuclear Science, NS-22, No. 6, pp. 2295-2302 (1975).

[32] G. F. Derbenwick, B. L. Gregory, IEEE Trans. on Nuclear Science, NS-22, No. 6, pp 2151-2156 (1975).

[33] K. M. Schlesier, IEEE Trans. on Nuclear Science, NS-21, pp. 152-158 (1974).

BIBLIOGRAPHY

Apparao, K. M. V., Composition of Cosmic Radiation, Gordon and Breach Science Publishers, 1975.

Aubuchon, K., "Radiation Hardening of P-MOS Devices by Optimization of the Thermal SiO_2 Gate Insulator", IEEE Trans. Nucl. Sci., NS-18, 117 (1971).

Brews, J. R., "Carrier Density Fluctuations and the IGFET Mobility Near Threshold," J. Appl. Phys., 46, 2181 (1975).

Brews, J. R., "Theory fo the Carrier-Density Fluctuations in an IGFET Near Threshold," J. Appl. Phys. 46, 2193 (1975).

Brucker, G. J., "Transient and Steady-State Radiation Response of CMOS/SOS," IEEE Trans. Nucl. Sci., NS-21, 6 (1974).

Brucker, G. J., Ohanian, R. S., and Stassinopoulos, E. G., "Successful Large-Scale Use of CMOS Devices on Spacecraft Traveling Through Intense Radiation Belts," IEEE Trans. on Aerospace and Electronic Systems, AES-12, 23 (1976).

Burghard, R. A., Gregory, B. L., Gwyn, C. W., and Derbenwick, G. F., "Process Dependence of Radiation Effects in CMOS Integrated Circuits," Final Report, AFWL Contract 75-198, May 1975.

Burrell, M., The Calculation of Proton Penetration and Dose Rates, NASA TMY-53063, (GMSFC).

Burrell, M., and Watts, J., Electron and Bremsstraklung Penetration and Dose Calculation, NASA TN D-6385, (GMSFC), 1971.

Churchill, J. N., Collins, T. W., and Holmstrom, "Electron Irradiation Effects in MOS Systems," IEEE Trans. Elec. Dev., ED-21, 768 (1974).

Cladis, J. B., Davidson, G. T., and Newkirk, L. L., Trapped Radiation Handbook, General Electric Company, Rept. DNA2524H, Dec. 1971.

Cliff, R. A., Danchenko, V., Stassinopoulos, E. G., and Sing, M., "Prediction and Measurement of Radiation Damage to CMOS Devices on Board Spacecraft," IEEE Trans. Nucl. Sci., NS-23, 1781 (1976).

Derbenwick, G. F., and Gregory, B. L., "Process Optimization of Radiation-Hardened CMOS Integrated Circuits," IEEE Trans. Nucl. Sci., NS-22, 2151 (1975).

Fossum, J. G., Derbenwick, G. F. and Grefory, B. L., "Design Optimization of Radiation-Hardened CMOS Integrated Circuits," IEEE Trans. Nucl. Sci., NS-22, 2208 (1975).

Gregory, B. L., "Process Controls for Radiation-Hardened Aluminum-Gate Bulk Silicon CMOS," IEEE Trans. Nucl. Sci., NS-22, 2295 (1975).

Grove, A. S., Physics and Technology of Semiconductor Devices, John Wiley and Sons, Inc., 1967 (Chapter 2).

Holmes-Siedle, A. G., and Zaininger, K. H., "The Physics of Failure of MOS Devices Under Irradiation," IEEE Trans. on Reliability R-17, 34 (1968).

Hughes, R. C., "Charge Carrier Transport Phenomena in Amorphous SiO_2: Direct Measurement of the Drift Mobility and Lifetime," Phys. Rev. Lett. 30, 1333 (1973).

Hughes, H., Baxter, R. D., and Phillips, B., "Dependence of MOS Device Radiation-Sensitivity on Oxide Impurities," IEEE Trans. Nucl. Sci. NS-19, 256 (1972).

Larin, F., Radiation Effects in Semiconductor Devices, John Wiley and Sons, Inc., (1968).

Lavine, J. P., and Vette, J. I., Models of the Trapped Radiation Environment, Volume VI: High Energy Protons, NASA, SP-3024, 1970.

Lavine, J. P., and Vette, J. I., Models of the Trapped Radiation Environment, Volume V: Inner Belt Protons, NASA SP-3024, 1969.

Maier, R. J., and Tallon, R. W., "Dose-Rate Effects in Permanent Threshold Voltage Shifts of MOS Transistors," IEEE Trans. Nucl. Sci., NS-22, 2214 (1975).

Mitchell, J. P., "Radiation-Induced Space-Charge Buildup in MOS Structures," IEEE Trans. Elec. Dev. ED-14, 764 (1967).

Peel, J. and Kinoshita, G., "Radiation-Hardened Complementary MOS Using SiO_2 Gate Insulators," IEEE Trans. Nucl. Sci. NS-19, 271 (1972).

Poch, W., and Holmes-Siedle, A., "The Long-term Effects of Radiation on CMOS Logic Networks," IEEE Trans. Nucl. Sci., NS-17, (Dec. 1970).

Powell, R. J. and Derbenwick, G. F., "Vacuum Ultraviolet Radiation Effects in SiO_2," IEEE Trans. Nucl. Sci., NS-18, 99 (1971).

Raider, S. I., Gdula, R. A., and Petrak, J. R., "Nitrogen Reaction at a Silicon-Silicon Dioxide Interface," Appl. Phys. Lett. 27, 150 (1975).

Schlesier, K. M. and Norris, P. E., "CMOS Hardening Techniques," IEEE Trans. Nucl. Sci. NS-19, 275 (1972).

Schlesier, K. M., "Radiation Hardening of CMOS/SOS Integrated Circuits," IEEE Trans. Nucl. Sci., NS-21, 152 (1974).

Schulz, M., and Lanzarotti, L. J., Particle Diffusion in the Radiation Belts, Springer-Verlag, 1974.

Snow, E. H., Grove, A. S., and Fitzgerald, D. J., "Effects of Ionizing Radiation on Oxidized Silicon Surfaces and Planar Devices," Proc. IEEE 55, 1168 (1967).

Srour, J. R., Curtis, O. L., Jr., and Chiu, K. Y., "Charge Transport Studies in SiO_2: Processing Effects and Implications for Radiation Hardening," IEEE Trans. Nucl. Sci., NS-21, 73 (1974).